

# UNIVERSITÄTSKLINIKUM HAMBURG-EPPENDORF

III. Medizinische Klinik und Poliklinik,  
Nephrologie, Rheumatologie und Endokrinologie

Prof. Dr. med. Tobias B. Huber

## **Selection and characterization of kidney-specific vectors from random adeno-associated virus display peptide libraries**

### **Dissertation**

zur Erlangung des Doktorgrades PhD  
an der Medizinischen Fakultät der Universität Hamburg.

vorgelegt von:

Guochao Wu  
aus Shanxi/ China

Hamburg 2023

**Angenommen von der**

**Medizinischen Fakultät der Universität Hamburg am: 05.12.2023**

**Veröffentlicht mit Genehmigung der**

**Medizinischen Fakultät der Universität Hamburg.**

**Prüfungsausschuss, der/die Vorsitzende: Prof. Dr. Tobias B. Huber**

**Prüfungsausschuss, zweite/r Gutachter/in: Prof. Dr. Friedrich Nolte**

## Table of Contents

<b>1</b>	<b>Introduction.....</b>	<b>1</b>
1.1	The adeno-associated virus (AAV) .....	1
1.1.1	General biological properties .....	1
1.1.2	Genome composition .....	1
1.1.3	Genome replication .....	2
1.1.4	AAV receptors and transduction pathway .....	4
1.2	AAV as a vector for gene therapy .....	6
1.2.1	Recombinant AAV vector .....	6
1.2.2	Immunogenicity of AAV vectors .....	8
1.2.3	AAV capsid engineering for tropism modification.....	9
1.2.4	Random AAV2 and AAV9-W503A display peptide libraries.....	11
1.2.5	Application of the next-generation sequencing in AAV peptide libraries.....	13
1.3	The kidney.....	14
1.3.1	The nephron .....	14
1.3.2	The glomerulus .....	15
1.3.3	The Juxtaglomerular apparatus .....	17
1.3.4	Gene therapy in kidney diseases .....	18
1.3.5	Kidney as a target for AAV transduction .....	20
1.4	Aim of the study .....	21
<b>2</b>	<b>Materials and Methods.....</b>	<b>23</b>
2.1	Materials.....	23
2.1.1	Devices, reagents, and disposables .....	23
2.1.2	Buffer composition .....	25
2.1.3	Enzymes .....	25

2.1.4 Antibodies .....	26
2.1.5 Synthetic oligonucleotides.....	27
2.1.6 Plasmids.....	28
2.2 Methods .....	29
2.2.1 Basic molecular biology methods.....	29
2.2.1.1 Polymerase chain reaction (PCR) .....	29
2.2.1.2 PCR purification and gel extraction .....	29
2.2.1.3 Restriction endonuclease and ligation.....	30
2.2.1.4 Plasmid DNA purification.....	30
2.2.2 Prokaryotic method .....	31
2.2.2.1 Preparation of competent E. coli bacteria.....	31
2.2.2.2 Transformation .....	32
2.2.2.3 Bacterial enrichment culture .....	33
2.2.3 Large-scale recombinant AAV production.....	33
2.2.3.1 Cell culture and triple transfection of HEK293T/17 cells .....	33
2.2.3.2 AAV harvest and PEG 8000 precipitate .....	34
2.2.3.3 Iodixanol-based density gradients AAV purification .....	34
2.2.3.4 AAV iodixanol buffer exchange .....	35
2.2.3.5 AAV titration by qPCR.....	35
2.2.3.6 Ligation of synthetic oligonucleotide inserts to ITR-less AAV rep/cap plasmid .....	36
2.2.4 In vivo selection of random AAV display peptide libraries.....	37
2.2.4.1 Intravenous injection of peptide library and tissue harvest.....	37
2.2.4.2 Tissue homogenization and total DNA extraction.....	37
2.2.4.3 PCR amplification of the library inserts.....	37

2.2.4.4	Digestion of library inserts and backbone plasmid .....	38
2.2.4.5	Ligation of plasmid and insert and large-scale electroporation .....	38
2.2.4.6	Production of secondary AAV libraries .....	38
2.2.4.7	Enrichment of library variants in subsequent rounds of selection .....	39
2.2.4.8	Glomerulus isolation .....	39
2.2.5	Next-generation sequencing .....	40
2.2.5.1	NGS samples preparation .....	40
2.2.5.2	Quality control and sequencing .....	41
2.2.5.3	Bioinformatics evaluation of the NGS data .....	42
2.2.5.4	Evaluation of variants based on rating scores .....	42
2.2.6	Evaluation of selected capsid variants .....	43
2.2.6.1	Animals and vector administration .....	43
2.2.6.2	Blood and urine collection .....	43
2.2.6.3	Tissue preparation .....	44
2.2.6.4	Immunofluorescence staining .....	45
2.2.6.5	Immunohistochemistry and hematoxylin and eosin staining .....	46
2.2.6.6	Immunogold labeling and electron microscope .....	46
2.2.6.7	Vector genome distribution quantification .....	47
2.2.6.8	Measurements of kidney and liver functions .....	47
2.2.6.9	Treatment of anti-GBM glomerulonephritis by AAV2-GEC delivered IdeS .....	48
2.2.6.10	Assessment of Nano-luciferase (Nluc) activity in serum .....	48
2.2.6.11	Statistics .....	48
<b>3</b>	<b>Results .....</b>	<b>49</b>
3.1	In vivo selection of AAV random display peptide libraries in the murine kidney ...	49

3.1.1	Generation of subsequent AAV libraries during selection in the kidney.....	49
3.1.2	Peptides enrichment during in vivo selection in the murine kidney.....	51
3.1.3	Peptide enrichment monitored by next-generation sequencing.....	53
3.1.4	Scoring of dominant peptides.....	54
3.2	Characterization of AAV2-QVLVYRE.....	56
3.2.1	AAV2-QVLVYRE specifically and efficiently transduced the GEC.....	56
3.2.2	AAV2-GEC maintained robust tropism in GFB-damaged mice.....	61
3.2.3	AAV2-GEC maintained robust tropism in Balb/c mice and SD rats.....	64
3.2.4	AAV2-GEC delivery of IdeS prevents anti-GBM glomerulonephritis.....	65
3.3	Characterization of AAV9-GGNYGLG.....	71
3.3.1	AAV9-GGNYGLG specifically targeted the distal tubule adjacent to the JGA71	
3.3.2	AAV9-JGA specifically targeted a subset of the TAL at the JGA.....	74
3.3.3	The SLC12A1/CLDN16-positive TAL cells at the JGA is generally susceptible to AAV transduction.....	76
3.3.4	AAV9-JGA targeted TAL cells through tubule-afferent arteriole contact.....	77
<b>4</b>	<b>Discussion.....</b>	<b>81</b>
4.1	Overview.....	81
4.2	The selection and NGS analysis processes of the random AAV display peptide library.....	82
4.3	The potential of AAV2-GEC as a gene manipulation tool.....	83
4.4	The potential of AAV9-JGA as a gene manipulation tool.....	85
4.5	A possible route of AAV9-JGA transduction of TALs after intravenous injection..	87
4.6	Outlook.....	88
<b>5</b>	<b>Summary.....</b>	<b>90</b>
<b>6</b>	<b>Zusammenfassung.....</b>	<b>91</b>
<b>7</b>	<b>List of abbreviations.....</b>	<b>92</b>

<b>8</b>	<b>Reference .....</b>	<b>96</b>
<b>9</b>	<b>Acknowledgment.....</b>	<b>114</b>
<b>10</b>	<b>Curriculum vitae .....</b>	<b>115</b>
<b>11</b>	<b>Eidesstattliche Versicherung .....</b>	<b>117</b>

# 1 Introduction

## 1.1 The adeno-associated virus (AAV)

### 1.1.1 General biological properties

Adeno-associated virus (AAV) is a non-enveloped icosahedral single-stranded DNA virus with a diameter of 22-26 nm <sup>1</sup>. Over 50 years ago, Dr. Bob Atchison and Dr. Wallace Rowe first described and named AAV as a contaminant in the preparation of adenovirus <sup>2</sup>. AAVs belong to the parvoviral family's dependovirus genus and require the presence of helper viruses like adenovirus, herpes simplex virus, and cytomegalovirus to complete their productive replication cycle in host cells <sup>3</sup>. Wild-type AAVs can site-specifically integrate into human chromosome 19 at 19q13.4qter, known as AAVS1, a region that may be related to the role of ITR and Rep proteins <sup>4</sup>. Various serotypes of AAVs have been identified, each of which can infect different tissues, but have not been linked to any human diseases.

### 1.1.2 Genome composition

The whole genome of AAV is approximately 4.7 kb in length and is flanked by two 145 bp inverted terminal repeats (ITRs) <sup>5</sup>. The ITR, containing cis-elements necessary for virus replication and packaging, can fold on the palindromic sequences to form a distinctive T-shaped hairpin structure <sup>6</sup>. The AAV genome encodes three gene clusters: replication (Rep), structural capsid, and assembly-activating protein (AAP) genes. The rep gene encodes four different proteins Rep78, Rep68, Rep52, and Rep40 that are essential for viral replication and assembly. The transcripts Rep78 and Rep68 are regulated by the P5 promoter, while the Rep52 and Rep40 are driven by the P19 promoter. Rep68 and Rep40 are formed by alternative splicing of Rep78 and Rep52, respectively. The cap gene regulated by the P40 promoter encodes three overlapping viral structural proteins (VP1, VP2, and VP3) that are responsible for viral genome protection, as well as receptor interaction and cell internalization <sup>7,8</sup>. The icosahedral virion capsid is composed of sixty copies of the VP1, VP2, and VP3 monomers in a 1:1:10 ratio. The AAP gene is located

in the alternative open reading frame of VP2/VP3 and necessary for capsid assembly in various AAV variants<sup>9,10</sup>. Recently, the membrane-associated accessory protein (MAAP) was identified to be overlapping with the open reading frame within the VP1 region of the AAV cap gene. MAAP was postulated to limit AAV production through competitive exclusion as a novel AAV egress factor<sup>11,12</sup>.

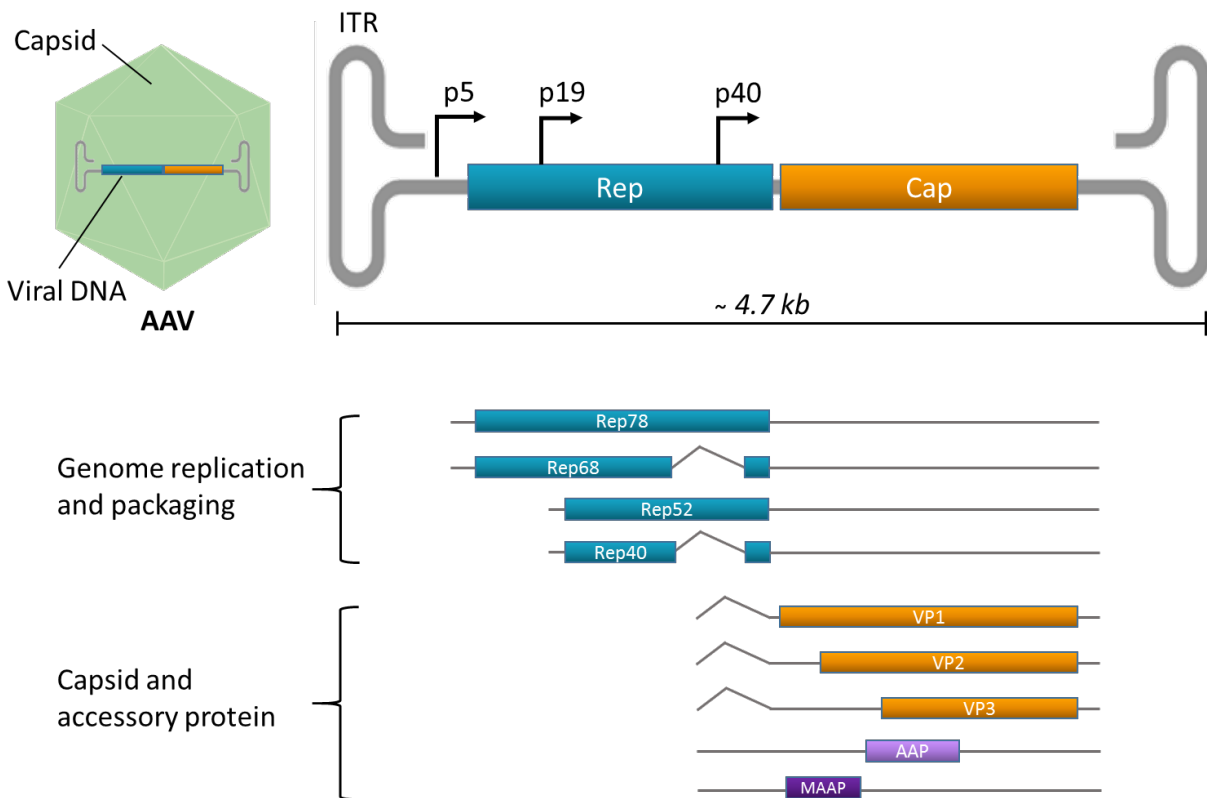


**Figure 1.1 Genome organization of AAV.** Two ITRs flank the AAV genome, which contains three promoters (p5, p19, p40) and four ORFs (Rep, Cap, AAP, MAAP). The rep gene encodes four proteins (Rep78, Rep68, Rep 52, and Rep40) respond to genome replication and packaging. Three overlapping VP proteins (VP1, VP2, and VP3) are expressed from the cap gene. AAP is expressed from a nonconventional start site nested in the VP2 and VP3 genes. MAAP is overlapping with VP1 as a novel AAV egress factor. Figure was created with BioRender.com.

### 1.1.3 Genome replication

AAV genome replication can proceed only in the presence of a helper virus, and the AdV5-dependent replication-rolling hairpin replication (RHR) mechanism of the AAV2 genome has been described as a textbook paradigm<sup>13</sup>. Like all single-strand DNA viruses,

AAV requires host-cell production of the complementary strand before gene expression. Once the AAV genome is released to the host nucleus, AAV begins to replicate its genome by an RHR mechanism<sup>14-16</sup> (Figure 1.2). Replication is initiated at the 3' end of ITR with the free 3'-OH terminus as a transcription primer. As a result, the second strand containing the 5' ITR is produced<sup>17</sup>. Subsequently, the replication of 5' ITR uses a new 3'-OH target site, which is nicked by a viral Rep protein at the terminal resolution site (TRS) in the 3' ITR<sup>17</sup>. There, a new 3'-OH primer is formed, and upon the synthesis of the complementary strand and strand displacement, a complete copy of the AAV genome is reproduced. Importantly, Meier et al.<sup>18</sup> recently described a new replication mechanism called rolling circle replication (RCR), which allows the formation of numerous double-stranded head-tail concatemers that cannot be explained by the RHR model during AAV replication in the presence of herpes simplex virus type 1 (HSV-1).

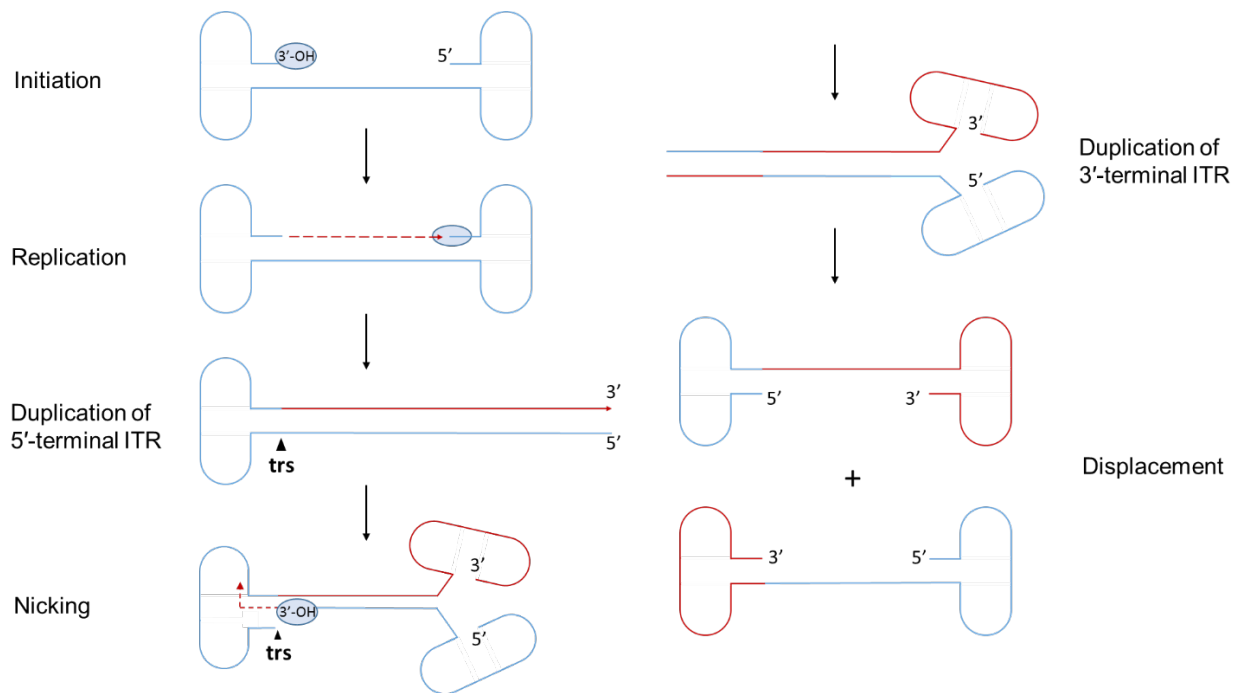


**Figure 1.2 Models for replication of the AAV genome.** Rolling hairpin replication of the AAV genome. Replication is initiated using the free 3'-OH and continues to duplicate the 5'-terminal ITR structure. A new 3'-OH target site was induced by a viral Rep protein at the palindromic terminal resolution site (TRS) allowing replication of the 3'-terminal ITR structure. Parental DNA is shown in blue and newly synthesized DNA is shown in red.

### 1.1.4 AAV receptors and transduction pathway

Initial attachment of AAV to target cells involves the interactions with the serotype-specific primary glycan receptors and the proteinaceous co-receptors on the cell surface <sup>19</sup>. For instance, the AAV2 capsid interacts with heparan sulfate proteoglycans (HSPG), a primary glycan receptor, for the initial cellular entry and then binds to co-receptors, such as fibroblast growth factor receptor 1 (FGFR1), hepatocyte growth factor receptor (HGFR), integrins ( $\alpha V\beta 5/\alpha 5\beta 1$ ), or laminin receptor (LamR) for the further cell entry <sup>19-22</sup>. Table 1.1 summarizes the identified glycan receptors and corresponding co-receptors for particular AAV serotypes. Additionally, several receptor binding sites on the AAV capsid surface have been identified and characterized by substituting crucial receptor binding residues <sup>23-25</sup> or determining the structure of the receptor-bound capsid <sup>26-29</sup>. This initial attachment facilitates viral internalization via clathrin-mediated endocytosis <sup>30,31</sup> (Figure 1.3). AAVs can also be internalized via caveolae-mediated endocytosis <sup>32</sup>, the CLIC/GEEC pathway <sup>33</sup>, and directly via RAC1-mediated micropinocytosis <sup>34</sup>. Some endocytic pathways contribute to effective transduction while others result in 'dead ends' <sup>32,34</sup>.

**Table 1.1 Cell receptors of different AAV serotypes**

Serotype	Attachment glycan receptor(s)	Co-receptor(s)	Entry factor(s)
AAV1	N-linked sialic acid <sup>35</sup>	Unknown	AAVR, GPR108
AAV2	HSPG <sup>21</sup>	FGFR1 <sup>36</sup> , HGFR <sup>20</sup> , LamR <sup>37</sup> , Integrin <sup>38</sup>	AAVR, GPR108
AAV3	HSPG <sup>39</sup>	HGFR <sup>40</sup> , LamR <sup>37</sup>	AAVR, GPR108
AAV4	O-linked sialic acid <sup>41</sup>	Unknown	GPR108
AAV5	N-linked sialic acid <sup>41</sup>	PDGFR <sup>42</sup>	AAVR
AAV6	HSPG <sup>43</sup> , N-linked sialic acid <sup>35</sup>	EGFR <sup>44</sup>	AAVR, GPR108
AAV7	Unknown	Unknown	Unknown
AAV8	Unknown	LamR <sup>37</sup>	AAVR, GPR108
AAV9	N-linked galactose <sup>45</sup>	LamR <sup>37</sup>	AAVR, GPR108
AAVrh10	keratan sulfate <sup>46</sup> , N-linked galactose <sup>47</sup>	Unknown	Unknown

**Note:** HSPG, heparan sulfate proteoglycans; FGFR1, human fibroblast growth factor receptor 1; HGFR, hepatocyte growth factor receptor; EGFR, epidermal growth factor receptor; PDGFR, platelet-derived growth factor receptor- $\alpha$ ; LamR, laminin receptor; AAVR, universal AAV receptor; GPR108, a member of the G protein-coupled receptor superfamily.

After entering the cell, AAV vectors were trafficked through endolysosomal vesicles and processed within vesicular and Golgi compartments to prime the AAV capsid for escaping toward the nuclear region <sup>31,48,49</sup>. During the transport in the endosomal compartment, AAV capsid exposes the N-termini of VP1 and VP2 owing to the acidification of the pH environment <sup>50-52</sup>. Interestingly, a multi-serotype AAV receptor (AAVR), which was recognized as the glycoprotein over 20 years ago and has lately been rediscovered as an essential host entry factor during the post-attachment step of AAV transduction <sup>53,54</sup>. The AAVR encodes five polycystic kidney disease (PKD1-5) domains on the ectodomain, which interacts with the most AAV capsids <sup>55,56</sup> except AAV4 and the closely related variant AAVrh32.33 <sup>57</sup>. More recently, a second highly conserved host entry factor for most AAV variants, GPR108, was identified by a genome-wide CRISPR screen using a divergent AAV serotype, rh32.33, which was previously reported to be independent of AAVR <sup>58</sup>. Both AAVR and GPR108 are predominantly localized intracellularly to the Golgi apparatus <sup>58-60</sup>, implying a potential role for AAVR and GPR108 in AAV trafficking to the Golgi apparatus. The exact roles of AAVR and GPR108 in AAV transduction remain unknown. Currently, the majority of AAVs used in research require both AAVR and GPR108 for cell entry, except AAV5 and AAV4, which requires only AAVR or GPR108, respectively.

Once within the nucleus, the AAV viral capsid is uncoated, and the single-stranded genome is released to synthesize a double-stranded genome capable of transcription, which results in transgenic expression <sup>50</sup>. During the uncoating process, some viral DNA can be released without the complete disassembly of the capsid <sup>61,62</sup>, and the kinetics of DNA release seem to differ among serotypes and cell types <sup>1</sup>. The AAV genome can persist in the nucleus in a concatemeric episomal form <sup>13</sup> or integrate into the host genome at very low frequencies <sup>63</sup>.

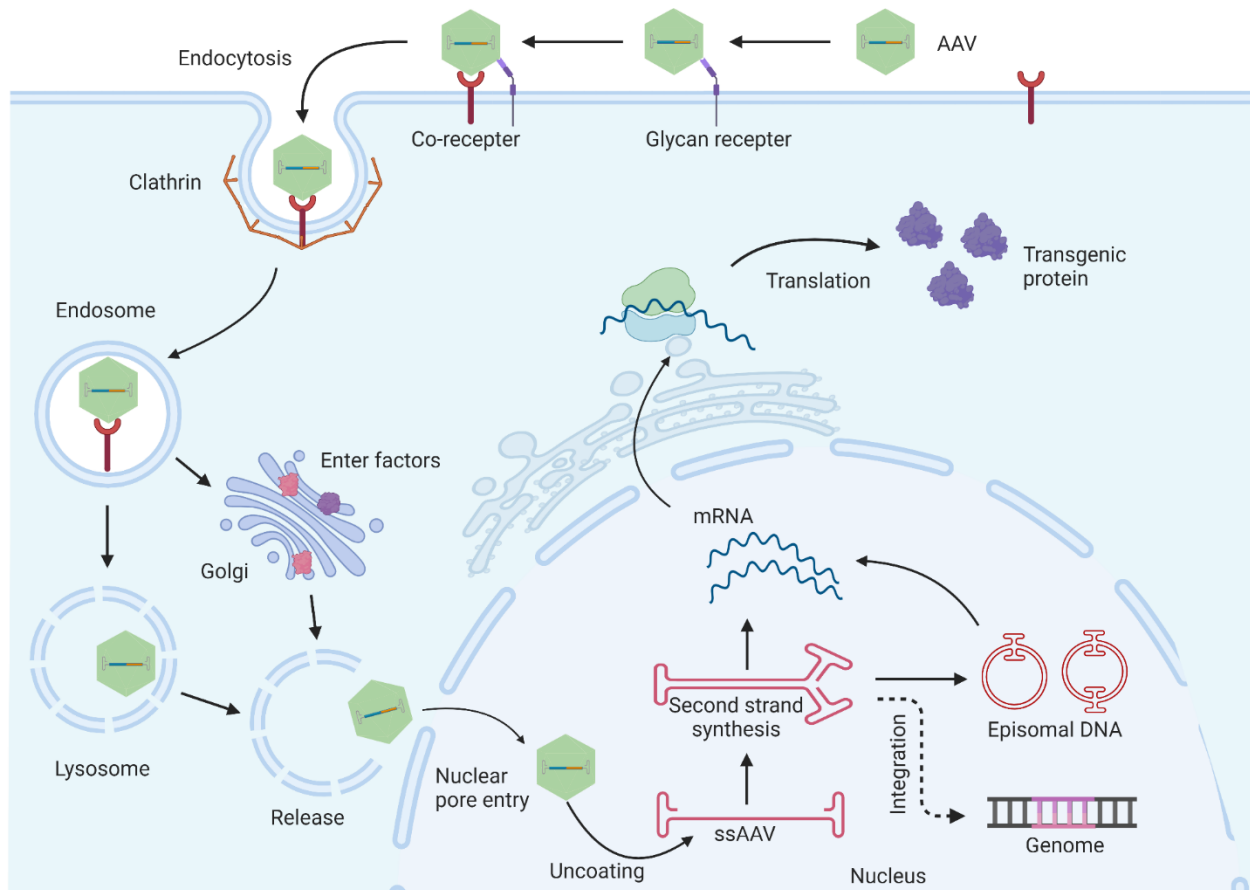


**Figure 1.3 AAV transduction pathway.** AAV vectors are recognized by primary glycan receptors and stabilized by secondary co-receptors. This triggers the virus internalization via clathrin-mediated endocytosis. The traffic through the endolysosomal vesicles and process within the vesicular and Golgi compartments prime the AAV capsid for escaping near the nuclear region. Entry factors (AAVR and GPR108) primarily located in the Golgi are essential for transduction. Once within the nucleus, the capsid is uncoated and the vector genome is released, followed by transcription, which results in the expression of transgene. Also, the AAV genome can persist in the nucleus in a concatemeric episomal form or integrate into the host genome at very low frequencies. Figure was created by BioRender.com.

## 1.2 AAV as a vector for gene therapy

### 1.2.1 Recombinant AAV vector

After decades of research on AAV, the basic biological properties<sup>2,5,64-66</sup> and some advantages of AAV have been characterized, including wide host range, high safety, and low immunogenicity<sup>67-72</sup>. These characteristics contributed to the idea of using AAV as a

gene therapy vector. Recombinant AAV (rAAV) vectors are generated by replacing the rep and cap genes of a wild-type AAV plasmid with a gene of interest. Only the ITRs is remained to guide genome replication and packaging during vector production. The majority of rAAV vectors contain the AAV2 ITRs, and their genome has a packaging capacity of approximately 4.7 kb.

**A** Wild-type AAV



**B** Recombinant AAV

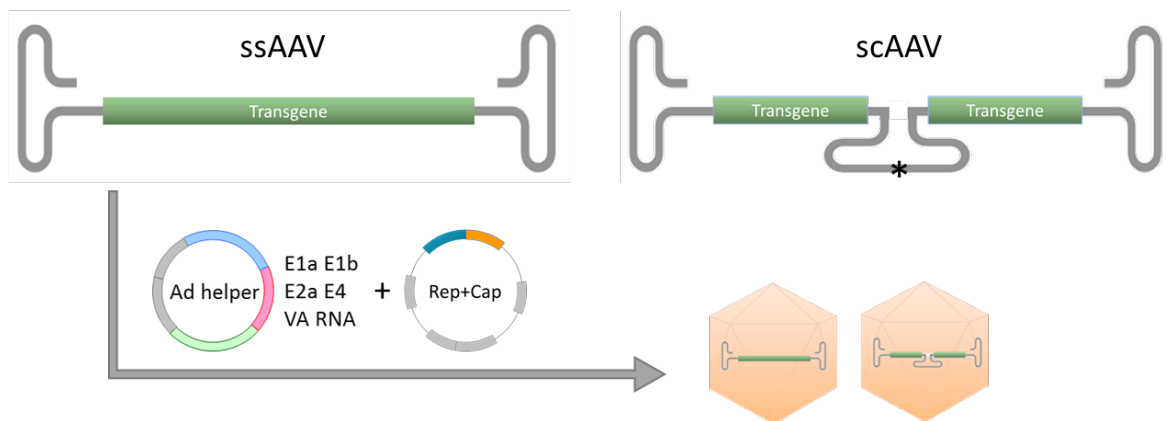


**Figure 1.4 Recombinant AAV vector genome systems.** (A) The wild-type AAV genome (rep and cap) is flanked by two inverted terminal repeats (ITRs). (B) The recombinant AAV vector is either single-stranded (ss) DNA that encodes ~4.5 kb transgene or self-complementary (sc) DNA that can encode ~2.2 kb transgene sequence in duplex form. The scAAV transgene is flanked by two wild-type ITRs and a mutated ITR (\*) at the axis of symmetry. Recombinant AAV vectors are produced by co-transfection of an ITR-flanked transgene cassette, an ad helper plasmid (E1a, E1b, E2a, E4, and VA RNA), and a plasmid encoding rep and cap.

rAAV is often synthesized by triple transfection of HEK293 cells, which comprises the vector plasmid containing the transgene flanked by ITRs, co-transfected with an ad helper plasmid (E1a, E1b, E2a, E4, and VA RNA), and a plasmid encoding rep and cap<sup>73</sup>. The

transduction of single-stranded AAV (ssAAV) requires the second-strand synthesis for gene transcription, which is rate-limiting for AAV synthesis<sup>74,75</sup>. In contrast, the use of self-complementary AAV (scAAV) allows more efficient transduction by introducing a mutation into one of the ITRs' terminal resolution sites<sup>76</sup>. The plus and minus strands of DNA tethered by the mutated ITR lead to concatemerization and circularization of the vector genome<sup>13</sup>. As a consequent, the packaging capacity of scAAV vectors is halved to approximately 2.2 kb<sup>13</sup> (Figure 1.4).

### 1.2.2 Immunogenicity of AAV vectors

AAV-based gene therapies have shown promise in curing a variety of human diseases. However, humoral and cellular immune responses against AAV vectors or transgenes pose a substantial barrier to the development of this field<sup>77,78</sup>. Pre-existing neutralizing antibodies (NAbs) against the AAV capsids in the human population can significantly reduce the effectiveness of rAAV, particularly when administered intravenously<sup>77</sup>. Additionally, rAAV administration can trigger a robust humoral immune response that produces capsid-specific NAbs, further hindering gene delivery<sup>79-81</sup>. In addition to antibody-mediated clearance, rAAV can also activate innate immunity via Toll-like receptor 2 (TLR2) and TLR9, which can subsequently promote adaptive immune responses<sup>79,80</sup>. For example, the capsid can be degraded by the proteasome and the resulting peptides are presented CD8+ T cells by major histocompatibility complex (MHC) class I molecules. The CD8+ T cells can then initiate cytotoxic effects, which eliminate rAAV-transduced cells and lead to loss of transgene expression<sup>79,80</sup>. Moreover, the transgene product can elicit a humoral immune response, resulting in the generation of transgene product-specific antibodies, which can suppress the long-term transgene expression<sup>80</sup>.

Due to the high prevalence of NAbs, several strategies have been developed to overcome this barrier, such as the use of immunosuppressive drugs to suppress humoral immunity<sup>82,83</sup>, the use of plasmapheresis to reduce circulating NAbs<sup>84</sup>, or the use of capsid engineering techniques to modify the recognition sites of NAbs to reduce immunogenicity<sup>85</sup>. However, all these strategies either do not effectively address high titers of neutralizing antibodies or tend to cause side effects. Recently, IgG-degrading enzyme of

*Streptococcus pyogenes* (IdeS) was shown to be effective in preclinical studies to mitigate the effects of pre-existing NABs<sup>86,87</sup>. IdeS reduced NAB and allowed effective hepatic transduction in mice and non-human primates in the presence of pre-existing humoral immunity and vector re-administration<sup>88-90</sup>. Unlike the humoral immune response, the cell-mediated immune response to AAV varies widely across patients and clinical trials. Some strategies to avoid the response were developed, including suppression of capsid-specific T-cell responses by immunosuppressive regimens, reduction of antigen presentation of AAV capsids by reducing therapeutic doses and empty capsids, and generation of Treg-mediated immune-tolerant capsids by AAV engineering<sup>79</sup>. Still, new approaches are needed to mitigate the cell-mediated immune response.

### **1.2.3 AAV capsid engineering for tropism modification**

AAV is a prospective platform for *in vivo* gene delivery. Several wild-type AAV-based gene therapies have been approved in clinical trials and achieved long-term therapeutic effects<sup>91-97</sup>. However, there are limited naturally occurring AAV variants, and most of them are unsuitable for direct clinical applications due to insufficient tissue specificity and immunogenicity. To circumvent these restrictions, strategies for optimizing AAV vectors for gene therapy applications have been extensively developed during the last three decades, including rational design and directed evolution. All of these strategies are referred to as capsid engineering.

Rational design is based on a comprehensive understanding of AAV biology and structure, and directly modifies the capsid structure via point mutations, motif insertions or chemical biology methods. Typically, these modifications focus on the surface-exposed regions of the AAV capsid<sup>98</sup>. Examples of these modifications include the substitution of two arginine residues with alanine in the GH12/GH13 loop of AAV2 to create a capsid with low-affinity to HSPG<sup>21</sup>; insertion of small targeting molecules by genetic fusion to AAV capsid proteins to allow AAV retargeting to cellular receptors<sup>99-101</sup>; and covalent modification of AAV with specific molecules to bridge AAV capsid with a targeting protein<sup>102</sup>. A more recent innovative rational design method predicts possible ancestral AAV capsids using computer approaches. These ancestral AAVs appear to be more

thermostable but exhibit similar transduction efficiency in different cell and tissue types compared to natural AAV serotypes<sup>103</sup>.

Directed evolution techniques can identify new AAV variants with beneficial properties by screening diverse AAV capsid libraries in vitro or in vivo under the certain selective pressure<sup>98</sup>. The main strategies to generate AAV capsid libraries include error-prone PCR, DNA family shuffling, random peptide insertion, and a combination of these strategies, thereby to generate new capsids with altered transduction efficiency and tissue tropism.

Error-prone PCR introduces random point mutations into the AAV capsid gene<sup>104</sup>. Although this approach is time-consuming and most point mutations are deleterious, a powerful variant EP1.9 was identified with a single amino acid mutant R459G, which achieved higher transduction efficiency than AAV2 wild-type in human embryonic stem cells<sup>105</sup>. Another AAV9 mutagenized variant N498I exhibited improved tropism for cardiac and skeletal muscles while de-targeting the liver<sup>106</sup>.

DNA family shuffling generates capsid chimeras based on the homologous recombination of variable regions on capsids among AAV serotypes<sup>107</sup>. This approach has yielded several novel capsids with improved transduction efficiency and tissue tropism. For example, AAV-DJ, a chimera of serotypes 2, 8, and 9, exhibits improved transduction in multiple cell lines and is more resistant to neutralizing antibodies than its parents<sup>108</sup>. Another chimera, AAV-LK03 (seven variations chimera), was selected from human hepatocytes in a xenograft mice model and is currently being investigated as a potential candidate vector for the treatment of hemophilia A<sup>109,110</sup>. In addition, combining the strategies of DNA family shuffling and error-prone PCR can generate more efficacy capsid libraries by using parental profiles with deterministic tropism<sup>111</sup>.

Random peptide insertion is also a powerful technology for generating AAV capsid libraries. The AAV2 serotype was utilized in the first attempt to generate peptide libraries by inserting randomized small peptides into exposed surface loops of the AAV2 capsid without changing the capsid assembly<sup>112</sup>. This technique was later extended to AAV9<sup>113</sup> and other serotypes<sup>114</sup>. The high throughput of randomized peptides displaying on the AAV capsid surface can bolster the chance of a successful selection of desired

candidates. This technique has already been validated in vitro and in vivo. In the context of AAV2, one effective variation 7m8 widely transduced retinal cells and rescued the disease phenotypes of X-linked retinoschisis and Leber's congenital amaurosis in mice<sup>115</sup>. AAV2.7m8 was identified as a potent viral vector for inner ear gene transfer due to its excellent transduction efficacy in the inner pillar and inner phalangeal cells<sup>116</sup>. Many other variants have been successfully identified from random peptide libraries with high tissue specificity and transduction efficiency in mammalian tissues, such as the central nervous system<sup>117-120</sup>, the lung tissues<sup>121,122</sup>, photoreceptors<sup>123</sup>, and cardiomyocytes<sup>124</sup>. In conclusion, directed evolution allows the generation of variants with distinct features from highly varied capsid libraries, especially when combined with high-throughput bioinformatics tools.

#### **1.2.4 Random AAV2 and AAV9-W503A display peptide libraries**

The random peptide insertion technology used in this study has been described by Müller and Varadi et al<sup>112,113</sup>. The designed strategies allow the insertion of small randomized peptides into a tolerated position within the AAV2 or AAV9 capsid surface to generate random peptide libraries. These modifications are located at prominent three-fold spike regions at the amino acid positions R588 (AAV2) and A589 (AAV9) (Figure 1.5, Figure 1.6B). The natural tropism of AAV serotypes hinders the selection of targeting variants from an AAV random peptide library, causing most variants to be trapped and limiting the number that can enter the target organ. Therefore, by mutagenesis the amino acid of the cell surface receptors specific to AAV serotypes can alter their tissue tropism, thereby reducing the capture of variants from the library by non-target tissues. The AAV9-W503A library used in this study is an example. AAV9 shows widespread systemic transduction, including in the heart, liver, and skeletal muscle<sup>125</sup>. Several specific amino acids in the AAV9 capsid are necessary for binding to galactose in hepatocytes<sup>24</sup>, among which the W503A mutation results in a liver-detargeting phenotype<sup>126,127</sup> (Figure 1.6A). The AAV9-W503A library was generated by using an AAV9-based library with the W503A mutation and the insertion of random 7-mer peptide sequences at capsid site A589 (VP1 numbering) (Figure 1.6B), which is located in the hypervariable region VIII of the AAV9 capsid and ensures the exposure of variable peptide sequences on the capsid surface<sup>24</sup>.

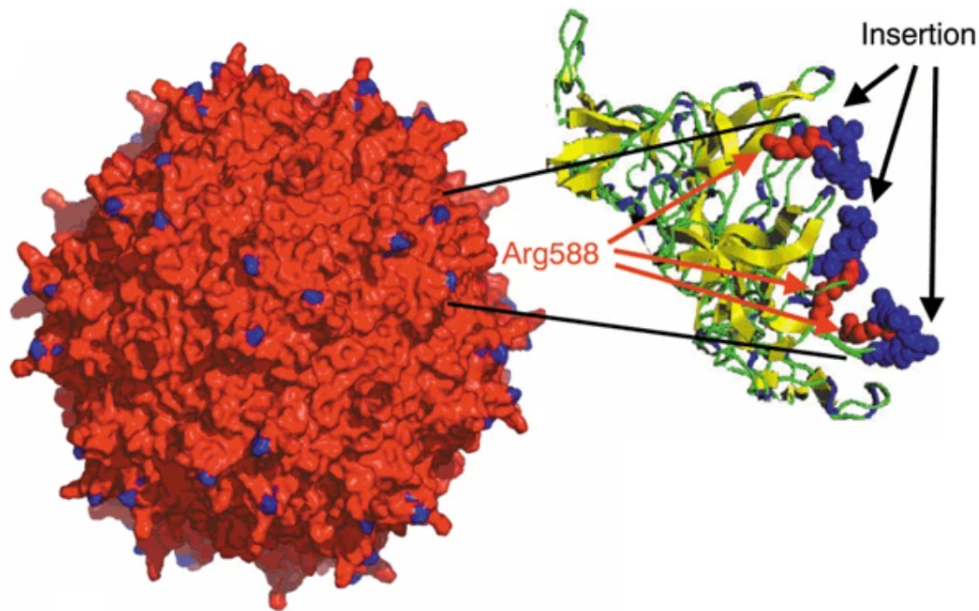


**Figure 1.5 Design and characteristics of the random peptide AAV display library construct.** The blue points indicate the location of 7-mer insertion close to the top of the threefold spikes on the AAV2 capsid surface. A spike region with Arg588 (red) is adjacent to library insertion (blue). The insertion area is within the binding domain of AAV, which binds to its natural receptors on the cell surface. Image was adapted from Müller et al. 2003 <sup>112</sup>.

Due to the limitation of transformation efficiency in library preparation, these libraries with seven random amino acid insertions yield approximately a diversity of  $1E+08$  AAV virions <sup>128</sup>. The random peptide insertion of AAV libraries can adopt the different amino acid coding schemes, such as NNK, NNB, NNS, NNN (N= A/C/G/T; B= C/G/T; K= G/T; S= C/G), and Trimer. Therefore, unlike other coding schemes, the Trimer technology requires only twenty codons to cover the twenty amino acids, resulting in no stop codon generation, no codon bias or no frameshifts, but a high sequence variety when compared to NNK or NNS libraries. Trimer and NNK formats were employed for the amino acid coding schemes of the AAV2 and AAV9-W503A libraries in this study, respectively.

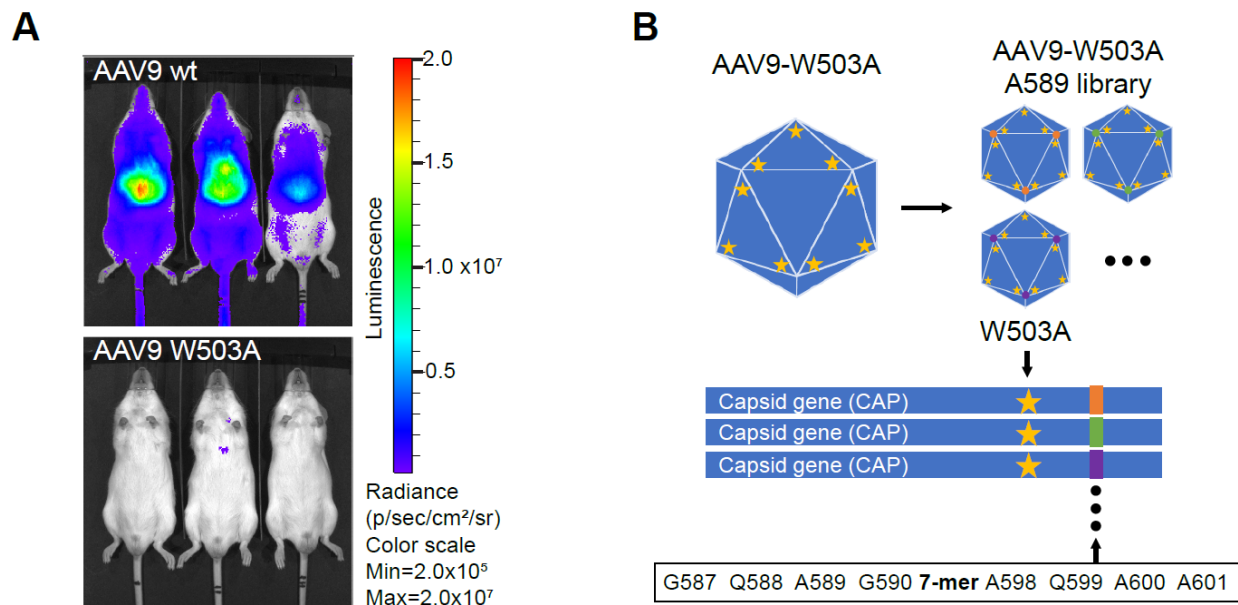


**Figure 1.6 AAV9-W503A-based peptide display library exhibited low transduction in the liver.** (A) In vivo luciferase imaging after tail vein injection of AAV9-WT and AAV9-W503A vectors carrying a luciferase reporter gene under the control of the CAG promoter. (B) Illustration of the construction of the AAV9-W503A-based peptide display library.

### 1.2.5 Application of the next-generation sequencing in AAV peptide libraries

The initial AAV peptide library needs to maintain a large diversity to ensure that the desired variants can be obtained after the library screening. In theory, library diversity should drop dramatically during each selection round and the potentially specific variants should be enriched in target tissues. However, considerable variants still exist even after the final selection round, which makes identification of the most promising candidates challenging. The selection of potentially tissue-specific clones can be simplified with the help of next-generation sequencing, which monitors the dynamics of the library and potentially improves the AAV capsid library screens during the selection. Especially, when combining next-generation sequencing with DNA barcoding technology, it is possible to correct over-represented sequences accumulated during library production, analyze the sequence of viral DNA extracts from target and non-target tissues, and determine the enrichment factors and enriched variants in selected tissues<sup>121,129</sup>. Körbelin et al. developed evaluation criteria based on the next-generation sequencing results to

determine the enrichment of certain sequences during selection and their specificity towards non-target organs. The most promising variants are identified by an enrichment score (E score), a general specificity score (GS score) and a combined score (C score)

<sup>121</sup>.

### **1.3 The kidney**

The primary function of the kidney is to filter and excrete waste substances from the blood. Other important functions of the kidney include acid-base and electrolyte homeostasis through reabsorption; regulates blood pressure through the renin-angiotensin-aldosterone system; and produces erythropoietin, active vitamin D3, prostaglandins, kinin, etc. Macroscopically, kidney is separated into the renal parenchyma and the renal pelvis. The renal parenchyma is further subdivided into the outer cortex and inner medulla (Figure 1.7A).

#### **1.3.1 The nephron**

The nephron is the functional unit of the kidney (Figure 1.7B). It consists of the renal corpuscle and renal tubule. The renal corpuscle in turn consists of a glomerulus surrounded by a Bowman's capsule. After the blood enters the glomerulus, primary urine is filtered out in the glomerular capillary tuft and released into Bowman's capsule. Subsequently, the primary urine flows through the different renal tubules (proximal convoluted tubule, the loop of Henle, distal convoluted tubule, and collecting tubule), while beneficial solutes, mostly water and salt are reabsorbed <sup>130</sup>. Each adult human kidney has up to 2.5 million nephrons <sup>131</sup>.

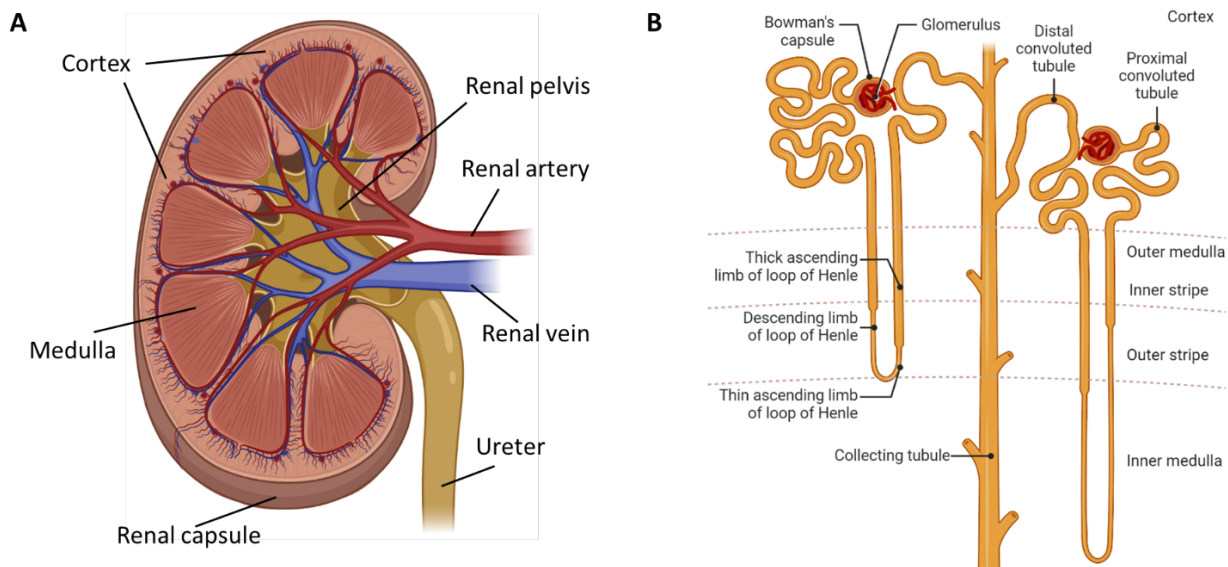


**Figure 1.7 Schematic diagram of the kidney and nephron.** (A) The anatomical structure of the kidney. The kidney mainly comprises of renal capsule, cortex, medulla, and renal pelvis. The blood flows into the kidney from the renal artery and flows out from the renal vein. The urine is collected by the renal pelvis and drained out of the kidney via the ureters. (B) The structure of a nephron. Each nephron consists of the glomerulus, proximal convoluted tubule, loop of Henle, distal convoluted tubule, and collecting duct. Figure was created by BioRender.com.

### 1.3.2 The glomerulus

The glomerulus is the filtration unit of the kidney and consists of a specialized bundle of capillaries<sup>132</sup>. These capillaries are uniquely located between two resistance vessels, creating a pressure gradient throughout the glomerulus for blood ultrafiltration. Parietal epithelial cells (PECs) adhere to the inner wall of Bowman's capsule as a monolayer and in continuity with the proximal tubular (PT) and podocytes. The blood enters the glomerulus via an afferent arteriole, then passes through the capillary network, which serves as the morphological basis of the blood-urinary barrier, and exits via an efferent arteriole.

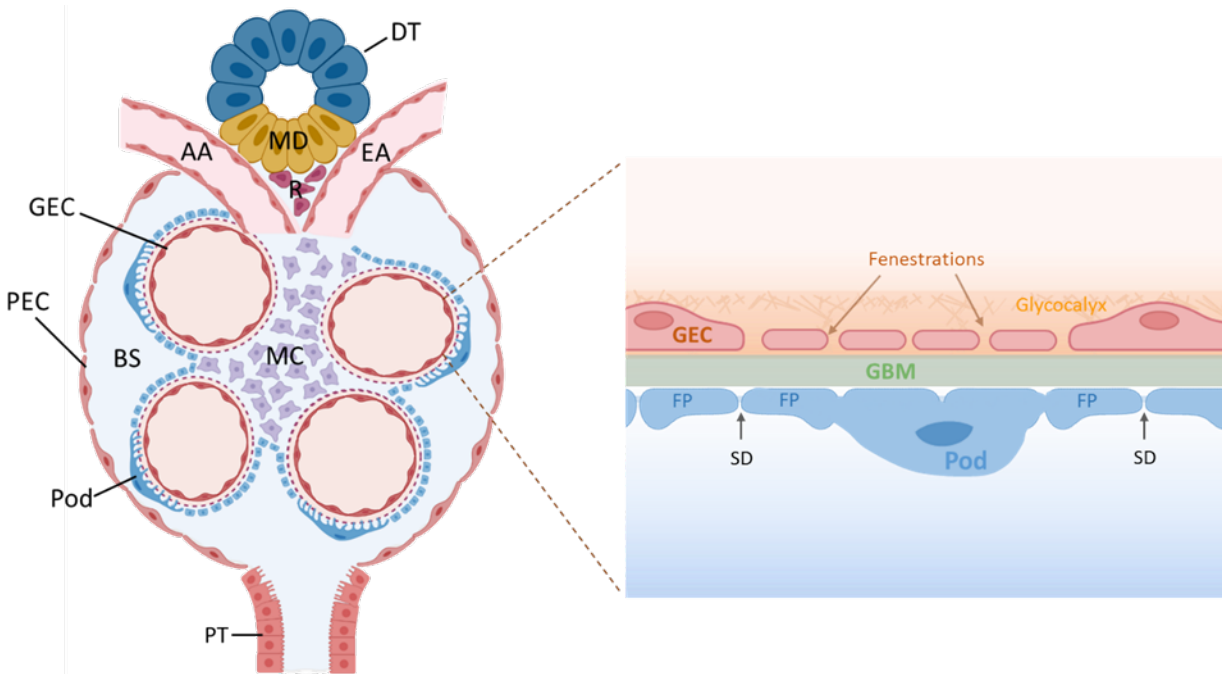


**Figure 1.8 Schematic diagram of the glomerulus and glomerular filtration barrier.** The glomerulus (left) is composed of capillaries that start from the afferent artery (AA) to the efferent artery (EA). These capillaries are comprised of glomerular endothelial cells (GECs) and wrapped by the podocytes (Pods). Parietal epithelial cells (PECs) line the Bowman's capsule (BS) and in continuity with the proximal tubular (PT) at the urinary pole. Between the glomerular capillary loops are the mesangial cells (MCs). Urine collects at Bowman space and passes through the proximal tubules. The macula densa and renin cells (R) between these arterioles and near the distal nephron (DT) are illustrated. The layers of the glomerular filtration barrier (GFB) are shown on the right panel. From the inner layer to the outer layer are glycocalyx, fenestrated endothelium, glomerular basement membrane (GBM), podocytes, and slit diaphragm (SD) between foot processes. Figure was created by BioRender.com.

The glomerular filtration barrier (GFB) comprises three layers: glomerular endothelial cells (GECs), glomerular basement membrane (GBM), and the visceral epithelial cells of Bowman's capsule, also called podocytes. The proximal component layer of the GFB is a fenestrated capillary endothelium, which contains numerous fenestrations with diameters ranging from 70 to 90 nm<sup>133</sup>. These fenestrations permit the filtration of fluid and small solute while retain a low permeability to macromolecules<sup>134</sup>. The glycocalyx of GEC is primarily composed of negatively charged glycosaminoglycans and repels the passage of negatively charged molecules (e.g. albumin)<sup>135</sup>. The GBM is the central layer of the GFB and acts as a physical scaffold between GECs and podocytes, allowing them

to cross-talk with one another via different signaling pathways <sup>136</sup>. The GBM is a ribbon-like extracellular matrix composed of four significant macromolecules including type IV collagen, laminins, heparan sulfate proteoglycan and nidogen, all of which create charge and size selectivity for blood filtration <sup>137</sup>. The distal layer of the GFB is formed by podocytes. These cells are characterized by foot-like processes that interdigitate with adjacent podocytes forming the filtration slit diaphragm <sup>138</sup>. The slit diaphragm serves as a final filtration barrier to maintain the equilibrium of ultrafiltration. In addition, between the glomerular capillary loops is a mesangium composed of mesangial cells and matrix. Mesangial cells in the mature glomerulus are directly in contact with GECs and GBM to regulate the capillary surface filtration area (Figure 1.8) <sup>139</sup>.

### **1.3.3 The Juxtaglomerular apparatus**

The Juxtaglomerular apparatus (JGA) is located at the glomerular vascular pole, where the thick ascending limb of Henle's loop rejoins its parent glomerulus, forming a triangular wedge bordered by the afferent and efferent arterioles <sup>140</sup> (Figure 1.9). The JGA is a kidney nephron component that functions as an intrarenal baroreceptor. The juxtaglomerular cells (also known as granular cells), the macula densa, and the extraglomerular mesangium make up the JGA. The granular cells are predominantly present in the terminal walls of the afferent arterioles and exhibit characteristics of both smooth muscle cells and secretory epithelial cells, allowing them to constrict when stimulated by renal sympathetic nerves and to synthesize and release renin into the bloodstream when stimulated by macula densa <sup>141</sup>. The macula densa is specialized epithelium cells located in the wall of the distal tubule, at the point of the TAL where it touches the glomerulus <sup>142</sup>. These cells sense sodium chloride concentration in the lumen via sodium-potassium-chloride cotransporter (NKCC2) and send signal to juxtaglomerular granular cells that adjust the renal blood flow and glomerular filtration rate (GFR) through tubuloglomerular feedback and renin release <sup>142</sup>. The extraglomerular mesangium unites all components of the glomerular entry in continuity with the intraglomerular mesangium and acts as a glomerular capillary anchor. Like the macula densa, The extraglomerular mesangium is involved in the regulation of systemic blood pressure <sup>143</sup>.

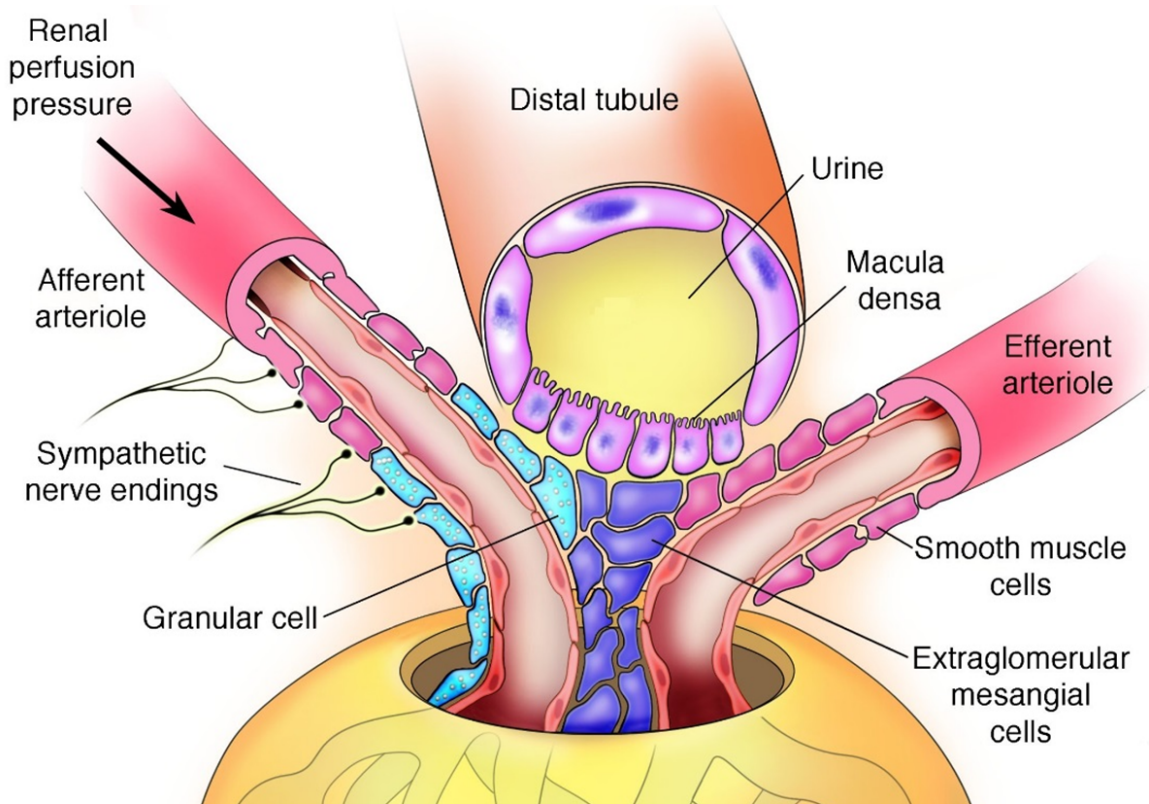


**Figure 1.9 Schematic diagram of the Juxtaglomerular apparatus.** The Juxtaglomerular apparatus (JGA) is located at the vascular pole of the glomerulus, where the thick ascending limb of Henle's loop (TAL) rejoins its parent glomerulus and forms a triangular wedge bordered with afferent and efferent arterioles. The JGA includes the macula densa, juxtaglomerular cells (granular cells), and extraglomerular mesangial cells. The figure was modified from Francois and Coffman <sup>144</sup>.

### 1.3.4 Gene therapy in kidney diseases

Over the past few decades, gene therapy has achieved dramatic improvements in the treatment of previously incurable inherited genetic diseases and acquired disorders <sup>145,146</sup>. An efficient delivery system is crucial to gene therapy effectiveness, which allows the therapeutic gene to be transferred and expressed locally within the target organ or tissue <sup>147</sup>. Current tools used for gene delivery include viral and nonviral approaches <sup>148,149</sup>. The delivered genetic material from these approaches can remain episomal or integrated into the genome to exert its effects through transcription and/or translation. In addition, the

CRISPR gene editing system is used as an extension of gene therapy <sup>150</sup>. Recent breakthroughs in the therapy of various genetic and metabolic illnesses, including lysosomal storage disorders, retinal degeneration, and spinal muscular atrophy, have resulted from the great diversity of delivery and editing technologies <sup>145,146</sup>. The development of gene therapy has achieved gene modifications within more easily targetable tissues, such as the eye, liver, muscle, and central nervous system <sup>94-97,145,146</sup>. However, the kidney is rarely mentioned in current gene therapy clinical trials.

Inherited kidney diseases are associated with a high prevalence of early-onset chronic kidney disease in adults, with many of them being monogenic diseases <sup>151</sup>, kidney-targeting gene therapy provides an opportunity for the treatment of inherited kidney diseases and the prevention of chronic kidney diseases. However, the complex structure of the kidney and also the multitude of different cell types and tissues make targeting specific kidney cell types difficult <sup>152</sup>. The glomerulus possesses an intrinsic blood-urinary barrier function that actively blocks proteins larger than 50 kDa in size or 10 nm in diameter <sup>133,152</sup>. This barrier makes it difficult for most gene therapy vectors, including relatively small AAV vectors, to penetrate glomerular cells via the intravenous route. This implies that, in general, optimizing targeting and transgenic expression for a certain cell type might be challenging.

Viral vectors are most potent for in vivo delivery, some viral vectors such as adenovirus, retrovirus, and AAV are the most commonly used for gene delivery in the kidney due to their transduction efficiency and longevity <sup>152</sup>. Although these viral vector systems come in various genetically diverse serotypes that are immunologically unique and can target multiple cells <sup>152,153</sup>, these viral vectors may not be specific or efficient enough to effectively treat kidney disease. Nonviral techniques have been developed as a safe and effective alternative to viral delivery for kidney therapy, with various applications such as naked DNA and lipoplexes transfection, nanoparticle administration, and extracellular vesicle delivery, and some nonviral vectors are not limited by the blood-urinary barrier <sup>154-158</sup>. Similar to the viral delivery approaches above, nonviral techniques often mediate inefficient gene expression or are not as specific to a particular cell type within the kidney, making them inadequate for most therapeutic approaches.

Several alternative delivery methods, such as intravenous injection, retrograde infusion into the ureter, and subcapsular injection via the kidney capsule, have been explored to improve gene transfer efficiency in the kidney<sup>153,159,160</sup>. These delivery routes allow the vector to get into the different parts of the kidney, however, most vectors tested result in either widespread off-target tissue transduction or inefficient transduction, making it crucial to optimize transgene expression and develop cell-specific targeting strategies to prevent off-target tissue transduction.

### **1.3.5 Kidney as a target for AAV transduction**

AAV stands out among the various viral vectors for gene therapy due to its molecular biology flexibility, which allows for engineering and modifications to reduce its immunogenicity and enhance its transduction efficiency, specificity, and longevity. Many AAV vectors have been approved in clinical trials for the treatment of genetic diseases<sup>94-97</sup>, however, the development of kidney cell-specific transduction vectors remains as a challenge. Recent studies have shown that AAV serotypes 1, 2, 8, 9, and rh10 mediate varied levels of gene delivery in the kidney<sup>160-166</sup>, but the data on their targeting specificity and transduction efficiency are inconsistent. This might be due to the differences in administration routes or doses. For instance, AAV serotype 9 has been identified as an efficient vector for mouse kidney transduction, especially when used at a high dose or in combination with a renal vein injection approach<sup>161,163,165</sup>, but other researchers have not observed such successful transduction in the kidney<sup>167,168</sup>. Similar to most delivery approaches, these AAV vectors usually mediate an unspecific transduction in the kidney, which might lead to extrarenal toxicity. Nevertheless, some approaches still achieved kidney-specific transduction locally. Laureano et al.<sup>169</sup> made an innovative attempt to obtain cell-specific expression by using an AAV9 vector carrying cell-type specific promoters in conjunction with the retrograde ureteral injection approach and achieved GFP-selective expression in the appropriate part of the kidney. A more recent study described a new synthetic AAV variant, Anc80, which allows reasonably selective and high-efficiency transduction of renal stroma and mesangial cells<sup>167</sup>. Notably, Anc80-mediated transport of Cre recombinase to the kidney was sufficient to alleviate renal fibrosis in mice<sup>167</sup>. These studies demonstrate the potential of using AAV for kidney-

targeting gene therapy, but further development of novel AAV capsids to improve the targeting specificity and transduction efficiency in kidney cells is required. AAV vector studies to the kidney are summarized in Table 1.2.

**Table 1.2 List of AAV vector studies to the kidney**

Variant	Promoter	Transgene	Species Strains	Dose (vg)	Injection route	Time (week)	Target tissues/cells	Ref.
AAVrh10	CMV	COMP-Ang1	db/db	2E+11	Left carotid artery	2	GEC	ref <sup>166</sup>
scAAV1	CMV	Cre	mT/mG	1E+12	Intravenous	3	Tubules	ref <sup>161</sup>
scAAV8	CMV	Cre	mT/mG	1E+12	Intravenous	3	GEC/PT	
scAAV9	CMV	Cre	mT/mG	1E+12	Intravenous	3	GEC/PT	
Anc80	CMV	GFP	C57BL/6	1E+11	Retro-orbital	3	Interstitial	ref <sup>167</sup>
AAV8	CAG	GFP	FVB	2E+11	RU/SC	4	Tubules /Glomerulus	ref <sup>160</sup>
AAV8	CMV	Cre	Ai14	3.16E+11	Intravenous	2	GEC/MC	ref <sup>164</sup>
AAV9	KSPC	GFP	C57BL/6	1E+11	RU	2	Nephron	ref <sup>169</sup>
AAV9	ECAD	GFP	C57BL/6	1E+11	RU	2	CD	
AAV9	SGLT2	GFP	C57BL/6	1E+11	RU	2	PT	
AAV9	NKCC2	GFP	C57BL/6	1E+11	RU	3	TALH	
AAV2	CAG	GFP	Lewis rats	1.25E+10	Renal artery	6	PT/CD	ref <sup>162</sup>
AAV9	CAG	hPRKAR1A	C57BL/6	2E+11	Retro-orbital	6	Tubules	ref <sup>163</sup>

Note: MC, mesangial cell; GEC, glomerular endothelial cells; ECAD, epithelial cadherin; NCAD, neural cadherin; KSPC, Ksp cadherin; CD, collecting duct; TALH, thick ascending limb of Henle's loop; ECAD, E-cadherin; NKCC2, sodium, potassium, 2 chloride co-transporter; PT, proximal tubule; RU, retrograde ureteral; SC, subcapsular injection.

## 1.4 Aim of the study

Gene therapy has been successfully applied in vivo for the treatment of genetic diseases affecting many organs. However, little progress has been made in applying gene therapies to genetic or acquired kidney diseases. Since kidneys are composed of a large number of different cell types, assembled in various tissues with highly diverging functions and disease susceptibilities, cell-specific targeting strategies are urgently needed. AAV as a promising in vivo gene delivery platform shows the advantage in delivering

therapeutic molecules to those difficult or non-druggable cells. However, natural AAV serotypes have insufficient targeting specificity and transduction efficiency in kidney cells, thus approaches to broaden the tropism of AAV and screenings for kidney-specific AAV vectors are particularly needed. Random AAV display peptide libraries have proven to be an effective tool for developing cell-specific vectors and have yielded attractive vectors for in vivo applications <sup>118,120,121</sup>. In this study, we developed a kidney-specific selection strategy based on the previously described methodology by improving the targeting resolution with glomerular separation technology to select two different AAV display peptide libraries. By integrating the experimental and bioinformatics workflows, the goal of this study was not only to establish an AAV in vivo screening approach for kidneys but also to generate new AAV vectors targeting kidney cells to broaden our current kidney gene delivery toolkit for research and clinical applications.

## 2 Materials and Methods

### 2.1 Materials

#### 2.1.1 Devices, reagents, and disposables

**Table 2.1 List of equipment**

<b>Application</b>	<b>Device</b>	<b>Manufacturer</b>
Cell culture	TC20™ automated cell counter	Bio-Rad
	Heracell™ 150i CO2 Incubator	Thermo Scientific
	VACUSAFE Aspiration System	Integra Biosciences
Bacteria culture	MaxQ™ 6000 Incubated/Refrigerated Stackable Shakers	Thermo Scientific
PCR	VWR® PCR Workstation	VWR
	C1000 Thermal Cycler	Bio-Rad
	QuantStudio 3 Real-Time PCR System	Thermo Scientific
Gel electrophoresis	Electrophoresis Power Supply EPS-601	Artisan Technology
	Alphaimager Mini Gel Documentation System	Group Cell-biosciences
Spectrophotometer	DS-11 Series Spectrophotometer	DeNovix
Ultramicrotome	EM UC6	Leica
Cryotome sectioning	CryoStar™ NX70 Cryostat	Thermo Scientific
pH meter	Lab 855	SI Analytics
Tube topper/sealer	Quick-Seal Cordless Tube Topper	Beckman Coulter
Microscopes	S6E	Leica
	Axio Scope A1	Carl Zeiss
	TCS SP5	Leica Carl
	ApoTome	Zeiss
Transmission Electron Microscope	Leo 910	Zeiss
Tissue dissociators	gentleMACS Dissociator	Miltenyi Biotec
Tissue homogenizer	Minilys	Bertin Instruments
Luminometer	Mithras LB 940	Berthold Technologies
Centrifuge	AVANTI J-20 XP	Beckman Coulter
	Centrifuge 5910 R	Eppendorf
	Fresco™ 17 Microcentrifuge	Thermo Scientific
	Optima LE-80K, Rotor: Type 70.1 Ti	Beckman Coulter
Electroporation system	MicroPulser Electroporator	Bio-Rad
DNA Fragment Analysis	Agilent 2100 Bioanalyzer	Agilent
Elisa	Sunrise(TM) plate reader	TECAN

**Table 2.2 List of kits, reagents, and disposables**

<b>Reagent</b>	<b>Name</b>	<b>Supplier</b>	
Kits	DNeasy® Blood & Tissue Kit	QIAGEN	
	AllPrep DNA/RNA Mini Kit	QIAGEN	
	Zyppy Plasmid Miniprep Kit	Zyppy Research	
	QIAfilter Plasmid Maxi Kit	QIAGEN	
	QIAquick PCR Purification Kit	QIAGEN	
	QIAquick Gel Extraction Kit	QIAGEN	
	MiSeq Reagent Kit v3	Illumina	
	Creatinine Jaffé Gen. 2	Roche Cobas	
	Liver function index	Roche Cobas	
	Nano-Glo® Luciferase Assay System	Promega	
Reagents	Polyethylene glycol 8000	Carl Roth	
	ProLong™ Gold Antifade Mountant	Invitrogen	
	HBSS, calcium, magnesium, no phenol red	Thermo Scientific	
	NEB® 10-beta/Stable Outgrowth Medium	New England Biolabs	
	PolyFect Transfection Reagent	QIAGEN	
	OptiPrep™	PROGEN Biotechnik	
	Polyethylenimine, Linear, 25kDa	Polysciences	
	Sheep Anti-Rat GBM Serum (PTX-001AGBM)	PROBETEX	
	TMB One Component Substrate	Biomol	
	Dynabeads® M-450 Tosylactivated	Invitrogen	
	Dynabeads® M-450 Epoxy	Invitrogen	
	Doxycycline hyclate	Sigma-Aldrich	
	Disposables	gentleMACS C Tubes (4x25 pieces)	Miltenyi Biotec
		pipettespitze mit Filter, 50-1250 ul, extra long	Sarstedt
DNA-lowbind tubes 1.5ml		Eppendorf	
DNA-lowbind tubes 2.0ml		Eppendorf	
Millex-GP Syringe Filter Unit, 0.22 µm, polyethersulfone, 33 mm, gamma		Merck Millipore	
Sterile Millex filter 0,22 µm		Millex	
CELLSTAR® Tissue Culture Dishes		Greiner Bio-One	
Beckman Coulter Tube, Quick-Seal®, Ultra-Clear, 13.5 mL, 16 x 76mm		Fisher Scientific	
Laboratory Pipetting Needles		Cadence Science	
pluriStrainer® 300 µm Cell Strainer non-sterile		pluriSelect	
pluriStrainer® 100 µm (Cell Strainer)		pluriSelect	
Ultracel-100 regenerated cellulose membrane		Merck Millipore	

## 2.1.2 Buffer composition

**Table 2.3 List of buffer composition**

<b>Buffer</b>	<b>Composition</b>
1x PBS-MK	2.5 mM KCl, 1 mM MgCl <sub>2</sub> in PBS
Phenol red solution	0.5% (w/v) phenol red
15% Iodixanol solution	25% (v/v) Iodixanol, 10% (v/v) 10x PBS-MK, 20% (v/v) 5M NaCl, 45% (v/v) ddH <sub>2</sub> O
25% Iodixanol solution	39.25% (v/v) Iodixanol, 10% (v/v) 10x PBS-MK, 0.75% (v/v) phenol red solution, 50% (v/v) ddH <sub>2</sub> O
40% Iodixanol solution	66.67% (v/v) Iodixanol, 10% (v/v) 10x PBS-MK, 23.33% (v/v) ddH <sub>2</sub> O
54% Iodixanol solution	89.25% Iodixanol (v/v), 10% (v/v) 10x PBS-MK, 0.75% (v/v) phenol red solution
PEI solution	0.1% (w/v) PEI in ddH <sub>2</sub> O, pH 7.0
50 x TAE buffer	1M Acetic acid, 50mM EDTA, 2M Tris
Elisa coating buffer	0.05 M Carbonate-Bicarbonat, pH 9.6
Elisa sample dilution buffer	50 mM TBS, 1% BSA, pH 8.0, 0.05% Tween 20
Post-coating buffer	50 mM TBS, 1% BSA, pH 8.0
Elisa washing buffer	50 mM TBS, 0.05% Tween 20, pH 8.0
Elisa stop solution	2 N H <sub>2</sub> SO <sub>4</sub>

## 2.1.3 Enzymes

**Table 2.4 List of enzymes**

<b>Name</b>	<b>Supplier</b>
Restriction endonucleases	New England Biolabs/Thermo Scientific
Collagenase Type V	Sigma-Aldrich
DNase I	New England Biolabs
T4 DNA Ligase	New England Biolabs
T4 Polynucleotide Kinase	New England Biolabs
Benzonase® Nuclease	Sigma-Aldrich
Phusion High-Fidelity DNA Polymerase	Thermo Scientific
DreamTaq Green PCR Master Mix (2X)	Thermo Scientific
RNase A	QIAGEN
PowerUp™ SYBR™ Green Master Mix	Applied Biosystems

## 2.1.4 Antibodies

**Table 2.5 List of antibodies**

<b>Description</b>	<b>Catalog</b>	<b>Supplier</b>
Rat Anti-Mouse CD31	550274	BD Pharmingen™
GFP Polyclonal Antibody	A10262	Thermo Scientific
Synaptopodin Polyclonal Guinea pig antiserum	163004	Synaptic Systems
Recombinant Anti-PDGFR alpha + PDGFR beta antibody [Y92] - C-terminal	ab32570	Abcam Biochemicals
Claudin 10 Polyclonal Antibody	38-8400	Thermo Scientific
Claudin-16 C-Terminus	00216	Bicell Scientific
Anti-SLC12A1 antibody [EPR11842]	ab171747	Abcam
NOS1 (A-11)	sc-5302	Santa Cruz Biotechnology
Anti-Renin antibody	ab212197	Abcam
Anti-GFP antibody (ab5450)	ab5450	Abcam
Anti-GFP antibody - ChIP Grade (ab290)	ab290	Abcam
Alexa Fluor®; 555 donkey anti-sheep IgG (H+L) *2 mg/mL*	A21436	Invitrogen
Anti-C1q antibody [4.8]	ab182451	Abcam
Complement C3 Antibody (11H9)	NB200-540SS	Novus Biologicals
Cy3™ Anti-α Smooth Muscle Actin Mouse Monoclonal Antibody	C6198-100UL	Sigma-Aldrich
Alexa Fluor®; 555 donkey anti-mouse IgG (H+L) *2 mg/mL*	A31570	Invitrogen
Goat anti-Mouse Albumin	A90-134A	Biomol
Goat anti-Mouse Albumin, HRP conjugated	A90-134P	Biomol
Endothelial Cells Antibody (RECA-1)	NB600-1388	Novus Biologicals
Anti-AAV9 mouse recombinant, ADK9-1R	610178S	Progen

## 2.1.5 Synthetic oligonucleotides

**Table 2.6 List of oligonucleotides**

<b>Name</b>	<b>Sequence (5' - 3')</b>
AAV2-R588 1st PCR F	ATGGCAAGCCACAAGGACGATG
AAV2-R588 1st PCR R	CGTGGAGTACTGTGTGATGAAG
AAV2-R588 2nd PCR F	GGTTCTCATCTTTGGGAAGCAAG
AAV2-R588 2nd PCR R	TGATGAGAATCTGTGGAGGAG
AAV9-A589 1st PCR F	GGAGCTTCTTCTTGGGCTCT
AAV9-A589 1st PCR R	AGCGGAGAAGGGTGAAAGTT
AAV9-A589 2nd PCR F	CAGCCACAAAGAAGGAGAGG
AAV9-A589 2nd PCR R	CCCGGAAGTATTCTTGGTT
AAV2-R588 NGS F	ACACTCTTTCCCTACACGACGCTCTTCCGATCTGCTCCAGAGA GGCCAGAGAG
AAV2-R588 NGS R	TGACTGGAGTTCAGACGTGTGCTCTTCCGATCTATGAGCATCT GCGGTGGCCGCCTG
AAV9-A589 NGS F	ACACTCTTTCCCTACACGACGCTCTTCCGATCTGCACCAGAGT GGCCAAGCAG
AAV9-A589 NGS R	TGACTGGAGTTCAGACGTGTGCTCTTCCGATCTATGAGCCCA GCCGGTGGCCGCCTG
AAV2/AAV9 Barcode F	AATGATACGGCGACCACCGAGATCTACACTCTTTCCCTACAC GAC
AAV2/AAV9 Barcode R	CAAGCAGAAGACGGCATAACGAGAT(7nt_index)GTGACTGGAG TTCAGACGTGTG
AAV Titration ITR F	GGAACCCCTAGTGATGGAGTT
AAV Titration ITR R	CGGCCTCAGTGAGCGA
AAV Titration CMV F	GGGACTTTCTACTTGGCA
AAV Titration CMV R	GGCGGAGTTGTTACGACAT
AAV Titration EGFP F	CTACGGCGTGCAAGTCTTCAG
AAV Titration EGFP R	CTTCAGCTCGATGCGGTTTAC
AAV2-QVLVYRE F	AGGCCAGGTTCTGGTTTACCGTGAAGCCCAGG
AAV2-QVLVYRE R	GGGCTTACGGTAAACCAGAACCTGGCCTCTC
AAV9-GGNYGLG F	AGGCGGGGTAATTATGGGTTGGGTGCCAGG
AAV9-GGNYGLG R	GGGCACCCAACCATAATTACCCCGCCTGCT

## 2.1.6 Plasmids

**Table 2.7 List of plasmids used**

<b>Name</b>	<b>Description</b>	<b>Source</b>
pXX2-187	AAV2 rep/AAV2 cap R588ins, Sfil sites, used for generation of single clone AAV2 R588 mutants	Michelfelder et al. <sup>170</sup>
pMT202-6	ITRs, AAV2 rep/AAV2 cap R588ins, Sfil sites, used for generation of random AAV2 display peptide libraries	Müller et al. <sup>112</sup>
pKV9K7-W503A	ITRs, AAV2 rep/AAV9 cap A589ins, Sfil sites, W503A mutant, used for generation of random AAV9 display peptide libraries	Gift from Jakob Körbelin
pXX2-9K7-W503A	AAV2 rep/AAV9 cap A589ins, Sfil sites, W503A mutant, used for generation of single clone AAV9 A589 mutants	Cloned during this study
pXX6	Adenoviral helper plasmid containing E1A, E1B, E2A, E4-orf6, VA, used for production of rAAV vectors	Xiao et al. <sup>73</sup>
AAV2/2	AAV2 rep/AAV2 cap	Addgene #104963
AAV2/3	AAV2 rep/AAV3 cap/adenovirus helper genes	Gift from Jakob Körbelin
AAV2/4	AAV2 rep/AAV4 cap/adenovirus helper genes	Gift from Jakob Körbelin
AAV2/5	AAV2 rep/AAV5 cap/adenovirus helper genes	Gift from Jakob Körbelin
AAV2/9	AAV2 rep/AAV9 cap	Addgene #112865
pscAAV-CMV-GFP	AAV expression cassette, self-complementary AAV vector bearing ITRs with CMV-eGFP with SV40	Addgene #32396
pAAV-CMV-GFP	AAV expression cassette, AAV vector bearing ITRs with CMV-eGFP-WPRE-SV40	Cloned during this study
pscAAV-CMV-Nluc	AAV expression cassette, self-complementary AAV vector bearing ITRs with CMV-Nluc with SV40	Cloned during this study
pscAAV-CMV-IdeS-Nluc	AAV expression cassette, self-complementary AAV vector bearing ITRs with CMV-IdeS-Nluc with SV40	Cloned during this study
pscAAV-CMV-Albsp-Flag-IdeS	AAV expression cassette, self-complementary AAV vector bearing ITRs with CMV-Albsp-Flag-IdeS-SV40; Albsp: Albumin signal peptide; IdeS gene: accession number JN035367.	Cloned during this study

## 2.2 Methods

### 2.2.1 Basic molecular biology methods

#### 2.2.1.1 Polymerase chain reaction (PCR)

The DNA fragments for subcloning were amplified by Phusion™ High-Fidelity DNA-Polymerase. Samples and reagents were prepared on ice. In one 50 µl reaction, 10 µl 5x Phusion HF or GC-Puffer, 0.4 µl dNTPs (25 mM), 0.5 µl Phusion® DNA polymerase, 1 µl forward primer (10 µM), 1 µl reverse primer (10 µM), 1.5 µl DMSO (optional), and 1 µl (1-10 ng) template DNA were mixed and filled up to 50 µl with PCR grade water. Then the PCR was run with initial denaturation for 30 s at 98°C, followed by 30-33 cycles of denaturation (98°C, 10 s), annealing (50-65°C, 30 s), and extension (72°C, 15 s per 1 kb). The final extension was performed for 5 min at 72°C, then hold at 4°C. The annealing temperature was depending on the primers.

A colony PCR was performed for rapidly screening bacteria colonies to verify that the desired genetic construct is present after a transformation step. A single clone was picked from the agar plate with a 10 µl pipet tip and stirred in 50 µl ddH<sub>2</sub>O in a PCR tube, then 25 µl DreamTaq Green PCR Master Mix (2x) was mixed with 1 µl forward primer (10 µM), 1 µl reverse primer (10 µM), 5 µl resuspended bacteria and filled up to 50 µl with ddH<sub>2</sub>O. After the initial denaturation step of 95°C for 3 min, followed by 35 cycles of denaturation (95°C, 30 s), annealing (50-60°C, 30 s), and extension (72°C, 30 s per 1 kb). The final extension was performed for 5 min at 72°C, then hold at 4°C. The annealing temperature was depending on the primers.

#### 2.2.1.2 PCR purification and gel extraction

For analytical purposes, the PCR products were loaded on a 1% (w/v) agarose gel with a 6x loading buffer and run with 100 V for 40 min. For the preparative purpose, DNA with a size between 70 bp to 10 kb from 2% (w/v) agarose gel was purified by using QIAquick Gel Extraction Kit according to the manufacturer's recommendation. DNA size was visualized or cut under UV light. Usually, PCR product with a size between 100 bp to 10 kb used for cloning insert was purified by using the QIAquick PCR Purification Kit. In the

case to purify the selected AAV library inserts, the QIAquick PCR purification kit was only used first four steps and the flow-through was kept.

#### 2.2.1.3 Restriction endonuclease and ligation

For restriction cloning purposes, 5 µg plasmid or the proper amount of PCR product was digested with 2 µl appropriate restriction enzyme, 5 µl of recommended 10x buffer, and filled up with 50 µl ddH<sub>2</sub>O. An analytical-scale restriction enzyme digestion to quickly check the identity of a plasmid was performed in a volume of 20 µl with 0.5-1 µg of substrate DNA and 1 µl enzyme. If two or more restriction enzymes were used, the amount of total enzyme did not exceed one-tenth of the total volume. Once all the ingredients were mixed, the reaction tube was incubated at the restriction enzyme's optimal temperature for 1 hour or an appropriate amount of time. Finally, agarose gel electrophoresis was performed to separate and visualize the digest fragments and purified them as the case may be for further experiments.

To construct a recombinant plasmid, if not stated otherwise, a ligation reaction mix was set up with 50 ng compatibly digested vector backbone, 1 µl T4 DNA ligase enzyme, 2 µl 10x NEB ligase buffer, an appropriate amount insert fragment, and filled up with ddH<sub>2</sub>O to a total volume of 20 µl. The molar ratio of vector to insert was applied from 1:3 to 1:30 on a case-by-case basis. Once all the components were mixed, the reaction tube was incubated at room temperature for 2 hours or overnight at 16°C. After ligation, the insert DNA was physically attached to the backbone and the complete plasmid was transformed into competent cells for propagation.

#### 2.2.1.4 Plasmid DNA purification

Highly purified and concentrated plasmid DNA was recovered from bacterial culture. Various volumes of bacterial culture were selected based on the plasmids required for the experiment. For small-scale use, plasmids were purified from 3 ml culture by using the Zyppe™ Plasmid Miniprep Kit following the manufacturer's instructions. Larger plasmid DNA amounts from 50 ml culture or 200 ml culture were purified using the QIAGEN Plasmid Midi Kit or QIAGEN Plasmid Maxi Kit according to the manufacturer's instructions.

### 2.2.1.5 DNA quantification

The purity and concentration of the DNA were determined by 260/280 nm absorbance measurement using the Denovix DS-11 spectrophotometer. The ratio of absorbance at 260/280 nm for DNA >1.8, indicates DNA is highly pure.

## 2.2.2 Prokaryotic method

### 2.2.2.1 Preparation of competent E. coli bacteria

To prepare the chemically competent bacteria, the DH5 $\alpha$  from frozen glycerol stock was streaked out onto an LB agar plate without antibiotics and the plate was grown overnight at 37°C. The day after, the single colony was picked and incubated with 4 ml fresh LB medium in a shaker overnight at 37°C. The next day, 400 ml pre-warmed LB medium was inoculated with 4 ml of the overnight bacteria and incubated at 37°C until OD<sub>600</sub> reached 0.35-0.40. Bacteria were put on ice immediately and chilled the culture for 30 min. The bacteria, and any materials that they come in contact with, must be pre-chilled to 4°C for the rest of the procedure. The chilled bacteria were harvested by centrifugation at 3,000 x g for 15 min at 4°C and resuspended in 30 ml 0.1 M CaCl<sub>2</sub>. After 20 min incubation on ice, the bacteria were harvested again by centrifugation at 2,000 x g for 15 min at 4°C. The cells were gently suspended in 5 ml 85% v/v 0.1 M CaCl<sub>2</sub> and 15% v/v glycerol solution and distributed 50  $\mu$ l bacteria to each 1.5 ml tube. Snap frozen in liquid nitrogen and stored at -80°C.

To construct the AAV peptide library, high-efficiency electrocompetent cells were prepared. A single colony was picked from the LB agar plate without antibiotics and inoculated with a 12 mL starter culture of LB medium. The culture was grown at 37°C in a shaker overnight. The day after, a 12 mL starter culture was inoculated in 1.2 L of LB medium and distributed in six 1L Erlenmeyer flasks. The medium was incubated at a 37°C shaker until the OD<sub>600</sub> reached 0.5. Bacteria were transferred to ice-cold 250 ml centrifugation bottles immediately and chilled on ice for 30 min. The bacteria were pellet at 1,000 x g for 20 min at 4°C and resuspended by pipetting up and down gently in 150 ml ice-cold sterilized ddH<sub>2</sub>O. Again, the bacteria were pellet at 1,000 x g for 20 min at 4°C and they were gently resuspended in 50 ml ice-cold sterilized ddH<sub>2</sub>O by pipetting them

up and down. Bacteria suspensions were combined into three centrifuge bottles and centrifuged at 1,000 x g for 20 min at 4°C. The supernatant was promptly discarded and the bacteria were resuspended in 20 ml ice-cold 10% (v/v) glycerol of each bottle. Bacteria suspensions were combined into two 50 ml ice-cold falcons (30 ml each falcon) and harvested at 1,000 x g for 20 min at 4°C. Each pellet was resuspended in a final volume of 2 mL ice-cold 10% (v/v) glycerol by gently swirling, and then the proper volume of bacteria was distributed to 1.5 ml tubes. Immediately put the aliquots into liquid nitrogen and stored them at -80°C. The tested efficiency of electrocompetent cells reached  $5 \times 10^8$  cfu/ $\mu$ g and was used for AAV library production.

#### 2.2.2.2 Transformation

For standard cloning purposes, the chemically competent cells were taken out of -80°C and thawed on ice (approximately 20-30 mins). The agar plate with the appropriate antibiotic was warmed up to room temperature before use. Subsequently, 50  $\mu$ l competent cells were mixed with 1-5  $\mu$ l DNA incubated on ice for 20 min followed by a heat shock at 42°C water bath for 45 s and immediately put back on the ice for 2 min afterward. Then, 450  $\mu$ l SOC medium was added to the tube and incubated at 1000 rpm for 30 min at 37°C in a Thermal Mixer. After reconstitution, 50  $\mu$ l bacteria were spread on an LB agar plate and incubated at 37°C overnight.

For the AAV library DNA transformation, each electroporation with 35  $\mu$ l of electrocompetent cells was thawed on ice and mixed with 1-2  $\mu$ l of the ligation reaction. The mixture was carefully transferred to an ice-cold 0.1 cm gap electroporation cuvette and tapped gently to remove air bubbles. The cuvette was put into the chamber slide and seated between the contacts in the base of the chamber. The program “Ec1” of the MicroPulser™ system was used for electroporation. After running the program, the cells in the cuvette were immediately suspended with 2 ml SOC medium and transferred to tubes followed by incubation at 200 rpm for 1h at 37°C. After reconstitution, the bacteria were plated on the selective medium or agar plate.

### 2.2.2.3 Bacterial enrichment culture

A single colony from agar plates for plasmid mini-preps usually started 3 ml LB-medium in a 15 ml falcon, while the plasmid large preps were carried out with 200 ml LB-medium in a 1L Erlenmeyer flask. Bacteria from mini-preps or glycerol stocks were added to large preps at the ratio of 1/500-1/1000. All the medium contained the appropriate antibiotic to the concentration and incubated overnight at 200 rpm and 37°C. In case the bacteria contain ITR-AAV plasmids were grown at 30°C and 175 rpm.

## 2.2.3 Large-scale recombinant AAV production

### 2.2.3.1 Cell culture and triple transfection of HEK293T/17 cells

HEK293T/17 cells were cultured in DMEM medium supplemented with 10% (v/v) FBS and 1% (v/v) P/S and incubated in a cell culture incubator at 37°C with 5% CO<sub>2</sub>. The cells were split at 1/5 to 1/10 when they reached 70% confluence. 24 h before transfection,  $1.1 \times 10^7$  HEK293T/17 cells were seeded per 145 mm dish and let grow until 80-90% confluence the next day. At the time of transfection, the fresh PEI + DPBS master mix and the DNA + DPBS solution (Table 2.8) were prepared in 15 ml falcon for each viral prep. Subsequently, the PEI + DPBS master mix was added to the DNA + DPBS solution and gently vortexed to mix. After 10 min incubation at room temperature, the required volume transfection mixture was dropped to each plate and swirled to mix before returning the plates to the cell culture incubator. Here, a total of 32 µg DNA was transfected for one plate and the plasmids (pXX6, pAAV ITR-transgene, pAAV Rep/Cap) were used in a ratio of 2:1:1 based on micrograms of DNA. 18 h after transfection, the medium was changed and cells were incubated for another 2 days.

**Table 2.8 Transfection mix for one 145-mm dish**

	<b>DPBS</b>	<b>PEI 1mg/ml</b>	<b>pXX6</b>	<b>transgene</b>	<b>pAAV Rep/Cap</b>
PEI+DPBS mix	1000 µl	140 µl	-	-	-
DNA+DPBS mix	500 µl	-	16 µg	8 µg	8 µg

### 2.2.3.2 AAV harvest and PEG 8000 precipitate

The cells were scraped off the plates at 72 h post-transfection, and the suspension was transferred to appropriate bottles for centrifugation at 1,000 x g for 5 min. The supernatant was removed and precipitated by adding 10 g PEG 8000 and 5.8 g NaCl per 100 ml volume. The PEG-media mixture was shaken until PEG 8000 and NaCl were completely dissolved and stored at 4°C for 18-72 h. The cell pellet was resuspended in 0.8 ml 1 x PBS-MK per plate and performed two freeze/thaw cycles to release viral particles between a dry ice-ethanol bath and a 37°C water bath. The cell suspension was then stored at -80°C after being frozen a third time. The next working day, the PEG-media mixture was centrifuged at 5,000 x g for 30 min at 4°C and the supernatant was poured out. Additional 2 min centrifugation was performed to completely remove the remaining supernatant from the pellet. The cell suspension was taken from -80°C and thawed in a 37°C water bath, and followed combined with the pellet of PEG-media mixture together resulting in approximately 5 ml total volume (no more than five 145 mm-plates). Subsequently, the combined cell suspension was digestion with Benzonase® Nuclease (50 U/ml) in a 37°C water bath for 30 min with inversion of the tube every 10 min. The cell debris was removed by centrifugation at 3,000 x g for 15 min at 4°C and the clarified viral suspension was kept at 4°C for the density centrifugation steps.

### 2.2.3.3 Iodixanol-based density gradients AAV purification

For the AAV purification, the 13.5 ml Quick-Seal™ Ultra-Clear™ Beckman Coulter Tubes and the Type 70.1 Ti rotor were used. One iodixanol density gradient is sufficient to purify the virus from up to five 145-mm dishes. The solutions were loaded into Quick-Seal tubes by using a 5 ml syringe and a Laboratory Pipetting Needles with the order of 3 mL clear 15% iodixanol, 2 ml red 25% iodixanol, followed by 1.6 ml clear 40% iodixanol, and continued with 1.6 ml red 54% iodixanol (Layers of increasing density added under the previous layer). The rest space above the 15% iodixanol layer of the gradient was loaded with approximately 5.3 ml of clarified viral suspension by using a 17 G needle and air bubbles were avoided. Once all the gradients were finished, the Quick-Seal tubes were sealed and balanced the error below 0.01 g with the help of different caps. The gradients were centrifuged at 58,000 rpm for 70 min at 18°C in an Optima™ LE-80K ultracentrifuge.

After centrifugation, the gradients were fixed and a 23 G needle was inserted at the top. Then, the virus was collected from the 40%/54% interface and 40% layer by puncturing the tube with another 23 G needle attached to a 2 ml syringe. The virus was stored at 4°C for buffer exchange (optional) or aliquoted as required and stored at -80°C.

#### 2.2.3.4 AAV iodixanol buffer exchange

For cell infection and high titer of AAV used, the iodixanol buffer exchange and concentration are necessary. The iodixanol solution with the virus was diluted 1:10 in DPBS and passed through the 0.22 µm syringe filter to an Amicon filter device. The virus/DPBS mixture was centrifuged at 3,000 x g at room temperature until 1-1.5 ml solution remained. The flow-through was discarded and a new diluted vector iodixanol solution was loaded to the same Amicon filter device (No more than 3.5 ml virus-contained initial iodixanol solution per Amicon filter device). Again, the virus/DPBS mixture was centrifuged at 3,000 x g at room temperature until 1-1.5 ml solution remained. Finally, the virus was washed with 10 ml DPBS two more times and remained 300-500 µl of solution in the top chamber in the last spin. Store at 4°C until titration by qPCR on the next day.

#### 2.2.3.5 AAV titration by qPCR

The genome copy numbers of the purified AAV were quantified by quantitative real-time PCR (qPCR). AAV samples were first treated with DNase I to eliminate DNA that was not packaged into the viral capsid. Therefore, the volume containing 5 µl samples, 39 µl ddH<sub>2</sub>O, 5 µl 10x DNase buffer, and 1 µl DNase I was gently mixed and incubated at 37°C for 30 minutes. To inactivate the DNase, 5 µl of EDTA were added to the tube and incubated in a 70°C metal bath for 10 min. The qPCR was measured in duplicate and the master mix for one reaction contained 10 µl 2x SYBR Green Master Mix, 1 µl forward primer (10 µM), 1 µl reverse primer (10 µM), 3 µl ddH<sub>2</sub>O, and 5 µl diluted samples or plasmid for the standard curve. Samples were usually diluted in 1:1,000 and 1: 5,000 for purified AAV. Once sample loading was complete, the plate was centrifuged at 2000 rpm for 2 min and then the PCR was run in QuantStudio 3 Real-Time PCR System with initial denaturation of 2 min at 95°C, followed by 40 cycles of denaturation at 95°C for 15 s, and combined annealing/ elongation for 30 s at 60°C. When the qPCR run was complete, the titer of the sample was calculated based on the Ct value of the standard curve which was

set up by dilution of an initial plasmid stock of  $2 \times 10^9$  molecules/ $\mu\text{l}$  to a range of  $2 \times 10^8$  to  $2 \times 10^3$  plasmid copies per reaction.

#### 2.2.3.6 Ligation of synthetic oligonucleotide inserts to ITR-less AAV rep/cap plasmid

To produce rAAV vectors with pre-selected peptide variants, the synthetic oligonucleotides encoding the seven amino acids of pre-selected variants at the position R588 of VP1 in AAV2 and A589 of VP1 in AAV9 were transferred into an ITR-less AAV rep/cap vector with cap insertion site. The oligonucleotides were showed below:

AAV2 library oligonucleotides	Forward primer: 5'-AGG C (X) <sub>21</sub> GCC CAG G-3'
	Reverse primer: 5'-GGG C (Z) <sub>21</sub> GCC TCT C-3'
AAV9 library oligonucleotides	Forward primer: 5'-AGG C (X) <sub>21</sub> GCC CAG G-3'
	Reverse primer: 5'-GGG C (Z) <sub>21</sub> GCC TGC T-3'

*(X)<sub>21</sub> = specific nucleotide sequence of peptide chosen for analyses; (Z)<sub>21</sub> = Reverse complement sequence of (X)<sub>21</sub>*

Each pair of oligonucleotides for peptide variants were set up in a 20  $\mu\text{l}$  phosphorylation/annealing reaction. One reaction contained 1  $\mu\text{l}$  forward primer (20  $\mu\text{M}$ ), 1  $\mu\text{l}$  reverse primer (20  $\mu\text{M}$ ), 1  $\mu\text{l}$  10x T4 Ligase Buffer (NEB), 6.5  $\mu\text{l}$  ddH<sub>2</sub>O and 0.5  $\mu\text{l}$  T4 Polynucleotide Kinase (NEB). The tube was incubated at 37°C for 30 min, 95°C for 5 min, and ramped down to 25°C at 5°C/min. Then, the phosphorylation/annealing reaction was diluted at 1:5 by adding 40  $\mu\text{l}$  ddH<sub>2</sub>O and mixed well for further ligation into the corresponding Sfil-digested ITR-less backbone plasmid (pXX2-187 or pXX2-9K7-W503A). For the ligation reactions, 1  $\mu\text{l}$  diluted phosphorylated oligonucleotides template was mixed with 1  $\mu\text{l}$  10x T4 Ligase Buffer (NEB), 1  $\mu\text{l}$  T4 DNA Ligase (40U/ $\mu\text{l}$ , NEB), 1  $\mu\text{l}$  ITR-less backbone plasmid (50 ng), and 6  $\mu\text{l}$  ddH<sub>2</sub>O and incubated at 16°C for 1-2 h. DH5 $\alpha$  E. coli cells were transformed by heat shock, the next day single colonies were picked and plasmids miniprep was performed for Sanger sequencing.

## 2.2.4 In vivo selection of random AAV display peptide libraries

The methods for in vivo selection of random AAV display peptide libraries described here were adapted from a previous protocol<sup>171</sup>.

### 2.2.4.1 Intravenous injection of peptide library and tissue harvest

C57BL/6J mice were injected with 1E+11 vg/mouse (n=3) random AAV display peptide libraries via the tail vein. Three or six days after injection, mice were sacrificed. The kidney as well as off-target organs (liver, lung, heart, pancreas, brain, spleen, skeletal muscle) were harvested for total DNA extraction.

### 2.2.4.2 Tissue homogenization and total DNA extraction

To extract total DNA, target and off-target tissues were diced on ice and dispensed into Precellys Lysing Kit (CK28) tubes filled with 180 µl of ATL buffer and 20 µl of proteinase K per 25 mg of tissue. Tissues were homogenized by Minilys at 5,000 rpm for 40 s and then purified using the DNeasy Blood & Tissue Kit according to the manufacturer's instructions. After elution, total DNA from the same organ was pooled in one tube for PCR amplification of AAV library inserts.

### 2.2.4.3 PCR amplification of the library inserts

The internalized peptide library in the cap gene region of the random AAV display peptide library was rescued from the total DNA of target tissues. To retain library diversity, the large-scale PCR of 20 reactions was performed for each round selection. Therefore, 500 ng total DNA served as a template for one reaction that mixed with 10 µl 5x Phusion HF buffer, 0.4 µl dNTPs (25 mM), 0.5 µl Phusion® DNA polymerase, 2.5 µl first forward primer (10 µM), 2.5 µl first reverse primer (10 µM) (Table 2.6), and filled up with water to 50 µl. To compare with the correct bands, the template controls of the plasmid library, insert-less plasmid library backbone, and ddH<sub>2</sub>O were used in the same batch PCR. Then the PCR was run with initial denaturation for 30 s at 98°C, followed by 30 cycles of denaturation (98°C, 10 s), annealing (65°C, 30 s), and extension (72°C, 10 s). The final extension was performed for 5 min at 72°C, then hold at 4°C. If an obvious band was yielded, the PCR products were used for further purification, otherwise nested PCR was performed under the same conditions using the second forward and reverse primers

(Table 2.6) and 2 µl of the product of the first PCR as a template. The samples were then purified (2.2.1.2) for restriction digestion.

#### 2.2.4.4 Digestion of library inserts and backbone plasmid

The purified library inserts (10-30 µg) were digested by BglI (2.2.1.3) at 37°C for 4 h and then purified with the QIAquick PCR Purification Kit (2.2.1.2) only with the first four steps. The flow-through contained the smaller library inserts that were precipitated by adding 1 vol DNA solution, 2 vol absolute ethanol, 1/10 vol 3 M sodium acetate, and 1 µl glycogen. The mix was incubated at -20°C for 2 h and centrifuged at 17,000 x g for 30 min. The DNA pellet was washed with 70 % ice-cold ethanol and dissolved in 30 µl ddH<sub>2</sub>O. The library backbone plasmid (5 µg) was digested by SfiI at 50°C overnight and then purified with the QIAquick PCR Purification Kit (2.2.1.2).

#### 2.2.4.5 Ligation of plasmid and insert and large-scale electroporation

A ligation mixture in a total volume of 25 µl was prepared with 2.5 µl 10x NEB ligase buffer, 2.5 µl T4 DNA ligase, 500 ng plasmid backbone (pMT202-6, pKV9K7-W503A), and 56 ng library inserts at a molar ratio of 1:30 and then incubated overnight at 16°C. To remove the buffer, the ligation product was precipitated by ethanol (2.2.4.4) as described and the pellet was dissolved in 25 µl ddH<sub>2</sub>O. 875 µl electrocompetent bacteria and 25 µl ligation product were premixed and distributed to 25 ice-cold cuvettes for electroporation (2.2.2.2). After reconstitution, 100 µl bacteria were spread on LB-AMP plates with the dilution of 1:10 and 1:100. The rest bacteria were cultured (2.2.2.3) in 1,200 ml LB-AMP medium in six 1L Erlenmeyer flasks overnight until the OD<sub>600</sub> reached to 2. The next day, the plasmid library was purified from the overnight bacteria culture using the QIAGEN Plasmid Maxi Kit (2.2.1.4). The number of colonies was counted on the plates to calculate the diversity of the plasmid library. The first round of pre-selected libraries usually yielded efficiencies more than  $1 \times 10^7$  and the subsequent selected round's efficiencies were in the range of  $1 \times 10^6$  to  $5 \times 10^6$ .

#### 2.2.4.6 Production of secondary AAV libraries

Secondary AAV display peptide libraries were produced by transfection of  $1 \times 10^8$  HEK293T/17 cells in ten 145-mm cell culture dishes. A one-step procedure that allows

the production of highly diverse AAV libraries to keep the maximal capsid-genome correlation of AAV particles was adopted. For each plate, 5 µg library plasmid (equal to 5,000 plasmids per cell) and 55 µg pXX6 plasmid were co-transfected with PolyFect Transfection Reagent. After three days, the AAV library was harvested (2.2.3.2) and purified by iodixanol density-gradient ultracentrifugation (2.2.3.3). The titer of the virus was determined by qPCR (2.2.3.5) using the ITR primers.

#### 2.2.4.7 Enrichment of library variants in subsequent rounds of selection

Secondary libraries were intravenously injected into C57BL/6J mice (n = 2) at a dose of  $1 \times 10^{11}$  vg/mouse. Four rounds of selection were performed in vivo. In the first two rounds of screening, the viral DNA corresponding to the insert-containing region was rescued from the whole kidney DNA. To provide selective pressure for capsids, in the third and fourth rounds, the virus circulation was extended to six days to better eliminate unspecific particles and the viral DNA was rescued from the isolated glomerulus (2.2.4.8). After each round of PCR amplification, 50 µl of library PCR products were kept for next-generation sequencing. And after each round of large-scale electroporation, 20 single clones were amplified (2.2.2.1) and sequenced to estimate the distribution of the library so that the screening process could be discontinued at the appropriate time point.

#### 2.2.4.8 Glomerulus isolation

The mice were euthanized and the aorta was opened along its longitudinal axis to expose the orifices of the renal arteries. Each kidney was perfused with 2 ml warm Dynabeads (37.5 µl of Dynabeads® M-450 Tosylactivated and 37.5 µl Dynabeads® M-450 Epoxy were mixed in 4.5ml 1x HBSS for one mouse) via the renal arteries. After perfusion, the renal papilla and capsule were removed. The mouse kidney was minced into small pieces on ice. Tissues were transferred to C-tube filled with 5.5 ml collagenase V solution (1 mg/ml collagenase from *Clostridium histolyticum* and 0.25 % BSA in DMEM/F-12 medium). The tissue was digested for 10 min at 37°C and homogenized every 5 min using a gentleMACS™ dissociator. Homogenized tissues were passed through the 300 µm cell strainer followed by a 100 µm cell strainer washed with ice-cold 1x HBSS. Tissue suspension was centrifuged at 300 x g for 4 min at 4°C, and the supernatant was discarded. The pellet was resuspended in 7.5 ml cold HBSS and distributed into 2 ml

tubes, washed over three times on the magnet. All glomerulus was pooled into a 2 ml tube for total DNA extraction.

### **2.2.5 Next-generation sequencing**

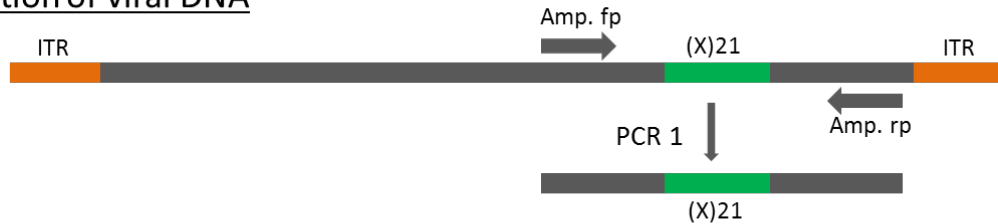
After in vivo screening, each round of target tissues and the final round of off-target tissues (liver, lung, heart, pancreas, brain, spleen, and skeletal muscle) were prepared for next-generation sequencing. At this point, three rounds of PCR were performed to generate a library. In the first PCR, enriched viral DNA was amplified from target and off-target organs. The linker sequences bound to viral DNA fragments were performed in subsequent second PCR. And in the third PCR, individual Illumina barcode adapters were ligated to the linker sequences allowing for multiple samples to be mixed and sequenced at the same time. During the whole process of library preparation, the appropriate measures were taken to minimize possible contamination. The PCR schematic is shown below.

#### **2.2.5.1 NGS samples preparation**

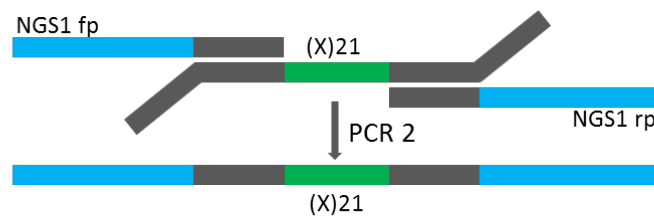
Total DNA isolation from target and off-target tissues and the AAV library DNA amplification were described in Chapters 2.2.4.2 and 2.2.4.3. For the library DNA amplification, 10 instead of 20 reactions were conducted in the off-target organs. The AAV library DNA was then purified (2.2.1.2) from a 2% agarose gel and served as a template for the linker primers binding in the second PCR. Therefore, PCR reactions (2.2.4.3) containing 10 ng purified AAV library DNA mixed with the suitable NGS linker primers (Table 2.6) were performed. To verify the PCR products were the right size possessed, the template controls of the plasmid library, insert-less plasmid library backbone, and ddH<sub>2</sub>O were used in the same batch PCR. A two-step PCR program for the linker attached was run with initial denaturation for 30 s at 98°C, followed by 30 cycles of denaturation (98°C, 10 s), annealing, and extension (72°C, 30 s). The final extension was performed for 5 min at 72°C, then hold at 4°C. Before the last PCR, in which the Illumina barcode adapter sequences were added, the products from the second PCR were examined by agarose gel electrophoresis and purified with QIAquick PCR Purification Kit (2.2.1.2). In the third PCR, a universal Illumina forward primer (Table 2.6) and individual barcode

adapter (Table 2.6) for each sample were ligated to 10 ng linker-bound DNA from the second PCR corresponding to the same conditions. Also, the template controls were set up in the third PCR with a 1 µl reaction mix from all controls of the second PCR. Finally, the DNA was examined by 2% agarose gel electrophoresis and then purified by gel extraction (2.2.1.2).

❖ Amplification of viral DNA



❖ Attach linker sequence



❖ Attach barcode adapters



2.2.5.2 Quality control and sequencing

The samples from different tissues and labeled by individual Illumina barcodes were pooled in a 150 µl mixture with 2 nmol/L per sample. Subsequently, the size and quality of DNA were assessed by Agilent 2100 Bioanalyzer system according to the manufacturer's recommendation. NGS and de-multiplexing were performed on an Illumina MiSeq sequencer (600-cycle, single-indexed, paired-end run) with MiSeq Reagent Kit v3. Approximately 100,000 reads per sample were yielded. The detailed processing and normalization for NGS were helped by Dr. Nuray Akyüz (UKE).

### 2.2.5.3 Bioinformatics evaluation of the NGS data

Bioinformatics evaluation of NGS raw data was analyzed by Dr. Malik Alawi (UKE). Known, invariable flanking sequences of length 10 bp (CCAGAGAGGC and GCCCAGGCGG for AAV2, CCAAGCAGGC and GCCCAGGCGG for AAV9) were used to extract only insert sequences of target length (21 bp) from the sequence reads. Reads not matching these flanking sequences exactly and reads with diverging insert sizes were removed from the analysis. Nucleotide insert sequences for which there was at least 100-fold more frequent insert sequence within an edit distance of 1 were considered possible artifacts and removed. Moreover, insert sequences with codons not matching the expected coding pattern (NNK or 2t7) were removed and the remaining sequences were translated into peptides.

### 2.2.5.4 Evaluation of variants based on rating scores

The AAV library enriched NGS data were evaluated by rating scores as described by Körbelin et al.<sup>121</sup>. In brief, to identify the most specific enriched AAV capsid candidates, three rating scores were established. The enrichment score ‘E’ was used to evaluate transduction efficacy in the target of each candidate reflecting changes in relative abundance from before-last to last selection. The general tissue specificity score ‘GS’ was used to assess the tropism of each candidate among target organs and other off-target organs (liver, lung, heart, pancreas, brain, spleen, and skeletal muscle) by multiplying the individual specificity scores (i.e.,  $S_{liver}$ ). To determine the most promising candidate regarding specificity and efficacy, a combined score “C”, was determined by multiplying E and GS. To calculate enrichment and specificity scores, the following formula was used.

$$E \text{ or } S_{\text{off-target}} = 1 - \frac{1}{1 + \frac{R_z}{R_y}}$$

*E score: Relative abundances third round ( $R_y$ ) and fourth round ( $R_z$ ) in target tissues*

*$S_{\text{off-target}}$  score: Relative abundances of fourth round off-target ( $R_y$ ) and the same round target ( $R_z$ )*

With the help of this formula, the ratios of the frequencies were calculated and converted into a value between 0 and 1. A value close to 1 means a strong enrichment or a high specificity. The enriched variants in the final round were sorted by the “C” score to determine the most promising variants for further validation.

## 2.2.6 Evaluation of selected capsid variants

### 2.2.6.1 Animals and vector administration

All animal procedures were performed in compliance with the National Institutes of Health Guide for the Care and Use of Laboratory Animals as well as the German law for the welfare of animals. Animal experiments were approved by the veterinary administration of the City of Hamburg under the license N054-2018 or N21-089. BTBR ob/+ (BTBR.Cg-Lep<sup>ob/wt<sup>WiscJ</sup></sup>) was purchased from JAX (Jax No. 004824, Bar Harbor, Maine, USA) to generate BTBR ob/ob mice. Neph1 floxed mice were crossed with Tg (Nphs1-rtTA\*3G)<sup>8Jhm</sup> (kind gift from Jeff Miner, Washington University, St. Louis, USA) and Tg(tetO-cre)<sup>1Jaw</sup> to yield Nphs1<sup>ΔiPod<sup>172</sup></sup>. Doxycyclin (2mg/ml in 5% sugar solution, Fagron, Barsbüttel, Germany) was administered for 7 days in the drinking water at an age of 5 weeks. Animals had free access to food and water and were kept on a 12-light/dark cycle. Purified AAV library particles and recombinant AAV vectors were injected into the tail vein of 8-12 weeks-old mice (strain C57BL/6J, BALB/c) or 6-8 weeks-old Sprague Dawley (SD) rats. The doses of AAV vectors administered intravenously were summarized in Table 2.9.

### 2.2.6.2 Blood and urine collection

Mice were anesthetized with isoflurane and blood was collected into a tube by a retro-orbital bleeding method. The blood was centrifuged at 1,500 x g for 10 min and the serum was collected and stored at -20°C. To collect the mouse urine, mice were held over a 96-well plate and manually applied pressure to the trans-abdominal area to force the urine out of the bladder. Then the urine was collected and centrifuged at 2,000 x g for 10 min. The supernatant was transferred to the new tube and stored at -20°C.

**Table 2.9 The doses of AAV vectors administered intravenously were summarized.**

<b>Vectors</b>	<b>Species</b>	<b>Dose vg per animal</b>
AAV9-JGA expressing GFP	C57BL/6J	1E+11
AAV9-WT expressing GFP	C57BL/6J	1E+11
AAV9-JGA expressing GFP	SD rat	1E+12
AAV9-JGA expressing GFP	C57BL/6J	2E+11
AAV1-WT expressing GFP	C57BL/6J	5E+11
AAV2-WT expressing GFP	C57BL/6J	1E+11
AAV3-WT expressing GFP	C57BL/6J	8E+10
AAV4-WT expressing GFP	C57BL/6J	3E+11
AAV5-WT expressing GFP	C57BL/6J	5E+11
AAV6-WT expressing GFP	C57BL/6J	3E+12
AAV7-WT expressing GFP	C57BL/6J	5E+11
AAV8-WT expressing GFP	C57BL/6J	1E+11
AAV9-WT expressing GFP	C57BL/6J	1E+11
AAVrh.10-WT expressing GFP	C57BL/6J	1E+11
AAV2-GEC expressing GFP	C57BL/6J	1E+11
AAV2-WT expressing GFP	C57BL/6J	1E+11
AAV2-GEC expressing GFP	BTBR ob/ob	2E+11
AAV2-GEC expressing GFP	Nphs1 <sup>ΔiPod</sup>	1E+11
AAV2-GEC expressing GFP	Balb/c	1E+11
AAV2-GEC expressing GFP	SD rat	1.5E+12
AAV2-GEC expressing IdeS	C57BL/6J	2E+11
AAV2-GEC expressing GFP	C57BL/6J	2E+11
AAV2-GEC expressing IdeS-Nluc	C57BL/6J	1E+11
AAV2-GEC expressing Nluc	C57BL/6J	1E+11

### 2.2.6.3 Tissue preparation

Mice were anesthetized with ketamine/xylazine and perfused via the left ventricle with 5 ml DPBS followed by 5 ml 4% PFA. Tissues were harvested and sliced into 2 mm pieces,

subsequently fixed in 4% PFA at 4°C overnight. The next day, for paraffin-embedded tissue, the fixed sample was washed with PBS three times and the automated tissue processor was used for tissue preparation and embedding with the help of our technician Melanie Schaper. For the frozen OCT-embedded tissues, the fixed sample was dehydrated in 15% sucrose in PBS at 4°C for 6 h and then 30% sucrose in PBS overnight until the tissue sank. The sample was put into cryomolds with OCT covered and frozen on the metal block with dry ice and subsequently stored at -80°C. For transmission electron microscopy samples, the PFA-perfused tissues were sliced into 1 mm and fixed in 4% PFA at 4°C overnight. The next day, the sample was handed over to the EM facility (UKE) for further processing.

#### 2.2.6.4 Immunofluorescence staining

OCT-embedded frozen tissues were sectioned into 7 µm and dried at room temperature for 30 min. The slides were washed with 1x PBS three times for 3 min and the tissues were circled with a barrier pen. After permeabilization with 0.1% Triton X-100, the nonspecific binding sites were blocked with 5% BSA in PBST supplemented with 0.3M Glycine. Then sections were incubated overnight at 4°C with the following primary antibodies: chicken anti-GFP (1:500), rabbit anti-SLC12A1 (1:200), mouse anti-NOS1 (1:200), rabbit anti-CLDN10 (1:200), rabbit anti-CLDN16 (1:100), rabbit anti-renin (1:200), rat anti-CD31 (1:200), guinea pig anti-Synaptopodin (1:200), rabbit anti-PDGFR (1:200), Alexa Fluor<sup>®</sup> 555 donkey anti-sheep IgG (1:1000), Alexa Fluor<sup>®</sup> 555 donkey anti-mouse IgG (1:1000), Cy3<sup>™</sup> mouse anti-αSMA (1:500), mouse anti-RECA-1 (1:200), rabbit anti-C1q (1:200), rat anti-C3 (1:200). The next day, sections were washed with 1x PBS and incubated at room temperature for 1 hour with Alexa Fluor 488-, 555-, 594-, or 647-labeled secondary antibodies. DAPI was used for staining nuclei. For CLDN16 antibody staining, fixation was prolonged in methanol/acetone (1:1) at -20°C. Samples were antigen retrieved with boiled Target Retrieval Solution, Citrate pH6 for 30 mins. Permeabilization, blocking, and antibody incubation were performed as described above. Sections were analyzed at 20x, 40x, or 63x magnification under Carl Zeiss ApoTome or Leica TCS SP5 microscope.

Paraffin-embedded tissues were sectioned into 2  $\mu\text{m}$  and dried at 40°C overnight. The next day, the tissues were deparaffinized and rehydrated by immersing sections in xylene for 3 x 5 min followed by 100% ethanol for 3 x 5 min, 70% ethanol for 2 x 5 min, 50% ethanol for 5 min, and 1x PBS for 5 min. The antigen retrieval was performed with Citrate Buffer pH 6.0 for 30 min at 100°C. The slides were cooled down to room temperature and washed with 1x PBS. And then the blocking and antibody incubation were performed as described in frozen tissue staining. Sections were analyzed at 20x magnification under a Carl Zeiss ApoTome microscope.

#### 2.2.6.5 Immunohistochemistry and hematoxylin and eosin staining

Paraffin-embedded tissues for Immunohistochemistry (IHC) and hematoxylin and eosin (HE) staining were sectioned, deparaffinized, and rehydrated as previously described in section 2.2.6.4. For the IHC staining, the antigen retrieval was performed with TRIS/EDTA Buffer pH9 for 30 min at 100°C. After washing with PBS, the tissue was stained with rabbit anti-GFP antibody, 1:200 according to the ZytoChem Plus AP Polymer Kit manufacturers' protocols. The HE staining was kindly performed by our technician Melanie Schaper followed by the standard protocol. Images were taken at 20x and 40x magnification under a Carl Zeiss Axio Scope A1 microscope.

#### 2.2.6.6 Immunogold labeling and electron microscope

For pre-embedding immunogold labeling, vibratome sections (50  $\mu\text{m}$  thickness) of the kidney (immersed fixed in 4% PFA) were incubated at 4°C overnight with the primary antibody anti-AAV9-capsid (1:100), then washed and incubated with the nano-gold coupled secondary antibody (1:100) at 4°C overnight. Finally, nano-gold particles were silver-enhanced in the dark on ice for 2 minutes. Sections were contrasted using 1% OsO<sub>4</sub> at RT for 1 hour and 1% uranyl acetate in 70% ethanol at RT for 30 min. After dehydration, sections were embedded in epoxy resin, and ultrathin sections of 50 nm thickness were cut using a Leica EM UC6 ultramicrotome. Sections were imaged using a Zeiss Leo 910 Transmission Electron Microscope and analyzed using ITEM software.

#### 2.2.6.7 Vector genome distribution quantification

Fourteen days after AAV injection, biodistribution of the AAV vectors containing the GFP gene was studied by quantifying GFP transgene copy numbers in the isolated glomerulus (2.2.4.8) and other relevant organs. After DNA extraction (2.2.4.2), 100 ng genomic DNA from each sample was analyzed by qPCR (2.2.3.5) with the GFP-specific primer (Table 2.6). The number of vector genomes was quantified and normalized to vector copy numbers per diploid genome (vg/dg). The corresponding plasmid (pscAAV-CMV-GFP) was serially diluted and used as a standard curve (2.2.3.5).

#### 2.2.6.8 Measurements of kidney and liver functions

Enzyme-linked immunosorbent assay (ELISA) is a method for the quantification of biomolecules such as peptides, proteins, and antibodies. Here, the ELISA was used for albumin detection from mouse urine. The high affinity, protein-binding 96-well ELISA plate was coated with goat anti-mouse albumin capture antibody in a final concentration of 10 µg/ml in 0.05M carbonate-bicarbonate buffer (pH 9.6). The plate was covered with adhesive plastic and incubated overnight at 4°C. The next day, the coated plate and buffer were warmed to room temperature before use. The coating solution was flicked off and the plate was rinsed with washing buffer (50mM TBS, 0.05% Tween 20 pH 8.0) three times. Non-specific binding sites were blocked by adding 150 µl post coat solution (50mM TBS, 1%BSA pH 8.0) to each well and the plate was sealed and incubated at room temperature for 1 hour. Meanwhile, the sample (1:100, 1:1000) and albumin standard dilutions were prepared duplicates in sample diluent buffer (50mM TBS, 1% BSA pH 8.0, 0.05% Tween20). After blocking and washing, 100 µl of each standard and sample was added into appropriate wells and incubated at room temperature for 1 h with gentle shaking. Then, the plate was rinsed with washing buffer five times and 100 µl of HRP conjugated goat anti-mouse albumin detection antibody was added at a dilution of 1:40,000. The plate was incubated for 1h at room temperature with gentle shaking. After incubation, the plate was rinsed with washing buffer five times, and 100 µl TMB substrate was added into each well for 5 min incubation in the dark. Then, the 100 µl stop solution (2N H<sub>2</sub>SO<sub>2</sub>) was added to the plate and the OD<sub>450nm</sub> was measured with a Tecan Elisa Reader. The albumin concentration of the urine samples was calculated based on the

logarithmic standard curve. For the urine creatinine, the sample was diluted at 1:6 with ddH<sub>2</sub>O and measured by using Creatinine Jaffé Gen. 2 kit according to the manufacturer's recommendation. Liver functional indexes levels were measured by using kits from Roche according to the instruction.

#### 2.2.6.9 Treatment of anti-GBM glomerulonephritis by AAV2-GEC delivered IdeS

Eight weeks old C57BL/6J male mice were randomly assigned to two groups. One group was injected with 2E+11vg AAV2-GEC-IdeS and the other group was injected with 2E+11vg AAV2-GEC-GFP by intravenous injection. 14 days after the AAV injection, both groups were injected with 150 µl of anti-GBM serum (PTX-001 sheep anti-rat GBM serum, Probetex Inc.) by intraperitoneal injection. Urine was collected (2.2.6.2) at before and 1, 3, and 7 days after the anti-GBM serum injection. Animals were sacrificed 7 days after the anti-GBM serum injection.

#### 2.2.6.10 Assessment of Nano-luciferase (Nluc) activity in serum

C57BL/6J mice were injected intravenously with AAV2-GEC-IdeS-Nluc and AAV2-GEC-Nluc. On day 3, 7, 14, 28, 56, 120 and 240 after injection, mice were anesthetized with isoflurane and blood was collected through the submandibular vein. Serum was diluted with distilled at a ratio of 1:10. 100 µl of diluted serum from each sample was then added to an opaque 96-well microtiter plate and one volume of Nano-Glo® Luciferase Assay Reagent equal to the sample volume was added to the same well. Mix well to achieve optimal concentration. After 5 minutes of incubation, the luminescence of the samples was measured using a luminometer.

#### 2.2.6.11 Statistics

Data were analyzed with GraphPad Prism 8 and shown as mean ± SEM and mean ± SD accordingly. Statistical significance between groups was determined by the Student's t-test. Levels of significance:  $p < 0.05 = *$ ;  $p < 0.01 = **$ ;  $p < 0.001 = ***$ ,  $p < 0.0001 = ****$ .

### 3 Results

#### 3.1 In vivo selection of AAV random display peptide libraries in the murine kidney

To select kidney-specific AAV capsids, we used an AAV2 and AAV9-W503A-displayed random heptamer peptide library (1.2.4), and we established an in vivo screening protocol for kidneys based on a previous report<sup>171</sup> (Figure 3.1).

##### 3.1.1 Generation of subsequent AAV libraries during selection in the kidney

In vivo selection of the AAV random peptide library is a multi-stage process (2.2.4) and this process is susceptible to experimental limitations and interference, leading to off-target effects. To minimize off-target effects, several parameters were optimized during the screening process to ensure the successful screening of putative AAV variants in the library (Table 3.1). In this study, both AAV2 and AAV9-W503A libraries were performed with four selection rounds. The assumed diversity of the initial library is  $1\text{E}+08\text{vg}$ <sup>128</sup> and would decrease during the selection process. All selection rounds for AAV2 and AAV9-W503A were injected with  $1\text{E}+11\text{vg}$  AAV particles, which corresponds theoretically to a 1000-fold coverage of the initial library diversity to ensure enough viral particles enriched in the target tissue. In the third and fourth selection rounds, the selection strategies no longer focused on the complete kidney but on glomeruli to achieve a very high selection pressure. In addition, the AAV circulation days in vivo were extended to six days in the third and fourth selection rounds. The amount of plasmid library transformed clones and subsequently generated AAV peptide library titers were controlled to ensure sufficient library diversity during the selection. After the first selection round, the large-scale electroporation for the second plasmid library resulted in over  $1\text{E}+07$  transformed clones for both AAV2 and AAV9-W503A libraries. For the subsequent selection round of both libraries, all the transformed clones were yielded over  $1\text{E}+06$ . For the titers for subsequent selection injection, each round of the AAV display library produced from  $1\text{E}+08$  HEK cells yielded over  $1\text{E}+12\text{vg}$  per ml (Table 3.1).

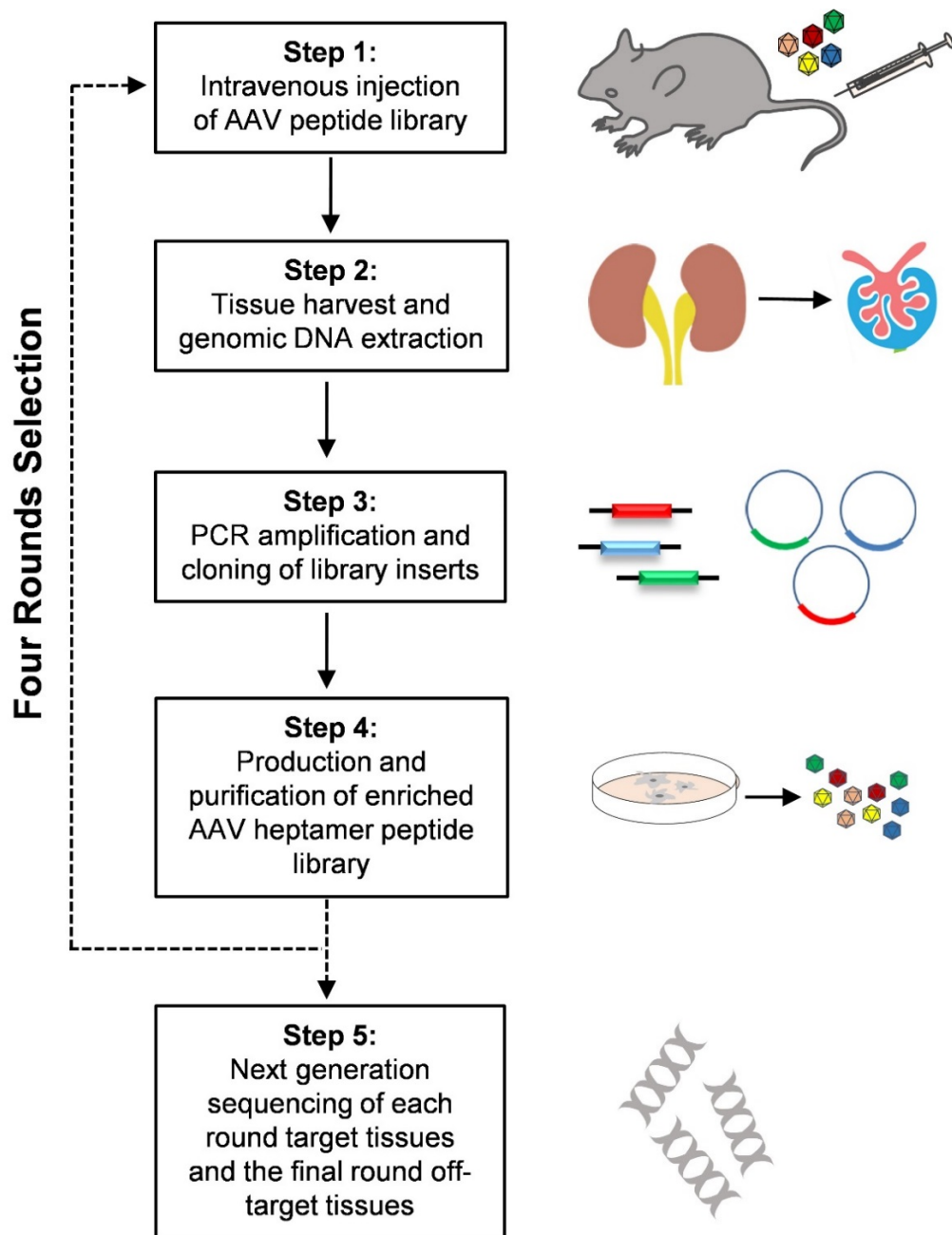


**Figure 3.1 Selection of the AAV heptamer peptide library in the murine kidney.** The random AAV display peptide library was injected intravenously in mice (step 1). After three days, the target tissues were harvested and genomic DNA (gDNA) was extracted (step 2) for library inserts amplification and library plasmid cloning (step 3). The secondary AAV display peptide library was produced by transfection library plasmid with HEK cells for subsequent rounds of selection (step 4). Four rounds of selection were performed. Each round of target tissues and the final round of off-target tissues were used for next-generation sequencing (step 5).

**Table 3.1 Summary of parameters for AAV display peptide library selection in the kidney**

Selection round	AAV injection dose (vg)	Circulation days	Target tissues	Plasmid library transformed clones	AAV peptide library titer (vg/ml)
<b>AAV2</b>					
R1	1E+11	3	kidney	2.08E+07	1.58E+12
R2	1E+11	3	kidney	3.03E+06	3.35E+12
R3	1E+11	6	glomerulus	2.44E+06	1.18E+12
R4	1E+11	6	glomerulus	6.05E+06	-
<b>AAV9</b>					
R1	1E+11	3	kidney	1.59E+07	1.18E+13
R2	1E+11	3	kidney	4.80E+06	1.05E+13
R3	1E+11	6	glomerulus	1.80E+06	1.61E+13
R4	1E+11	6	glomerulus	8.25E+06	-

### 3.1.2 Peptides enrichment during in vivo selection in the murine kidney

After large-scale electroporation of each round of library selection, twenty single clones were picked randomly from the corresponding pre-selected plasmid library (2.2.4.7) and the peptide insert-encoding fragment of the cap gene was Sanger sequenced. All the twenty sequenced clones displayed different heptapeptides in the first three selection rounds of both AAV2 and AAV9-W503A libraries (Table 3.2, Table 3.3). However, in the fourth round selection, seven out of twenty clones (NDIKPQP) displayed the same heptapeptides in the AAV2 library and eight out of twenty clones (GVNYGLG) displayed the same heptapeptides in the AAV9-W503A library. In this case, each of the libraries occurred one dominant peptide with a ratio of more than 30%, indicating that the screening process could be discontinued at this time point.

**Table 3.2 Peptides enrichment during the AAV2 library selection in the murine kidney**

<b>1st round</b>	<b>2nd round</b>	<b>3rd round</b>	<b>4th round</b>
AAQPPAG	AIESQNP	AQAAVAQ	DGAHQPA
AAQQLAH	DADSGAR	DAQPAGD	DGAHQPA
AELQIQR	DLAEGSE	EIQGTAQ	EDQHNGG
AIQTTFA	DLEQRMA	ENRGDSV	GDGPMSW
DEQLLQP	DMQLLLG	EQHVSPG	GNTQPPQ
EHSNACP	DNTIYNP	ESSMTQQ	GQGADGP
EPGTMFM	DSHTYPP	GALTDQV	HGQDKVA
GDQLGIR	EDDPVSW	GDGPMSW	KDNEPMQ
GEDWLAQ	ERQEPGA	GEDQWQG	<b>NDIKPQP</b>
HGQHYDN	GAITEWQ	GQVTAAM	<b>NDIKPQP</b>
PGPQELT	GVGALLQ	IDQGHAQ	<b>NDIKPQP</b>
PQQEQEQ	HNRADVP	NDIKPQP	<b>NDIKPQP</b>
QDGSWPP	IQITTAM	NGTGRPT	<b>NDIKPQP</b>
QHFDLPR	LENQNQP	QDADGWK	<b>NDIKPQP</b>
QNSQWQQ	NEPTPPF	QDAGIGT	<b>NDIKPQP</b>
QYQQQYG	QPISENN	QEPQPQP	NSIQPPK
SLPHASV	QQHGQAG	QIDQTRA	NSTQQLQ
TNEDLPY	TETVADP	QPRELPI	QANFTNN
TNVQQQL	YHPGAGH	QQIPFPE	QDAGIGT
VDGWEMK	YIYHAEQ	QQEQQAG	QVLVYRE

**Table 3.3 Peptides enrichment during the AAV9-W503A library selection in the murine kidney**

<b>1st round</b>	<b>2nd round</b>	<b>3rd round</b>	<b>4th round</b>
AGWSR*W	DRVCRGG	AGCRMGS	AANCVGG
CDDGGGV	ECGSGSY	ASGVRFV	EGVRCGL
CDRVSGV	ECVDKWW	DEGNCR L	GECRGSV
DDVQRGS	EGRCLVG	DSSGRLS	GGNGGVV
EGGAWLK	EQLRCGV	DYGGMAG	GIGCSKG
EVRSVHV	ERMGGIV	EGMGGCK	GRCGRSE
GCMSWLI	ESYREGE	GECGRVS	GSGQFVG
GGTGVGD	GCVDRLV	GEGGGM Y	GVCRDTF
GKCASGL	GEAGLGL	GEKGTAM	GVHVAWR
GKERGQN	GSEGTHS	GGCGIRQ	<b>GVNYGLG</b>
GNIVTGC	GSVGSV	GEGGCSI	<b>GVNYGLG</b>
GVAGAAI	SCVMFGG	GGMLCTG	<b>GVNYGLG</b>
GVGC SER	SDTRCGG	GSVGSV	<b>GVNYGLG</b>
RVEGGCQ	VCLSKSM	GVGSNSV	<b>GVNYGLG</b>
VDGSYGL	VECSLAV	NGGGGRC	<b>GVNYGLG</b>
VEKAGWR	VFVEC*N	SDGVGGA	<b>GVNYGLG</b>
VGIMDWR	VGCGFGL	VEGVPMC	<b>GVNYGLG</b>
VGVKNME	VGECQAR	VGETLAE	GVRCVVV
VWARDRW	VGSGGSM	VGNVRCM	VGGLCVR
WCVDGMR	VVSILPM	VGSRMCI	VVSVACM

### 3.1.3 Peptide enrichment monitored by next-generation sequencing

Sanger sequencing results provided limited information about library diversity and enrichment of individual clones (3.1.2). Therefore, we guided our selection by next-generation sequencing to thoroughly analyze each round of enriched peptides from target and non-target tissues in mice. The summary of NGS readout for AAV2 and AAV9-W503A libraries selection in the kidney was shown in Table 3.4. The number of DNA sequences remained at a similar magnitude across the screening rounds, while the number of library diversity peptide sequences decreased during the screening process. In both the AAV2 and AAV9-W503A libraries, the proportion of the top 100 most predominant peptides among all peptides increased during the selection (Figure 3.2).

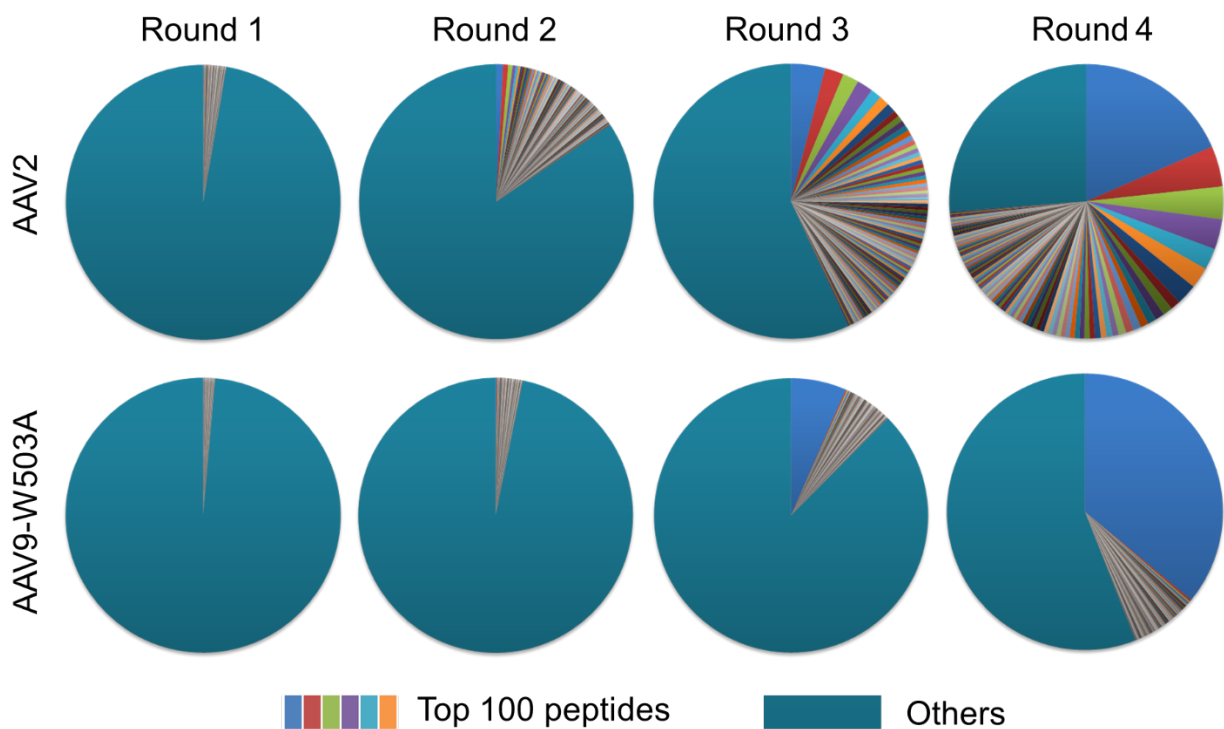


**Figure 3.2 Distribution of peptide variants in each selection round.** Pie charts indicate the frequency of particular peptide inserts was determined by NGS. “Others” indicates the occurrence of peptide variants ranked below the “top 100 peptides” in the total pool.

**Table 3.4 Summary of NGS readout for the random peptide libraries in the kidney.**

Library	Round	Number of DNA sequences	Number of peptide sequences	The percentage of top 100 peptides
AAV2	1	131040	49064	2.72
	2	152188	9253	15.57
	3	122338	3314	43.12
	4	57592	1233	68.99
AAV9-W503A	1	102412	38780	1.41
	2	129134	34467	3.19
	3	88978	23888	12.49
	4	111611	17799	44.03

### 3.1.4 Scoring of dominant peptides

The NGS data presented here indicate that there was no general correlation between most enriched peptides and their tissue specificity. Even after four rounds of screening, the library still had a large diversity. To select the most promising candidates, peptides enriched in the renal glomerulus were evaluated by an NGS-based scoring system (2.2.5.4) and ranked according to three rating scores: enrichment score (E score), general tissue specificity score (GS score), and combined score (C score).

All peptides were scored using the calculation mentioned above. In the AAV2 library, peptides with a relative abundance higher than 0.1% and E score greater than 0.5 were maintained and ranked by C scores. Likewise, peptides with a relative abundance higher than 0.05% and E score greater than 0.5 were maintained in the AAV9 library and ranked by C scores. Irrelevant and less abundant peptides were removed from the subsequent analysis. Only the candidates with a high C score were obtained when both the E and GS scores were relatively higher as well. The Top 10 candidates with the highest C score were shown in Figure 3.3. QVLVYRE and GGNVGLG didn't have the highest E score, but it outperformed other sequences by a better GS score, suggesting that it was not only abundantly but also high-specifically enriched in glomeruli.

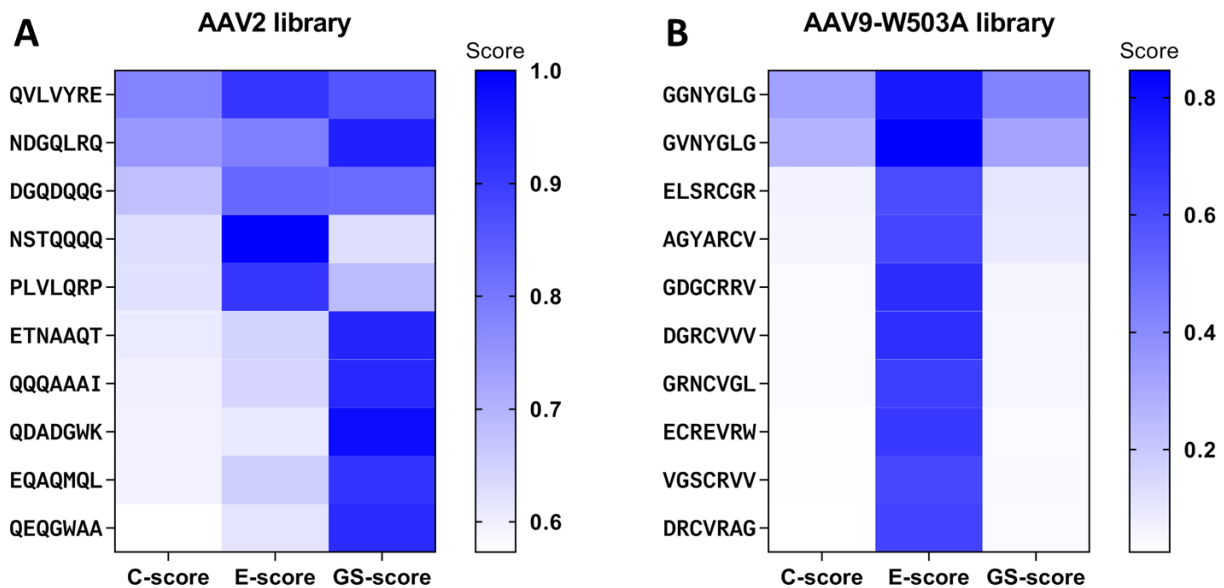


**Figure 3.3 Identification of AAV2-QVLVYRE and AAV9-GGNYGLG by rating scores.** (A) Top ten peptides enriched from the AAV2 library scored by C score. (B) Top ten peptides enriched from the AAV9-W503A library scored by C score. The combined C score (by multiplying GS and E) described the peptide performance regarding specificity (GS score) and efficacy (E score) with an ideal value of 1.

## 3.2 Characterization of AAV2-QVLVYRE

### 3.2.1 AAV2-QVLVYRE specifically and efficiently transduced the GEC

To evaluate the in vivo transduction profile of the AAV2-QVLVYRE variant, we generated scAAV reporter vector, which contained the GFP cDNA driven by the constitutive CMV promoter. The AAV vector was intravenously injected into 8-12 weeks old C57BL/6J mice with a dose of  $1E+11$  vg per mouse ( $n = 3$ ). After 14 days, the transgene expression was analyzed in different organs.

In the kidney, IF staining showed that the GFP expression mediated by AAV2-QVLVYRE was restricted to the glomerulus and revealed excellent transduction efficiency in all renal glomeruli (Figure 3.4). We further confirmed that AAV2-QVLVYRE specifically transduced the GEC, which was marked by CD31, but not podocytes marked by Synaptopodin (SYNPO), or mesangial cells marked by platelet-derived growth factor receptor  $\beta$  (PDGFRB) ((Figure 3.5). We thus termed AAV2-QVLVYRE as AAV2-GEC.

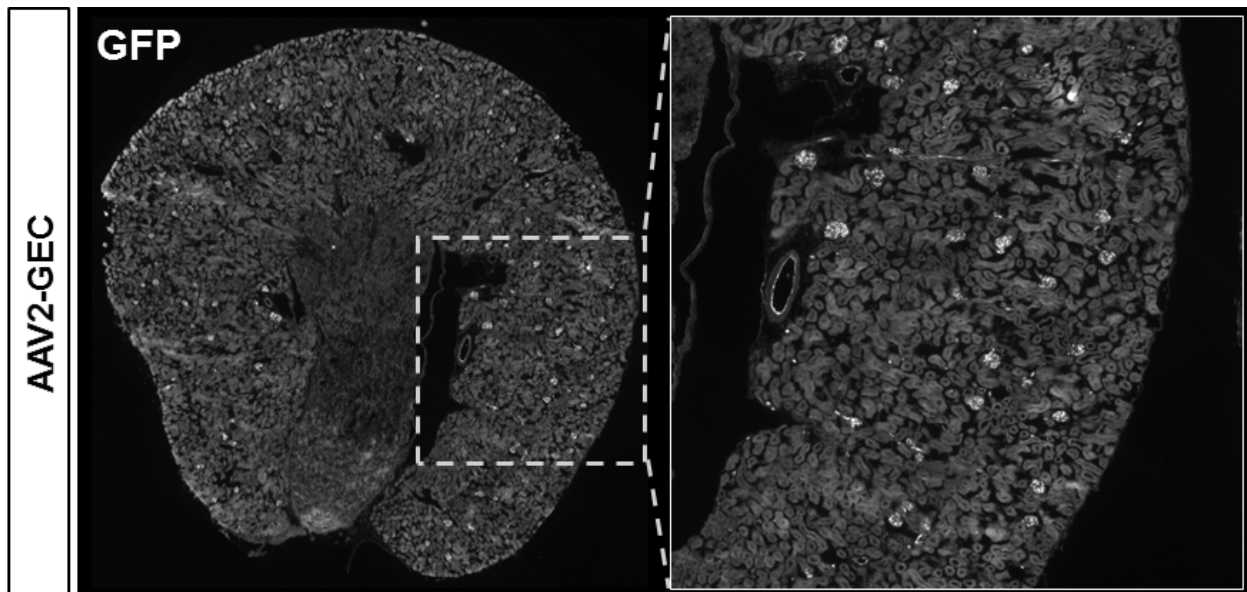


**Figure 3.4 AAV2-GEC mediated GFP expression in the kidney.** Representative overview images of AAV2-GEC mediated GFP expression in kidney cross sections from C57BL/6J mice.

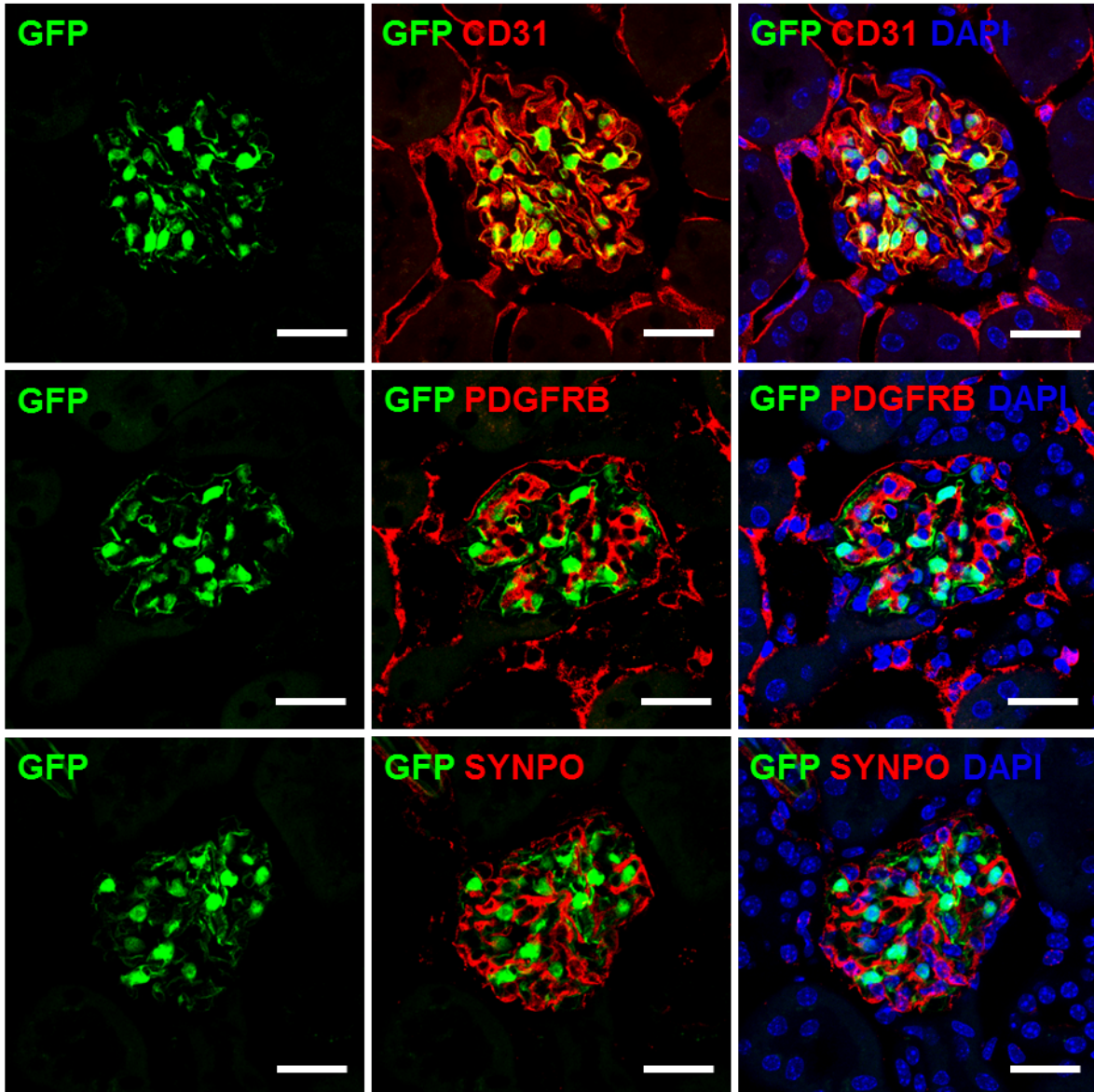


**Figure 3.5 AAV2-GEC specifically transduced the glomerular endothelial cells.** AAV2-GEC mediated GFP expression was found in the glomerular endothelial cells marked by anti-CD31 antibody in kidneys from C57BL/6J mice. Mesangial cells were marked by anti-PDGFRB antibody and podocytes were marked by anti-SYNPO antibody. Nuclei were counterstained with DAPI. Scale bar: 25  $\mu$ m.

The transduction properties of AAV2-GEC were compared to its parental wild-type AAV2 (AAV2-WT). No GFP expression was detected in the kidney of AAV2-WT injected mice (Figure 3.6). GFP expression was strong in the liver and heart, and moderate in the spleen of the AAV2-WT injected mice, whereas it was far weaker in all of these organs of the AAV2-GEC injected mice (Figure 3.7). In addition, Quantitative PCR (qPCR) showed that AAV2-QVLVYRE was at least 10-fold dominant in glomeruli compared to other organs including the whole kidney (Figure 3.8).

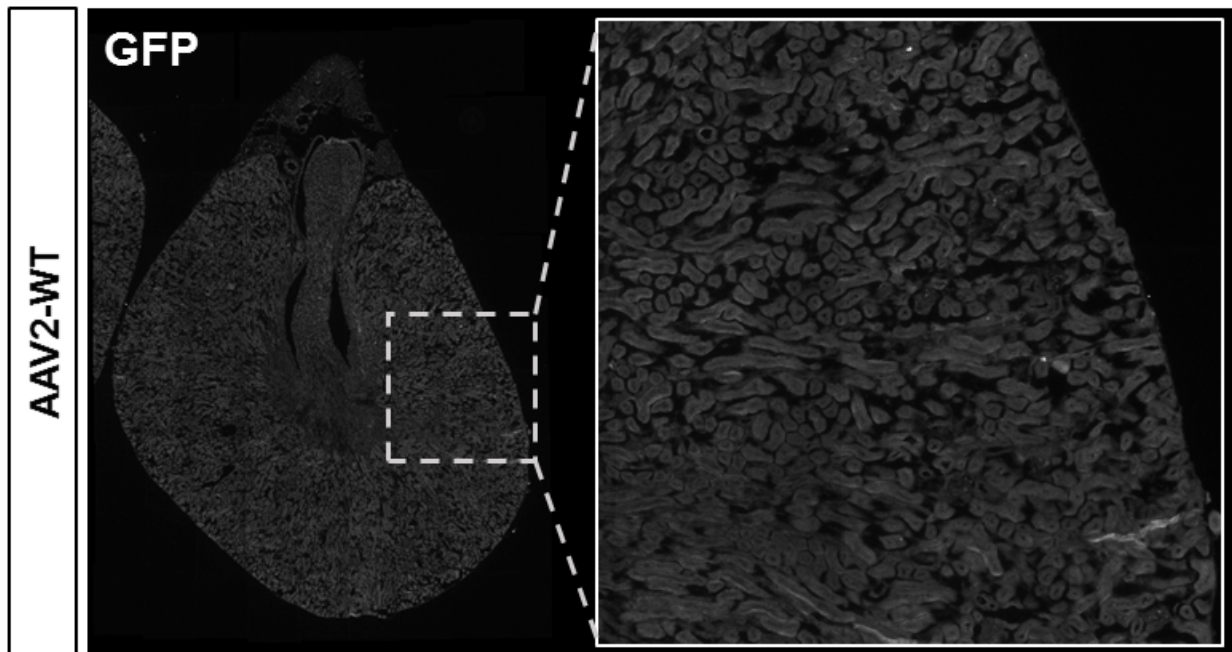


**Figure 3.6 AAV2-WT mediated GFP expression in the kidney.** Representative overview images of AAV2-WT mediated GFP expression in kidney cross sections from C57BL/6J mice.

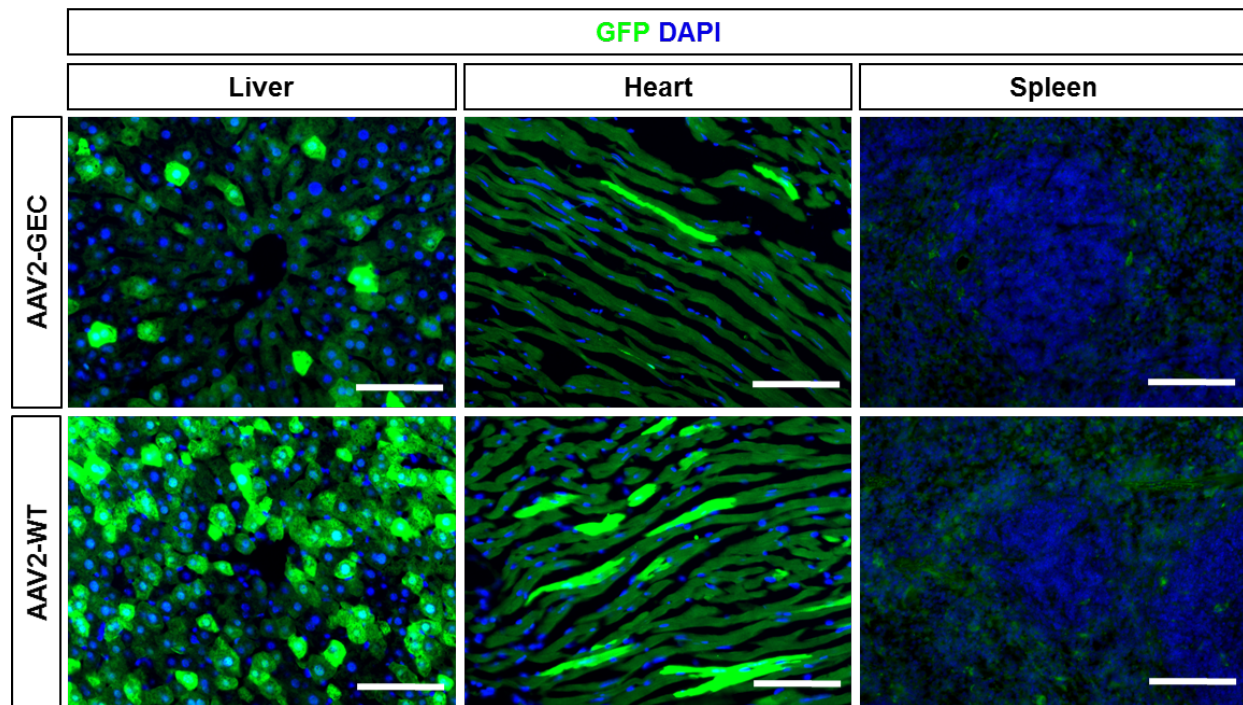


**Figure 3.7 AAV2-GEC mediated GFP expression in off-target organs.** Representative images of AAV2-GEC mediated GFP expression in the off-target organs (liver, heart, and spleen) compared to AAV2-WT mediated GFP expression. Nuclei were counterstained with DAPI. Scale bar: 100  $\mu$ m.

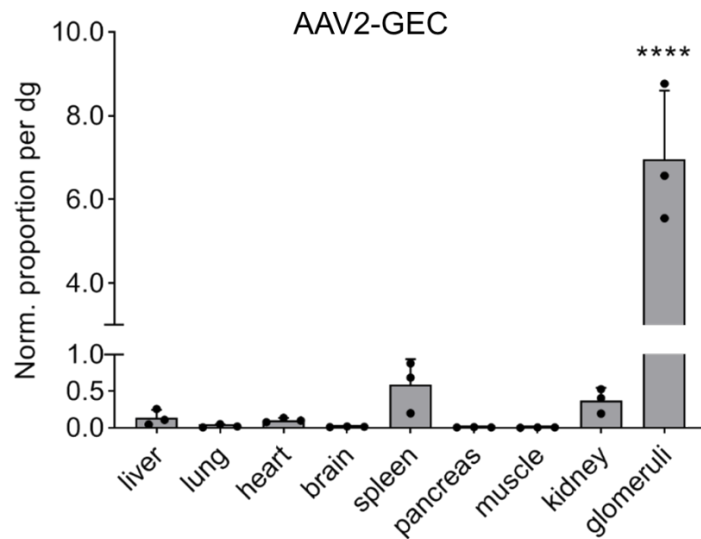


**Figure 3.8 Quantification of vector genome distribution by qPCR.** The number of vector genomes was quantified and normalized to vector copy numbers per diploid genome (vg/dg). Values are mean  $\pm$  SD. Significance: multiple t tests, \*\*\*\* $P$  < 0.0001 in all comparisons (glomeruli vs. other organs).

AAV2-GEC mediated GFP expression was analyzed over 360 days after intravenous injection (Figure 3.9A) and the GFP signal intensity was quantified (Figure 3.9B). Throughout the whole period, glomerular GFP peaked at day 14, was stable at high levels until day 120 and decreased from day 240. GFP signal was dominant in glomeruli, but from day 120 it was also detected in endothelial cells in the tubular segment. Additionally, liver and spleen histology was analyzed (Figure 3.10). No obvious histological lesions in the liver and spleen over 360 days, indicating no tissue toxicity due to the injection of AAV2-GEC. Taken together, AAV2-GEC mediates specific and prolonged GFP expression in the GEC for at least 120 days upon intravenous injection.

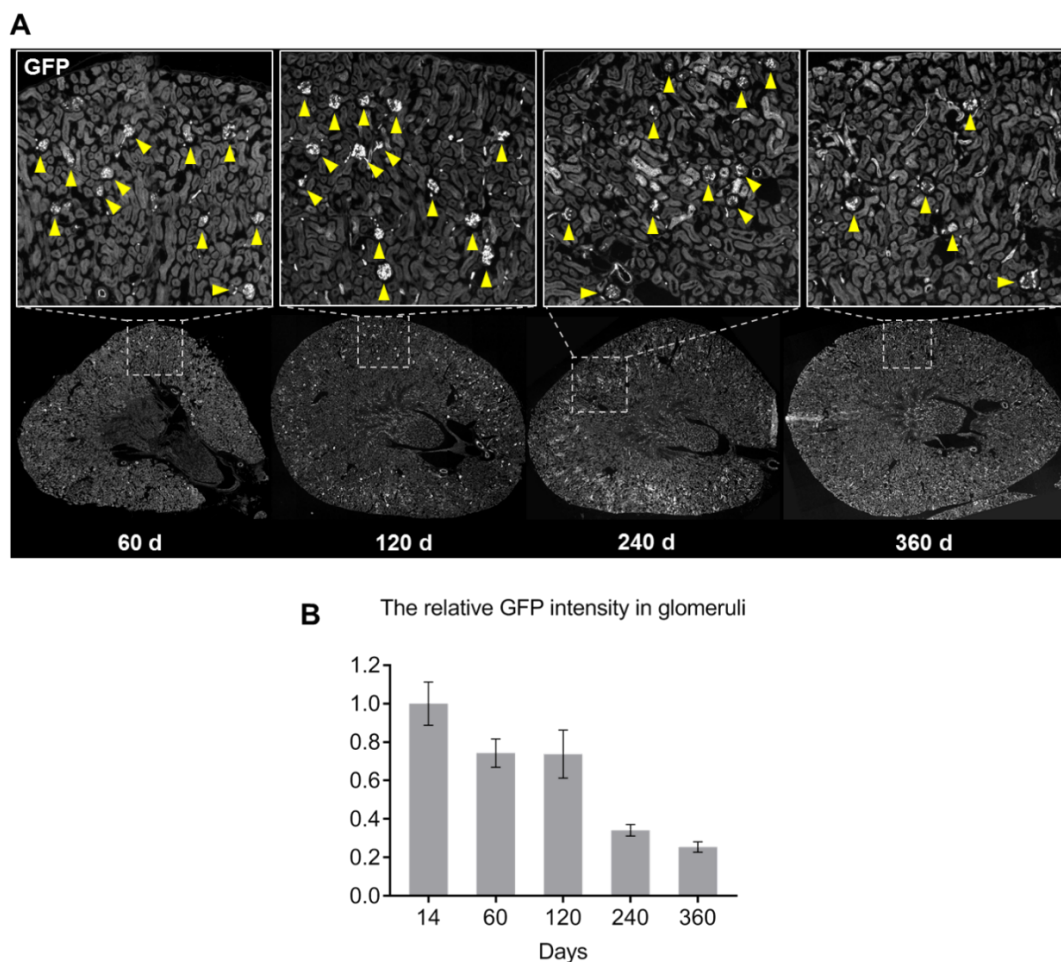


**Figure 3.9 AAV2-GEC mediated long-term GFP expression in the kidney. (A)** Representative overview images of AAV2-GEC mediated GFP expression in kidneys from C57BL/6J mice 60, 120, 240, and 360 days after intravenous injection. Arrows indicate GFP-positive glomeruli. **(B)** Quantification of GFP signal intensity. Ten images from each kidney (n=4) (incl. 20-30 gloms) were taken and the mean intensity was used for quantification. The final data were presented as relative expressions compared to the 14-day data. Values are mean  $\pm$  SEM.

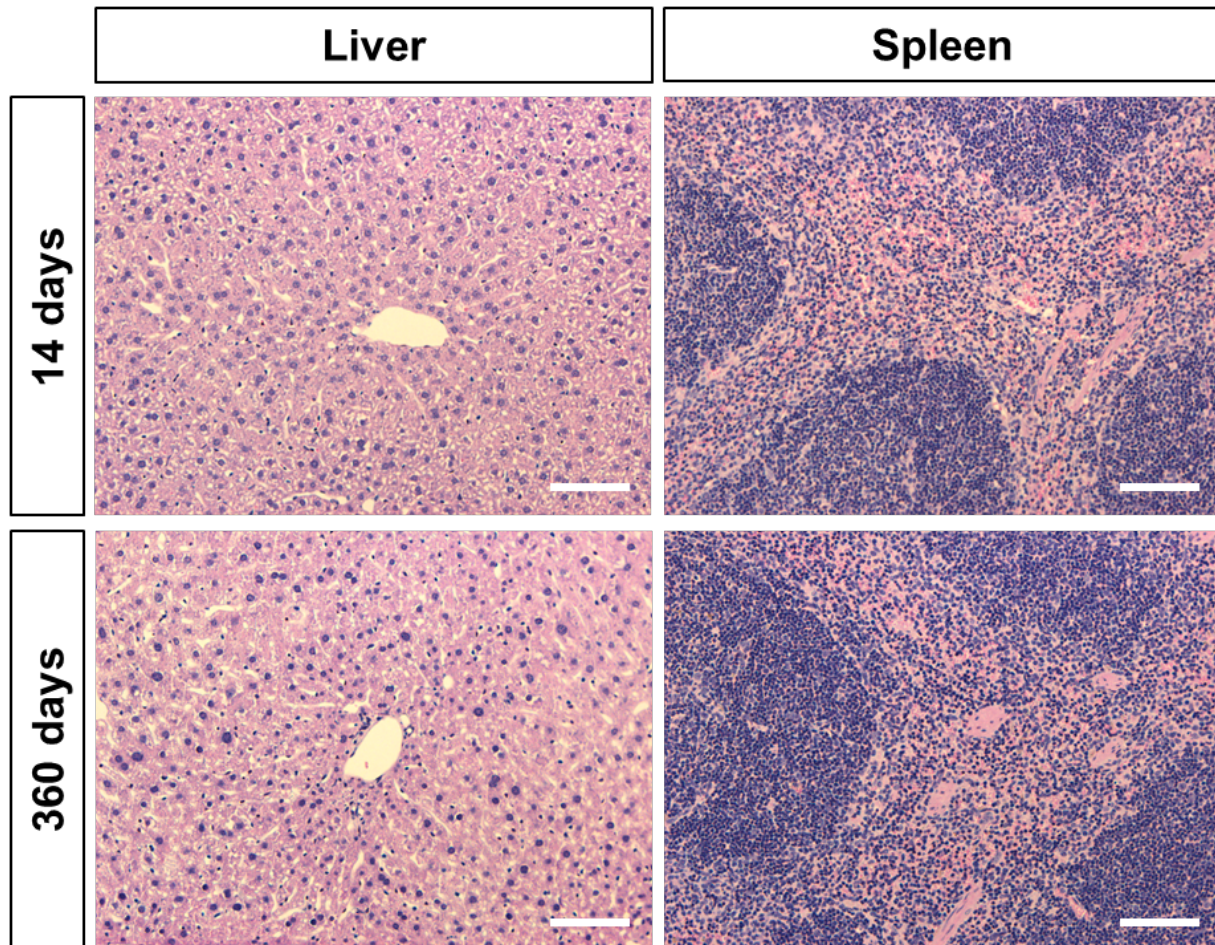


**Figure 3.10 Assessment of liver and spleen histology in AAV2-GEC transduced mice.** H&E staining in livers and spleens from AAV2-GEC transduced C57BL/6J mice 14 and 360 days after intravenously injection. No obvious histological lesions were observed. Scale bar: 100  $\mu$ m.

### 3.2.2 AAV2-GEC maintained robust tropism in GFB-damaged mice

GEC are highly differentiated endothelial cells characterized by their unique fenestrae and surface layer glycocalyx, which are essential for the filtration function. The differentiation and permeability of GEC are also regulated by podocytes. Under disease conditions, the breakdown of the GFB due to the injury of GEC or podocytes could lead to changes in the GEC tropism. Therefore, we evaluated the GEC tropism in mouse models with damaged GFB.

The loss of fenestrae and glycocalyx disruption in GEC are typically induced by hyperglycemia in diabetic kidney disease (DKD)<sup>173</sup>. We evaluated the transduction profile

of AAV2-GEC in BTBR *ob/ob* mice, which is a well-characterized DKD mouse model, exhibiting an early onset of hyperglycemia from 6 weeks<sup>174</sup> of age and significant changes in GEC fenestrae from 10 weeks of age<sup>175</sup>. AAV2-GEC-GFP was intravenously injected in 16-18 weeks BTBR *ob/ob* mice with a dose of 2E+11 vg. The dose was increased according to the body weight since this mouse model developed obesity from 6 weeks of age<sup>174</sup>. After two weeks, IF was performed on the kidney sections. Robust and efficient GFP expression was observed in the GEC of the BTBR *ob/ob* mice (Figure 3.11).

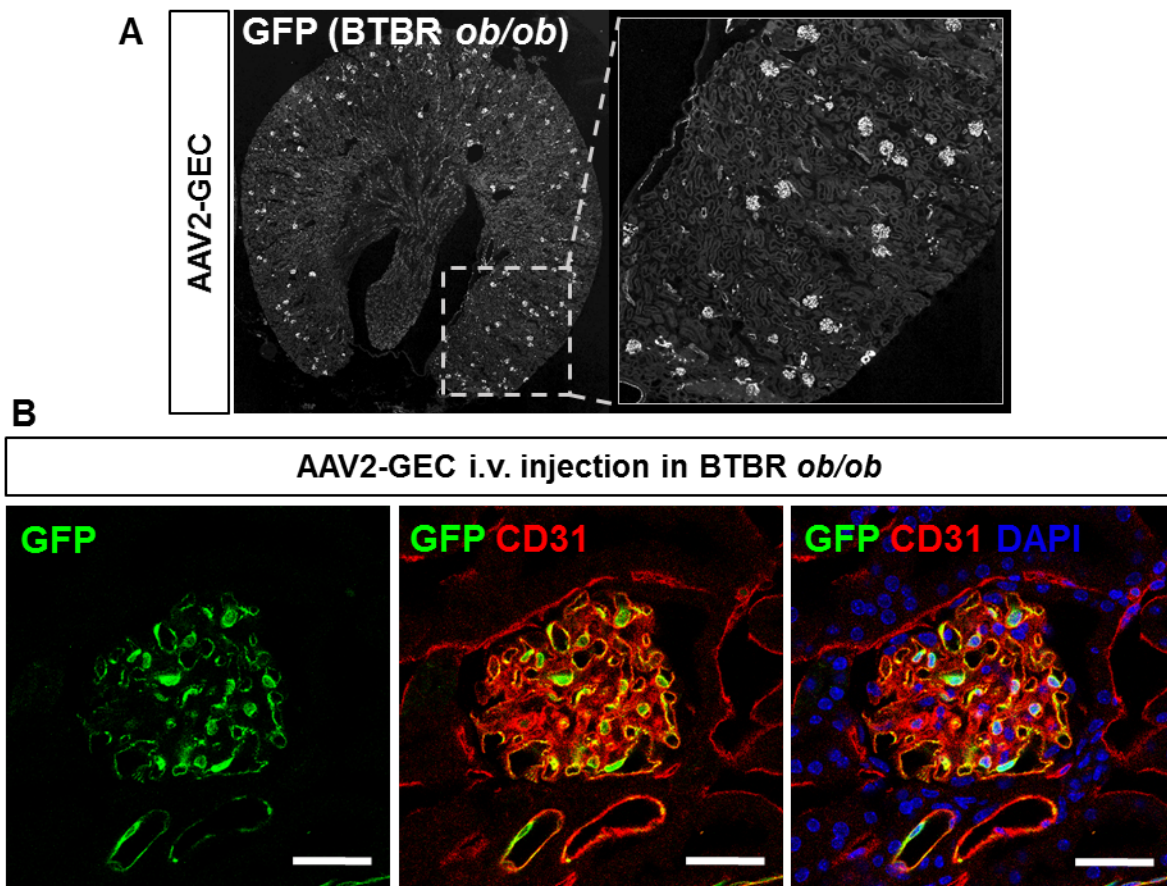


**Figure 3.11 AAV2-GEC maintained robust tropism in BTBR *ob/ob* mice. (A)** Representative overview images of AAV2-GEC mediated GFP expression in kidneys from BTBR *ob/ob* mice. **(B)** GFP expression was detected in the GEC marked by anti-CD31 antibody. Nuclei were counterstained with DAPI. Scale bar: 25  $\mu$ m.

We also evaluated the tropism of AAV2-GEC in  $Nphs1^{\Delta iPod}$  mice, which have induced Nephrin-deficiency in podocytes after doxycycline administration<sup>170</sup>. Nephrin is one of the essential slit diaphragm proteins in podocytes. Loss of Nephrin in adult mice leads to podocytes injury and the GFB leakage<sup>170</sup>. AAV2-GEC-GFP was intravenously injected in  $Nphs1^{\Delta iPod}$  mice 12 weeks after the knock-out induction with a dose of  $1E+11$  vg. After two weeks, IF was performed on the kidney sections. Robust and efficient GFP expression was observed in the GEC of the  $Nphs1^{\Delta iPod}$  mice (Figure 3.12).

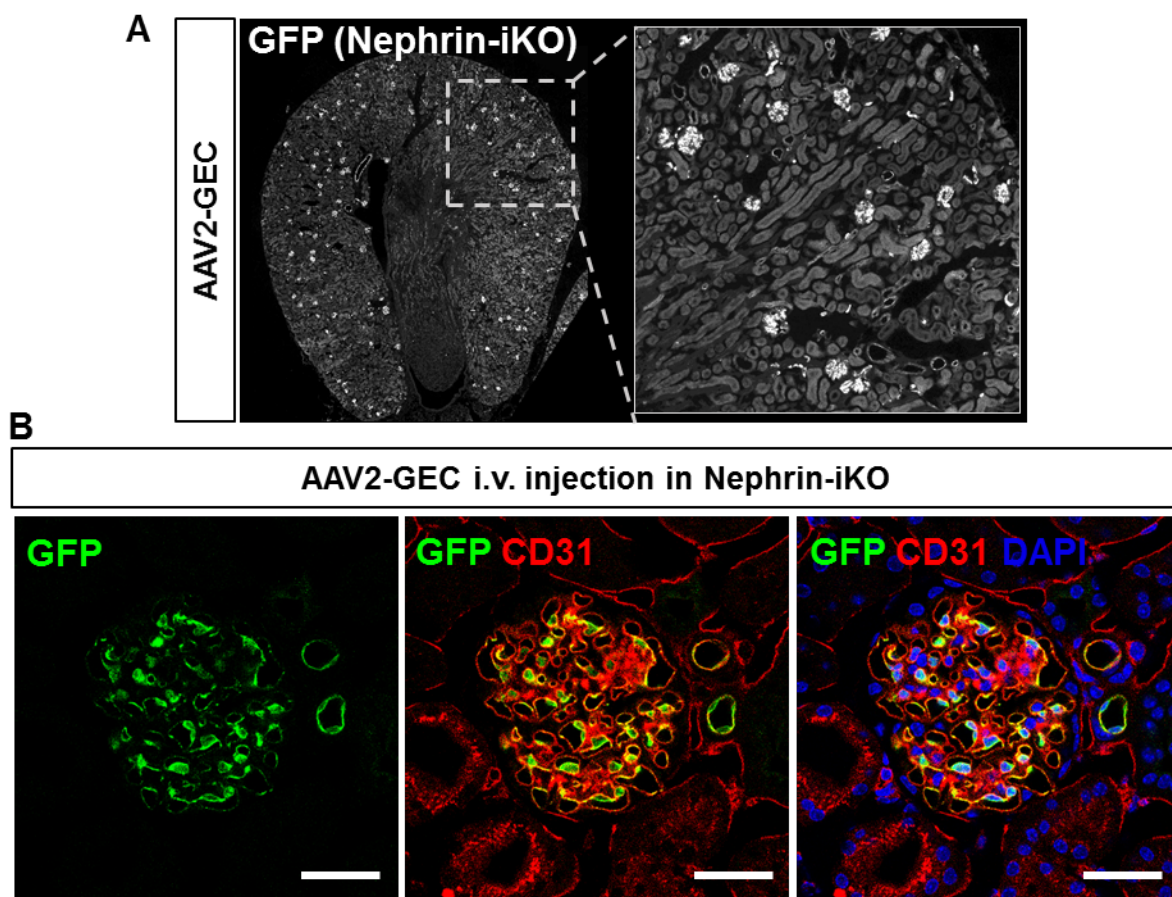


**Figure 3.12 AAV2-GEC maintained robust tropism in  $Nphs1^{\Delta iPod}$  mice.** (A) Representative overview images of AAV2-GEC mediated GFP expression in kidneys from  $Nphs1^{\Delta iPod}$  mice. (B) GFP expression was detected in the GEC marked by anti-CD31 antibody. Nuclei were counterstained with DAPI. Scale bar: 25  $\mu$ m.

### 3.2.3 AAV2-GEC maintained robust tropism in Balb/c mice and SD rats

Since the transduction by AAV vectors may vary substantially between strains and species<sup>176-179</sup>, we evaluated AAV2-GEC tropism in adult Balb/c mice and SD rats. AAV2-GEC-GFP was intravenously injected in Balb/c mice with a dose of 1E+11vg. After two weeks, IF was performed on the kidney sections. We observed robust and efficient GFP expression in the GEC of the Balb/c mice (Figure 3.13). Similar tropism of AAV2-GEC was also determined in the SD rat, in which the GEC were marked by endothelial cell-specific biomarker rat endothelial cell antigen 1 (RECA-1) (Figure 3.14).

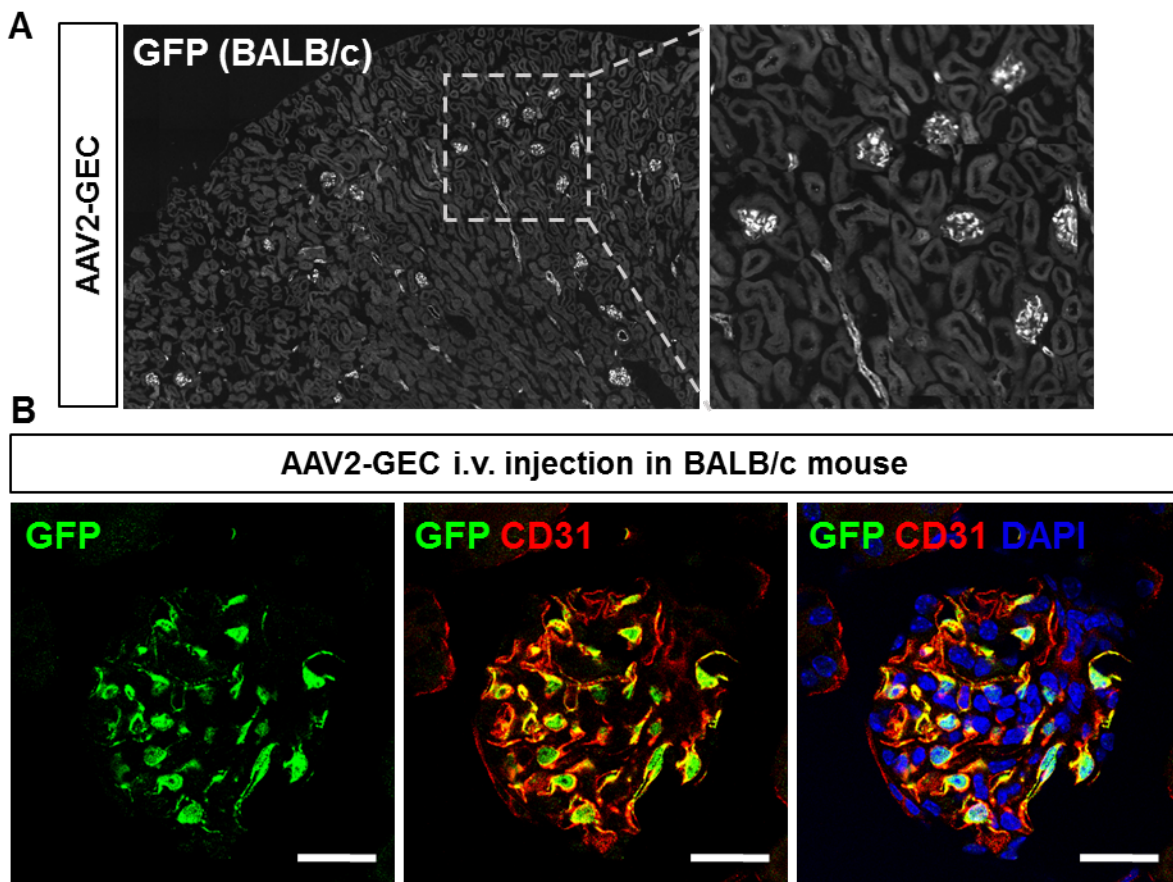


**Figure 3.13 AAV2-GEC maintained robust tropism in Balb/c.** (A) Representative overview images of AAV2-GEC mediated GFP expression in kidney cross sections from Balb/c mice. (B) GFP was found in the glomerular endothelial cells marked by anti-CD31 antibody in kidneys from Balb/c mice. Nuclei were counterstained with DAPI. Scale bar: 25  $\mu$ m.

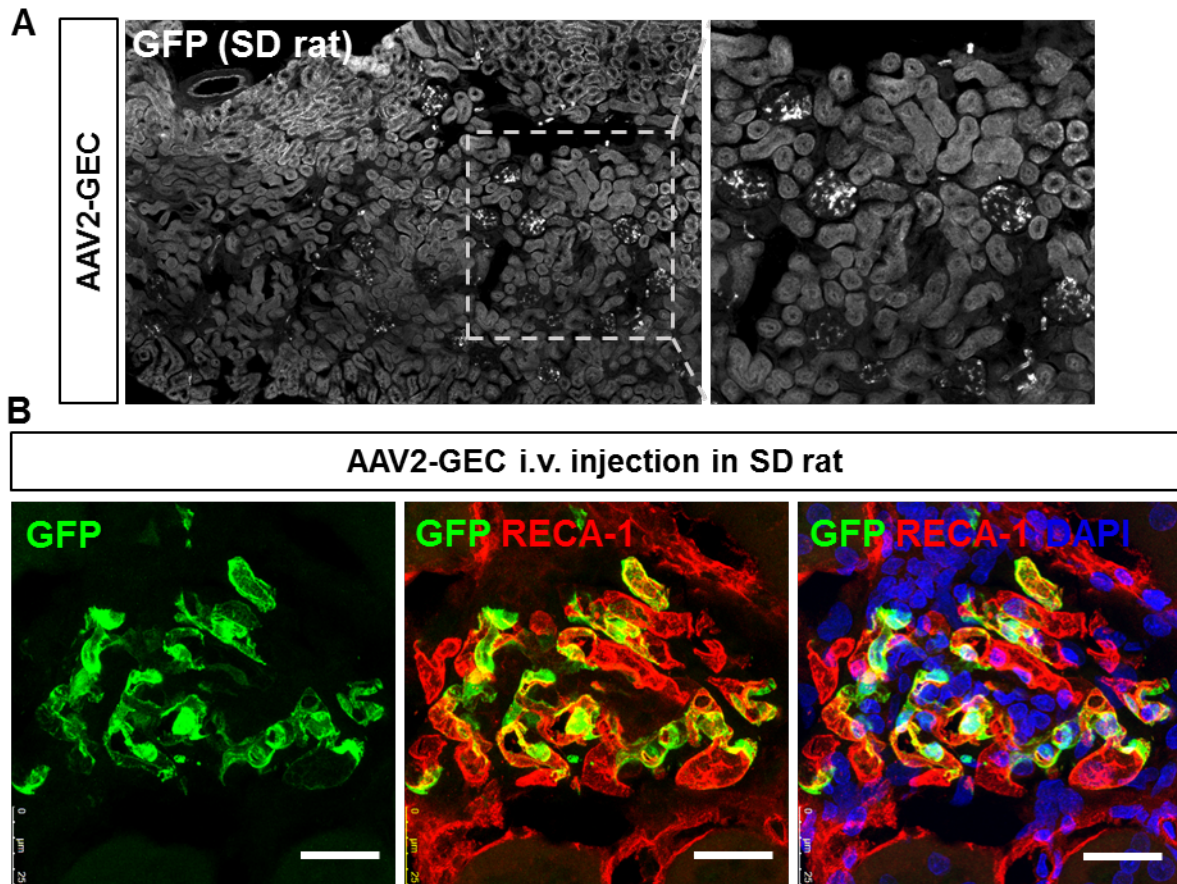


**Figure 3.14 AAV2-GEC maintained robust tropism in SD rats.** (A) Representative overview images of AAV2-GEC mediated GFP expression in kidney cross sections from SD rats. (B) GFP was found in the glomerular endothelial cells marked by anti-RECA-1 antibody in kidneys from SD rats. Nuclei were counterstained with DAPI. Scale bar: 25  $\mu$ m.

### 3.2.4 AAV2-GEC delivery of IdeS prevents anti-GBM glomerulonephritis

To investigate the therapeutic feasibility of AAV2-GEC, we developed a treatment strategy for anti-GBM glomerulonephritis for proof of concept (2.2.6.9). The experiment protocol is shown in Figure 3.15. AAV2-GEC vectors carrying IdeS and GFP under the control of the CMV promoter were used as treatment and control vectors, respectively. The vectors were intravenously injected in adult C57BL/6J male mice with a dose of  $2E+11$  vg. Two weeks after the AAV injection, all mice were administrated with 150  $\mu$ l anti-GBM serum to induce anti-GBM glomerulonephritis.



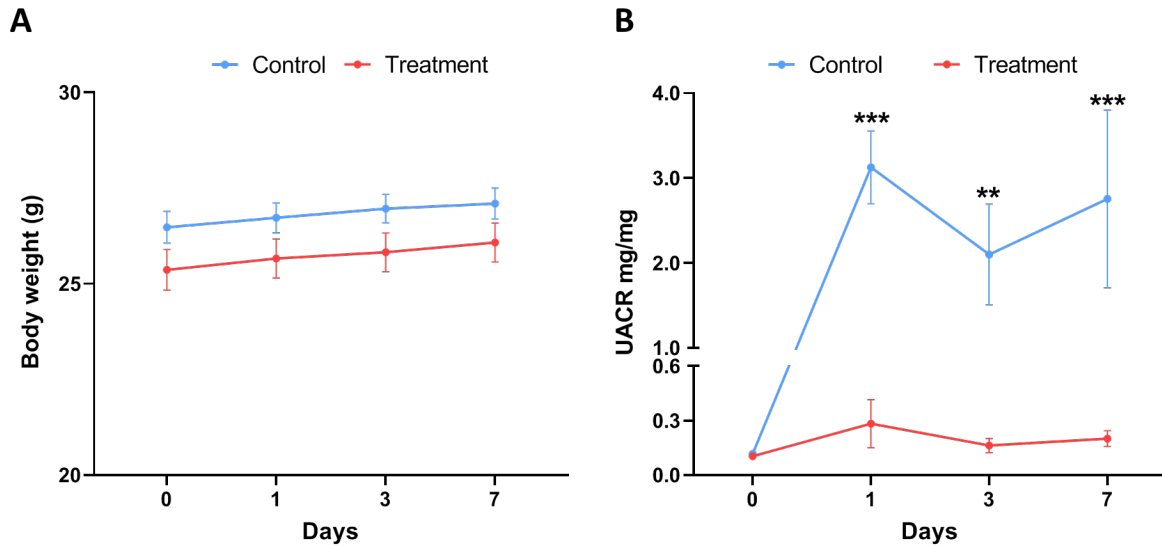


**Figure 3.16 Body weight and UACR of BL6 mice. (A)** Body weight (g) of control (AAV2-GEC-IdeS) and treatment (AAV2-GEC-GFP injected) mice were measured on days 0, 1, 3, and 7 after anti-GBM injection. There was no significant difference at any measurement point of the body weight between IdeS-treatment mice and GFP-control mice. **(B)** UACR was measured at before and 1, 3 and 7 days after anti-GBM injection from control and treatment groups. Values are mean  $\pm$  SEM. Significance: multiple t tests,  $**P < 0.01$ ,  $***P < 0.001$ , only statistically significant comparisons are shown.

Consistently, IF staining in the kidney sections showed that the whole sheep IgG (Figure 3.17D-F) was barely to detect in the treated mice compared to the control mice (Figure 3.17A-C), indicating that the GEC efficiently expressed IdeS, which cleaved circulating sheep IgG, thereby prevented the deposition of sheep IgG on the GBM. Due to the effective cleavage of sheep IgG by IdeS, the accumulation of mouse IgG on the GBM was also prominently prevented (Figure 3.17J-L), which then significantly reduced the deposition of complement C1q (Figure 3.18D-F) and C3 (Figure 3.18J-L) in treated kidneys compared with controls (Figure 3.18A-B, G-I). Additionally, serum liver function indexes (ALTL, ASTL, GGT12, CHOL2, TRIGL, and BILD2) were normal in both treated and control mice (Figure 3.19), indicating no liver toxicity caused by AAV2-GEC-IdeS injection. The long-term expression of IdeS was analyzed by monitoring its serum level for 240 days (Figure 3.20). IdeS was fused with Nano-luciferase (Nluc) and delivered to GEC by intravenous injection of AAV2-GEC-IdeS-Nluc. The concentration of circulating

IdeS was maintained from day 3 until day 240, indicating a stable expression of IdeS by transduced GEC.

Taken together, these results suggest that intravenous administration of AAV2-GEC-IdeS successfully prevented the progression of anti-GBM glomerulonephritis.

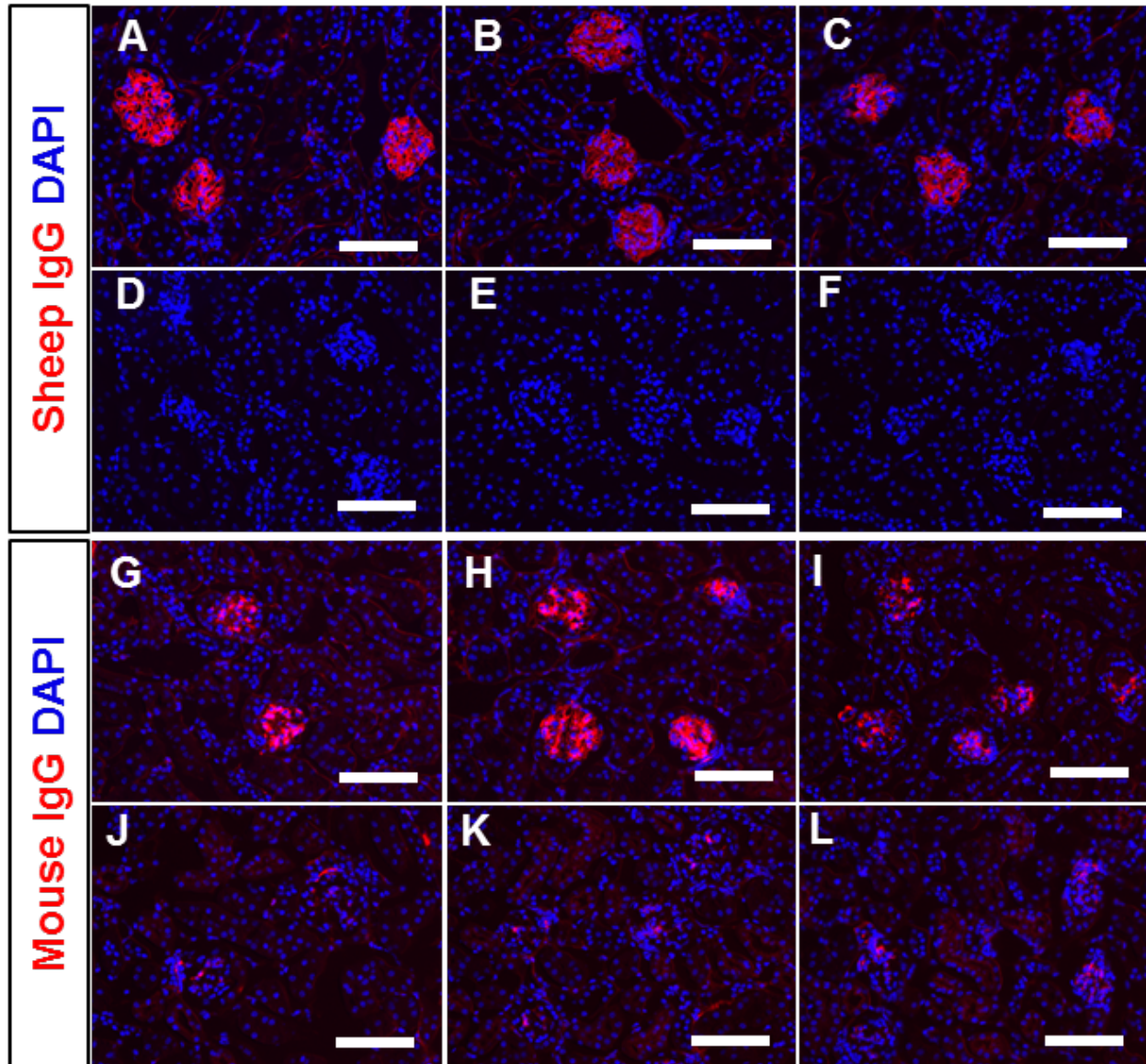


**Figure 3.17** Representative images showing the remaining sheep anti-GBM IgG detected using AL555-conjugated donkey anti-sheep IgG from AAV2-GEC-GFP control group (A–C) and AAV2-GEC-IdeS treated group (D–F). Deposition of mouse IgG detected using AF555-conjugated donkey anti-mouse IgG antibody. (G–I) show samples from the AAV2-GEC-GFP control group, while (J–L) represents the AAV2-GEC-IdeS treatment group. Nuclei were counterstained with DAPI. Scale bar: 100  $\mu$ m.

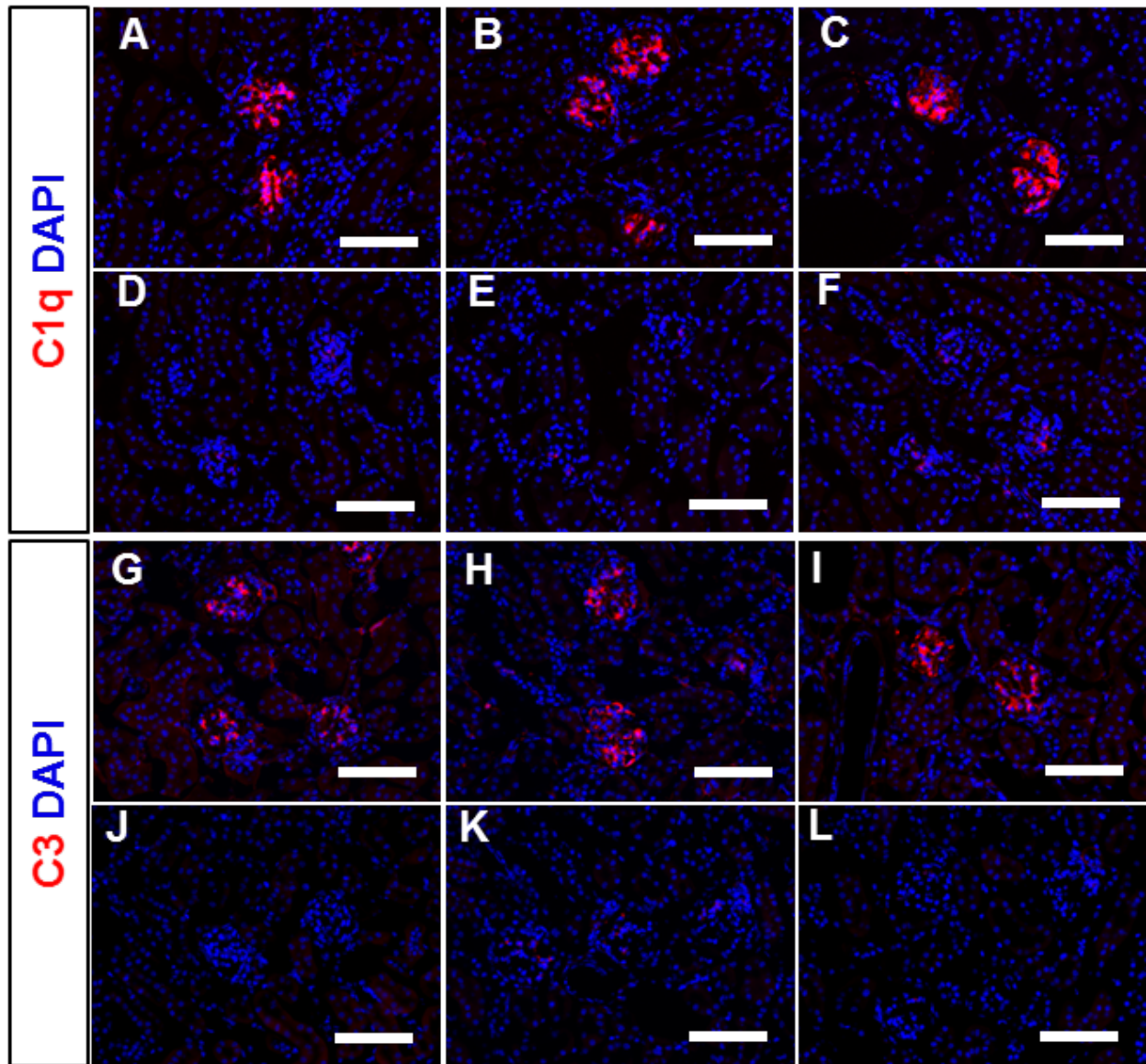


**Figure 3.18** Representative images showing the deposition of C1q from the AAV2-GEC-GFP control group (A–C) and AAV2-GEC-IdeS treatment group (D–F). Deposition of C3 in the kidneys. (G–I) show samples from the AAV2-GEC-GFP control group, while (J–L) represents the AAV2-GEC-IdeS treatment group. Nuclei were counterstained with DAPI. Scale bar: 100  $\mu$ m.

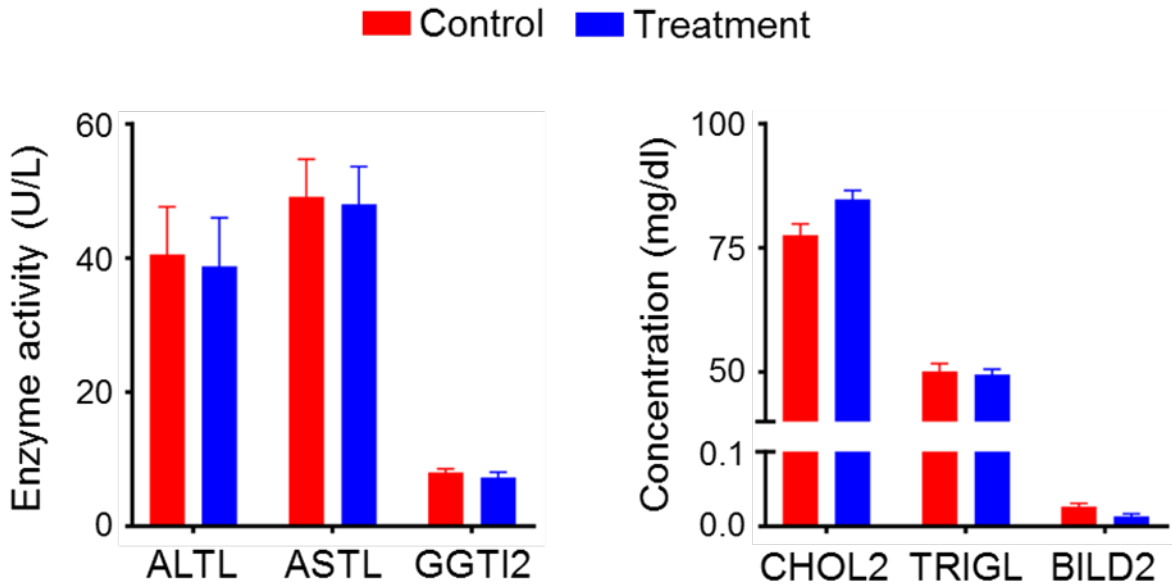


**Figure 3.19 Assessment of liver functions in AAV2-GEC-IdeS treated mice.** Liver functions were evaluated in mice serum from treatment (AAV2-GEC-IdeS) and control (AAV2-GEC-GFP) groups. No statistically significant differences were found.

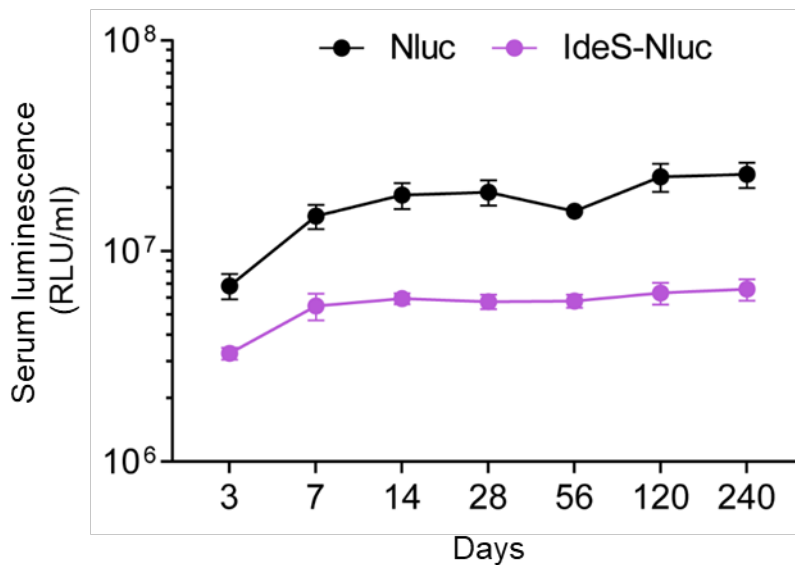


**Figure 3.20 Serum IdeS concentration in AAV2-GEC-IdeS mice.** C57BL/6J mice were injected intravenously with AAV2-GEC-Nluc (shown as Nluc) and AAV2-GEC-IdeS-Nluc (shown as IdeS-Nluc). The serum IdeS concentration was measured by the luminescence at 3, 7, 14, 28, 56, 120 and 240 days after injection.

### **3.3 Characterization of AAV9-GGNYGLG**

#### **3.3.1 AAV9-GGNYGLG specifically targeted the distal tubule adjacent to the JGA**

To evaluate the in vivo transduction profile of the AAV9-GGNYGLG variant, we generated a single-stranded (ss) AAV reporter vector, which contained the GFP cDNA driven by the constitutive CMV promoter. The AAV vector was intravenously injected into 8-12 weeks old C57BL/6J mice with a dose of  $1E+11$  vg per mouse ( $n = 3$ ). After 14 days, the transgene expression was analyzed in different organs. AAV9-GGNYGLG obviously transduced the TAL cells adjacent to the glomerulus, which were recognized as the JGA (Figure 3.21A). We thus termed this variant as AAV9-JGA. The targeting specificity and transduction efficiency of AAV9-JGA were compared to its parental wild-type AAV9 (AAV9-WT). Both AAV9-JGA and AAV9-WT transduced the TAL cells adjacent to the JGA in the kidney, but AAV9-JGA showed a greater fluorescence intensity and higher specificity, while AAV9-WT also transduced the glomerular cells (Figure 3.21B).

AAV9-WT injected mice showed strong GFP expression in the liver, but AAV9-JGA injected mice showed a much weaker GFP expression in the liver. AAV9-JGA mediated a stable GFP expression and the fluorescence intensity was maintained over 360 days after intravenous injection (Figure 3.22). Taken together, AAV9-JGA mediated specific targeting and efficient transduction to TAL cells adjacent to the JGA.

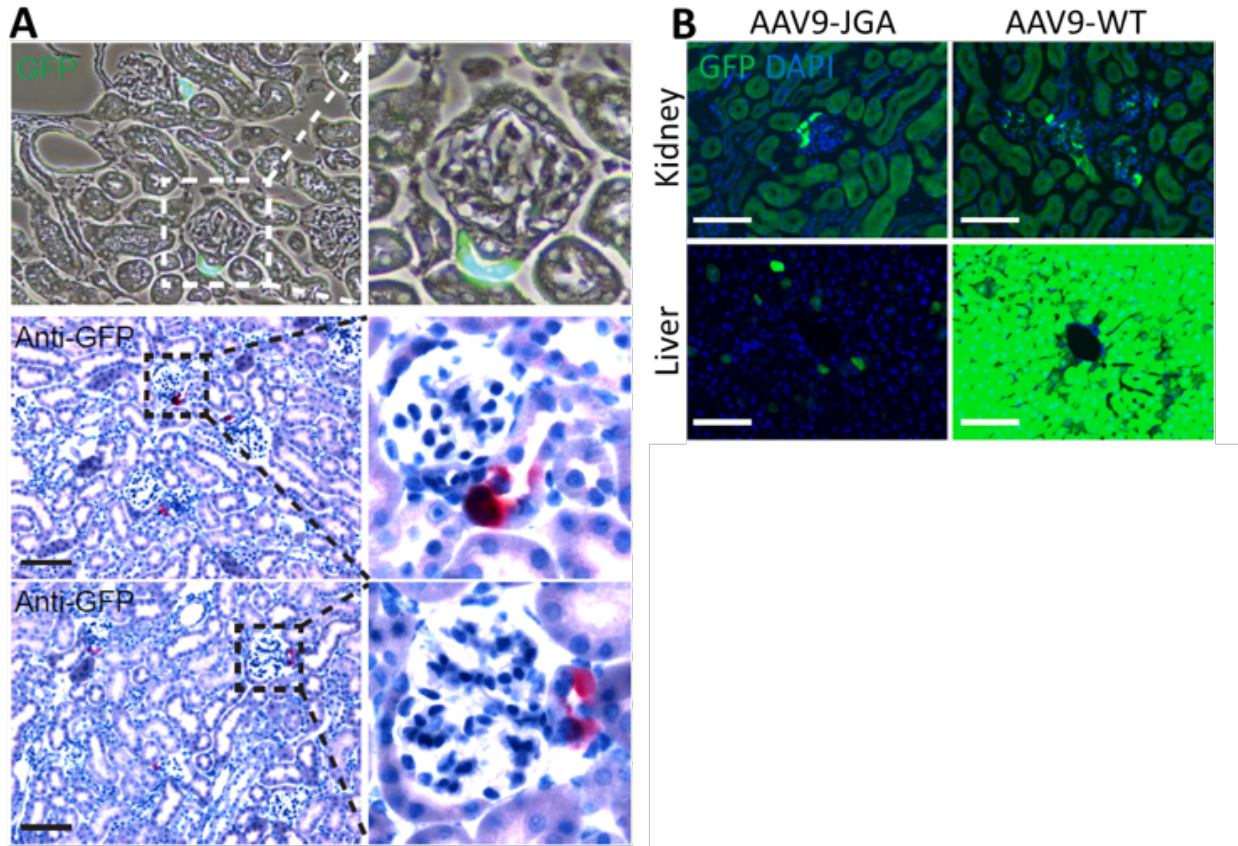


**Figure 3.21 AAV9-JGA specifically targeting TAL adjacent to the JGA in the kidney. (A)** Images of AAV9-JGA-mediated GFP expression in the kidney. Bright-field microscopy and immunohistochemistry staining against GFP indicated that AAV9-JGA specifically targeted TAL adjacent to JGA. Scale bar: 100  $\mu$ m. **(B)** Images of AAV9-JGA-mediated GFP expression in the kidney and off-target organs (liver, heart, and pancreas) compared with AAV9-WT-mediated GFP expression. Nuclei were counterstained with DAPI. Scale bar: 100  $\mu$ m. TAL: Thick ascending limb, JGA: Juxtaglomerular apparatus, WT: Wildtype.

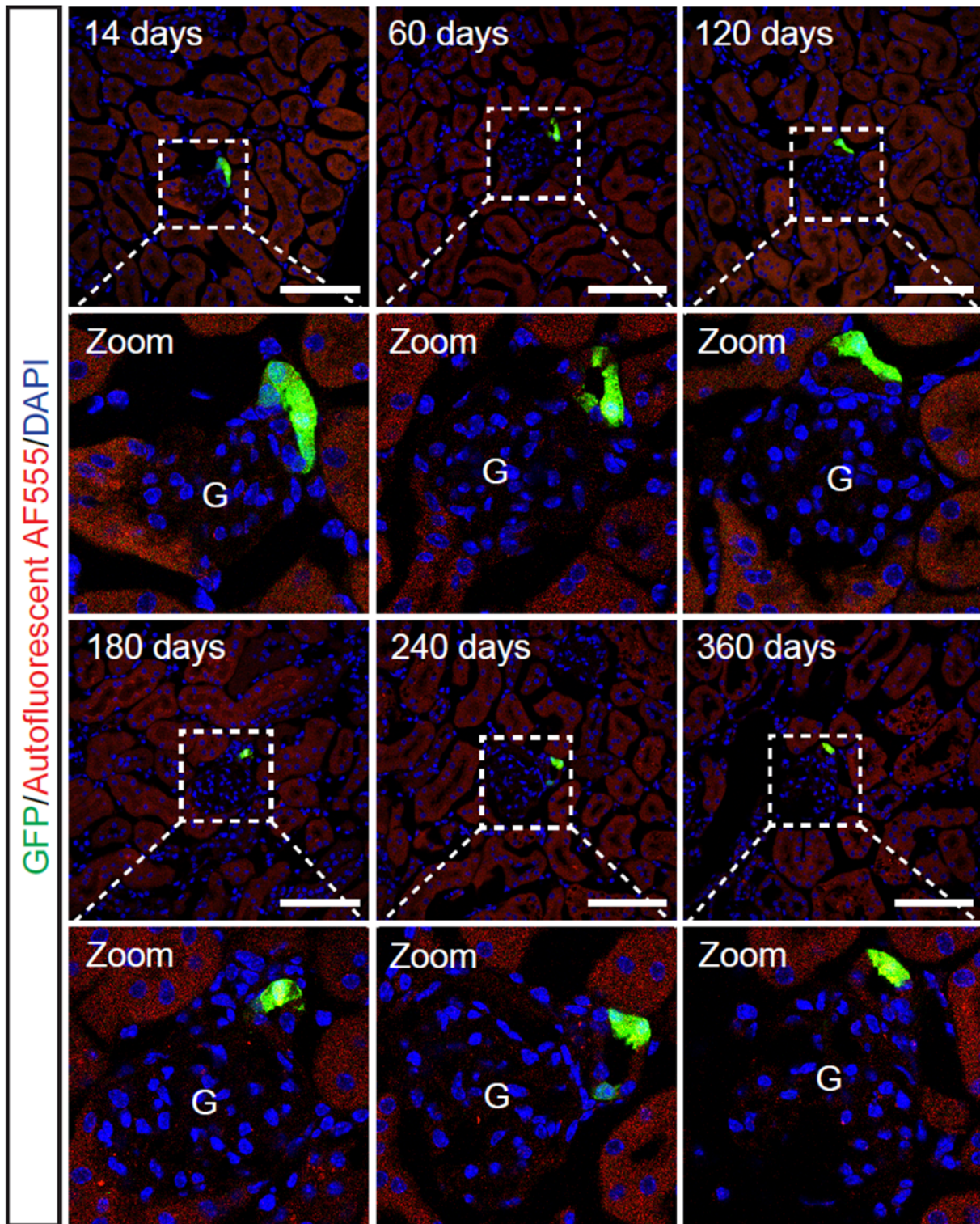


**Figure 3.22 AAV9-JGA mediated GFP expression over prolonged periods in the kidney.** Images of AAV9-JGA-mediated GFP expression in the kidney over 360 days. G indicates a glomerulus. Scale bar: 100  $\mu$ m.

### 3.3.2 AAV9-JGA specifically targeted a subset of the TAL at the JGA

To further characterize which cell type was transduced by AAV9-JGA, immunofluorescent (IF) staining was performed on the kidney sections of AAV9-JGA-GFP injected mice. Vector-mediated GFP expression was detected in the TAL cells, which were marked by Solute Carrier Family 12 Member 1 (SLC12A1), whereas no GFP expression could be detected in the macula densa marked by for nitric oxide synthase 1 (NOS1) or granular cells (GC) marked by for Renin (Figure 3.23A).

Interestingly, we observed that AAV9-JGA transduced only a part of the TAL epithelia. TAL was reported as a nephron segment that reabsorbs Na<sup>+</sup>, Ca<sup>2+</sup>, and Mg<sup>2+</sup> via the claudins mosaic pattern of tight junction paracellular pathway<sup>180</sup>. Recent single-cell data identified three distinct cell subtypes of the TAL: MD cells, Claudin-10 (Cldn10) positive cells, and Claudin-16 (Cldn16) positive cells<sup>181</sup>. IF staining showed that AAV9-JGA transduced the cells co-stained with CLDN16 but not with CLDN10 (Figure 3.23A). Cell types existing in the JGA are illustrated in Figure 3.23B. Taken together, AAV9-JGA specifically targeted a subset of the TAL epithelial cells adjacent to the JGA, which were characterized as SLC12A1/CLDN16-positive cells.

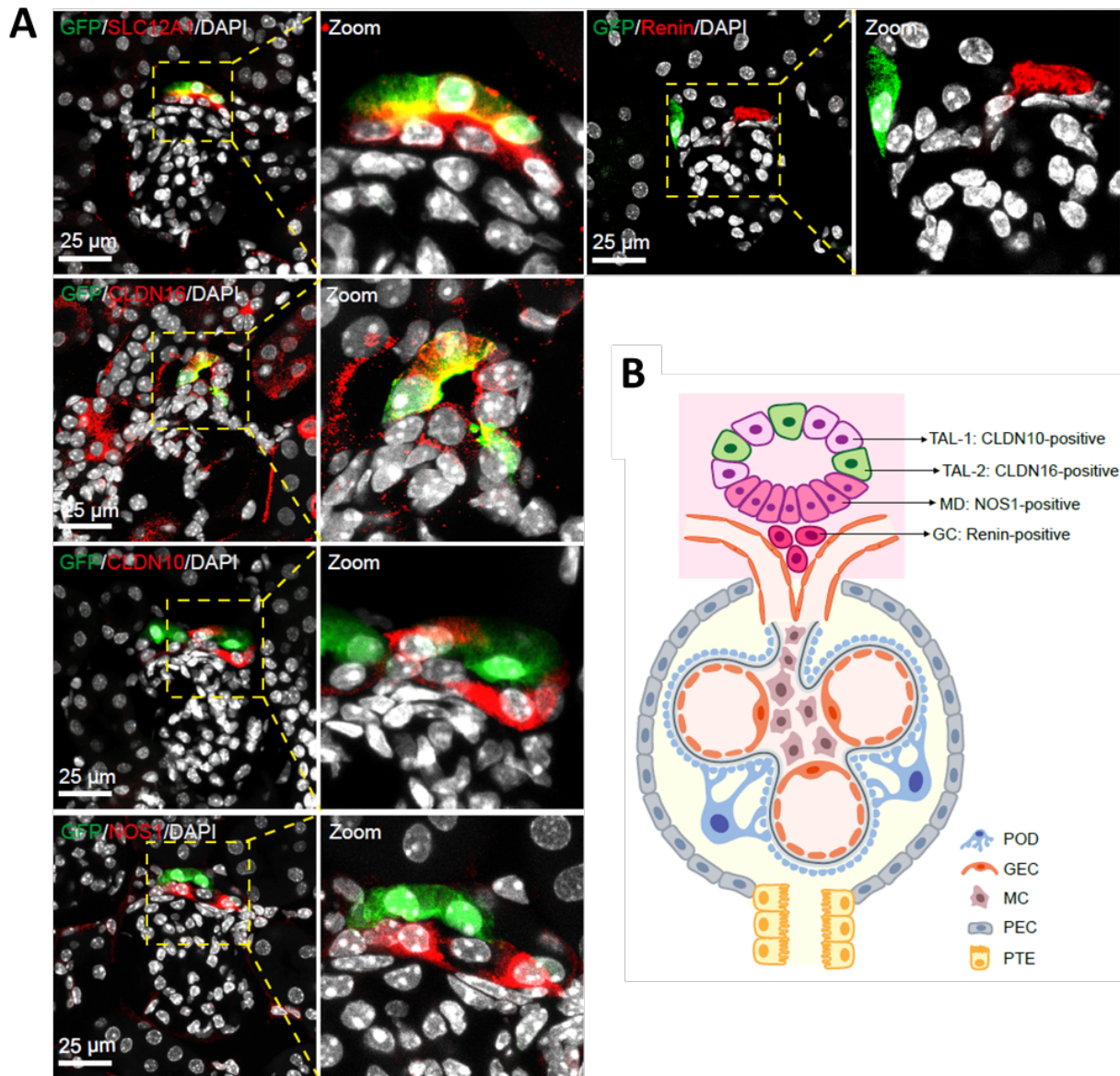


**Figure 3.23 AAV9-JGA specifically targeted Slc12a1-Cldn16-positive cells in TAL at the JGA. (A)** Images of AAV9-JGA-mediated GFP expression in the kidney. The TAL cells were marked by anti-SLC12A1 antibody. The MD cells were marked by anti-NOS1 antibody. The GC cells were marked by anti-Renin antibody. **(B)** The scheme shows the different cell types in the JGA and the renal corpuscle. MD: Macula densa, GC: Granular cells, POD: Podocytes, GEC: glomerular endothelial cells, MC: Mesangial cells, PEC: Parietal epithelial cells, PTE: Proximal tubular epithelial cells. The subtype cells of TAL were marked by anti-CLDN16 and anti-CLDN10 antibodies. Nuclei were counterstained with DAPI.

### **3.3.3 The SLC12A1/CLDN16-positive TAL cells at the JGA is generally susceptible to AAV transduction**

Previous studies have reported transduction of the distal tubule epithelia adjacent to the glomerulus after intravenous injection of wild-type and synthetic AAVs <sup>167</sup>. Ikeda et al. showed that the synthetic AAV (Anc80) always transduces a subtype of epithelia found in a tubule adjacent to the glomerulus, which is positive for SLC12A1 but negative for NOS1 and Renin <sup>167</sup>. These findings are consistent with the results in the current study. It raises the question, whether this subset of TAL at the JGA is generally susceptible to AAV transduction.

Thus, we intravenously injected mice with AAV serotypes 1-9 and AAVrh.10 expressing GFP. Kidney tissues were analyzed two weeks after injection. Interestingly, all the AAV serotypes transduced the subset of SLC12A1-positive TAL at the JGA, though they exhibited diverse intensities of GFP expression (Figure 3.24A). When compared to the AAV9-JGA selected in this current study, all AAV serotypes exhibited substantially less transduction specificity, as they also transduced the cells in the glomerulus and the other part of the tubule epithelia (Figure 3.24A). The cells transduced by these natural AAV serotypes were also negative for CLDN10 (Figure 3.24B). These results suggest that a subset of TAL at JGA is generally susceptible to AAV transduction.

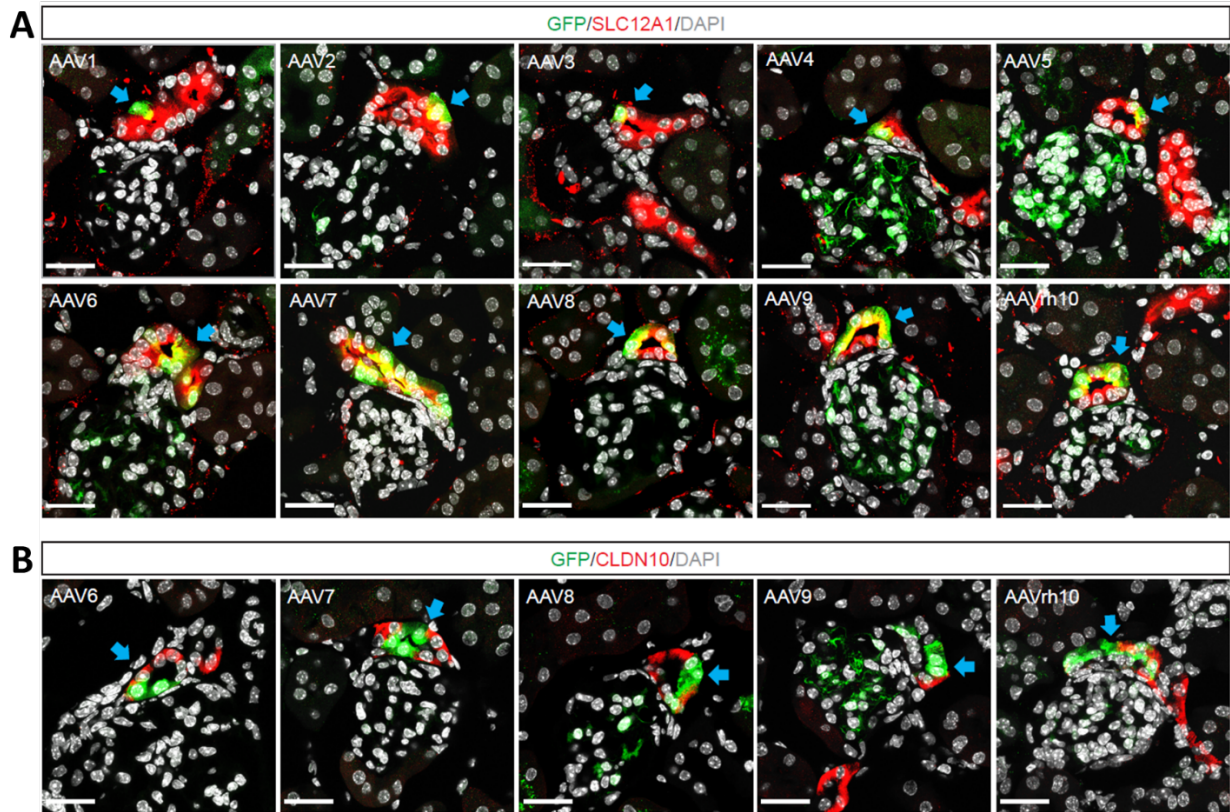


**Figure 3.24 AAV serotypes exhibited transduction of a subset of TAL at JGA. (A)** Images of AAV (serotype 1-9 and rh10)-mediated GFP expression in the kidney. All of the AAV serotypes transduced a subset of TAL adjacent to JGA. Arrows indicate co-localization of GFP with TAL marker SLC12A1. **(B)** Images of AAV (serotype 6/7/8/9- and rh10)-mediated GFP expression. GFP-positive cells were negative for CLDN10. Nuclei were counterstained with DAPI. Scale bar: 25  $\mu$ m.

### 3.3.4 AAV9-JGA targeted TAL cells through tubule-afferent arteriole contact

AAV9-JGA exhibited significantly higher and stronger transduction specificity and efficiency at the JGA than the AAV serotypes. Importantly, immunohistochemistry indicated that the GFP-positive cells were always contacted the arteriole joining the glomerulus, which was recognized by morphology and labeled by the endothelium and vascular smooth muscle markers CD31 (also known as PECAM-1: platelet endothelial cell adhesion molecule) and alpha-smooth muscle actin ( $\alpha$ SMA), respectively (Figure 3.25A). The anatomical contact between the distal nephron and the afferent arteriole of the same nephron (hereafter referred to as tubule-afferent arteriole contact) has been

suggested to play an important role in renal autoregulation<sup>182-184</sup>. Since AAV9-JGA and AAV serotypes were systemically administered in mice, we suspect that AAVs may preferentially reach the TAL cells at the JGA through tubule-afferent arteriole contact in the kidney.

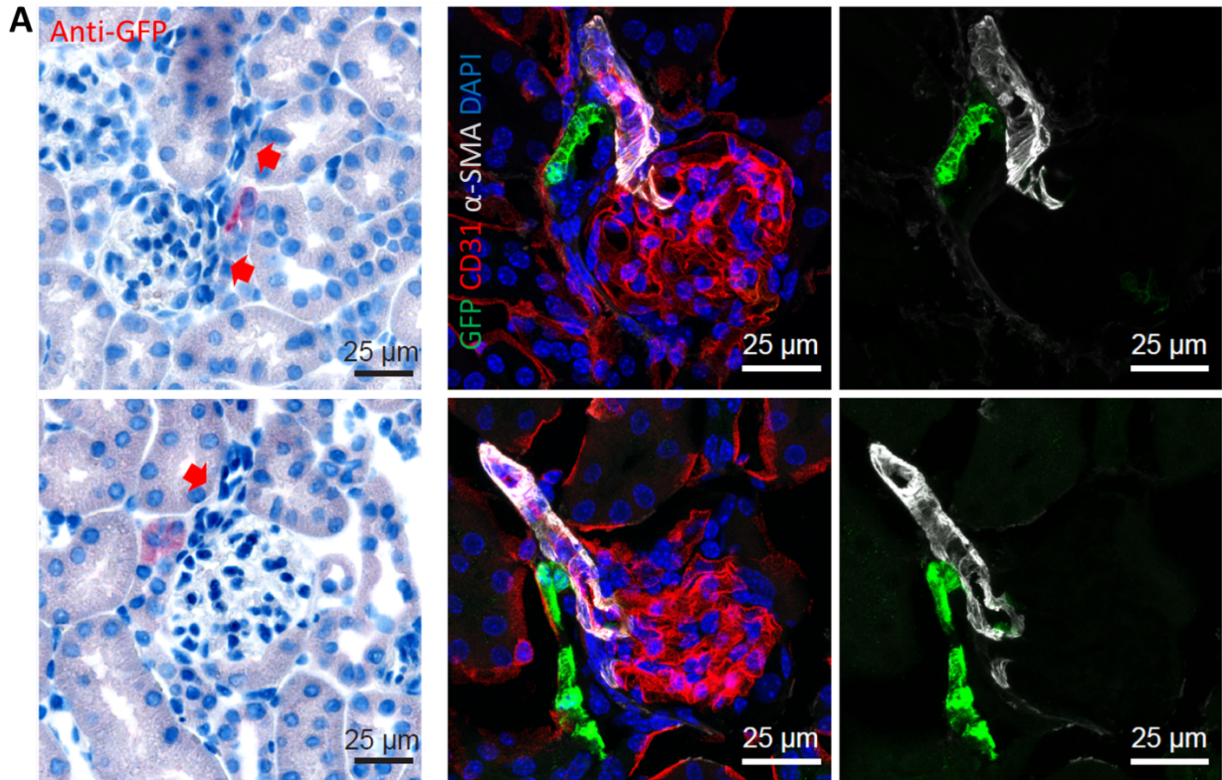


**Figure 3.25 (A) AAV9-JGA targeted the TAL cells through the tubule-afferent arteriole contact.** (A) AAV9-JGA-mediated GFP expression in mouse kidneys. Left panel: GFP was stained in red. Arrows indicate the direct contact of AAV9-JGA-targeted TAL cells with the afferent arteriole. Right panel: Endothelial cells were marked by anti-CD31 antibody, and vascular smooth muscle cells were marked by anti- $\alpha$ SMA antibody. Nuclei were counterstained with DAPI.

To determine the possible transduction route, we intravenously injected mice with AAV9-JGA and investigated the kidneys by electron microscopy (EM) 1.5 h after injection. The area of the JGA was studied, including the junction of the afferent arteriole (AA) and glomerulus, the MD cells adjacent to the glomerulus, and the targeted TAL cells on the opposite site of the MD (Figure 3.25B, upper left panel). We found vesicle-like structures approximately 27 nm in diameter in the region between the AA endothelium and the TAL basement membrane (Figure 3.25B, upper right panel). Notably, we observed

fenestration of the AA endothelium in this area (Figure 3.25B, lower panel). To further confirm that these vesicle-like structures were AAVs, we used anti-AAV9 capsid antibody to label the injected AAV9-JGA. As expected, we found AAV particles in the TAL basement membrane adjacent to the AA (Figure 3.25C).

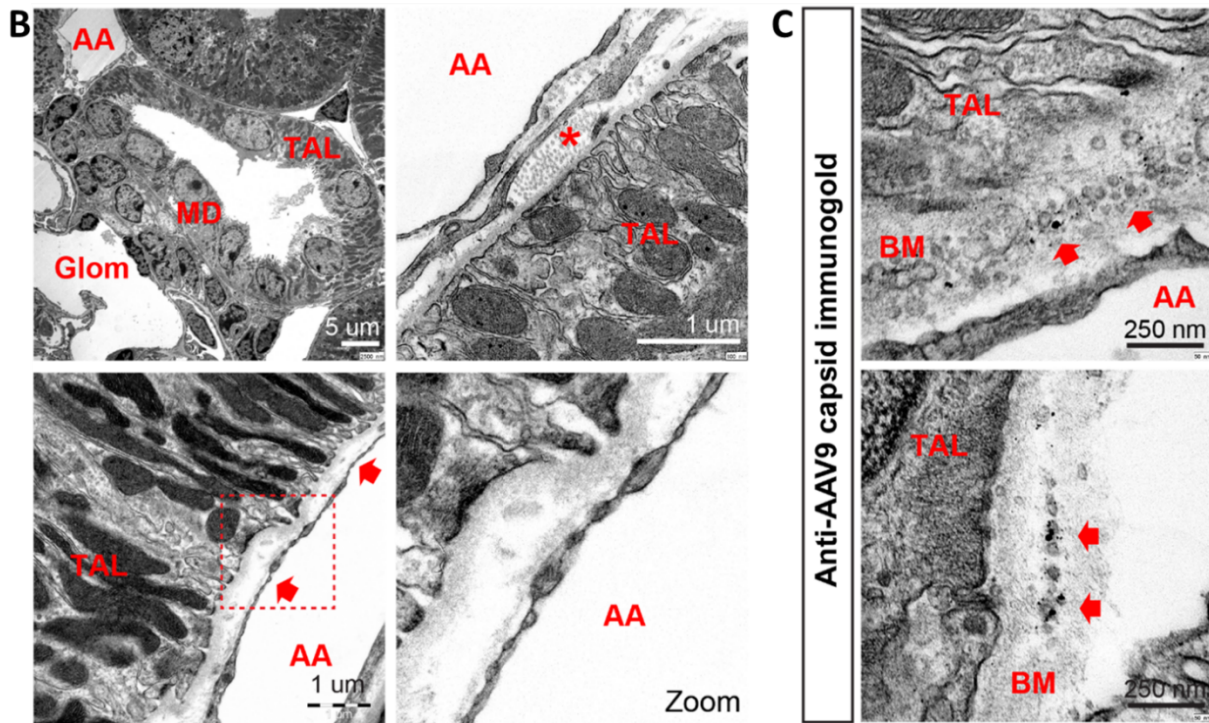


**Figure 3.25 (B&C) AAV9-JGA targeted the TAL cells through the tubule-afferent arteriole contact. (B)** After 1.5 h AAV9-JGA intravenous injection, mouse kidneys were investigated by electron microscopy. The area of interest demonstrating the JGA including the joint point of the afferent arteriole (AA) to the glomerulus (Glom), macula densa cells adjacent to the glomerulus, and the targeted thick ascending limb in the opposite site to MD. AAV particles (\*) were found in the region between the AA endothelium and the TAL basement membrane (BM). Arrows indicate the fenestrated endothelium of the AA. Asterisk indicates AAV particles. The dotted line square indicates the zoom area. **(C)** Anti-AAV9 capsid immunogold staining confirmed the AAV9-JGA particles in the TAL basement membrane adjacent to the AA.

Since the structure of JGA is conserved in mammals including humans<sup>185</sup>, the AAV9-JGA could also target this subset of TAL cells at the JGA in other mammals. We intravenously injected AAV9-JGA GFP into SD rats. As expected, GFP-positive cells were found in the subset of the TAL cells at the JGA, which contacted the blood vessel at the junction of the AA and glomerulus (Figure 3.26).

These observations suggest that the circulating AAV9-JGA probably passed through the fenestrated endothelium of the AA at the JGA, thereby entered the kidney and reached the TAL cells through the tubule-afferent arteriole contact.

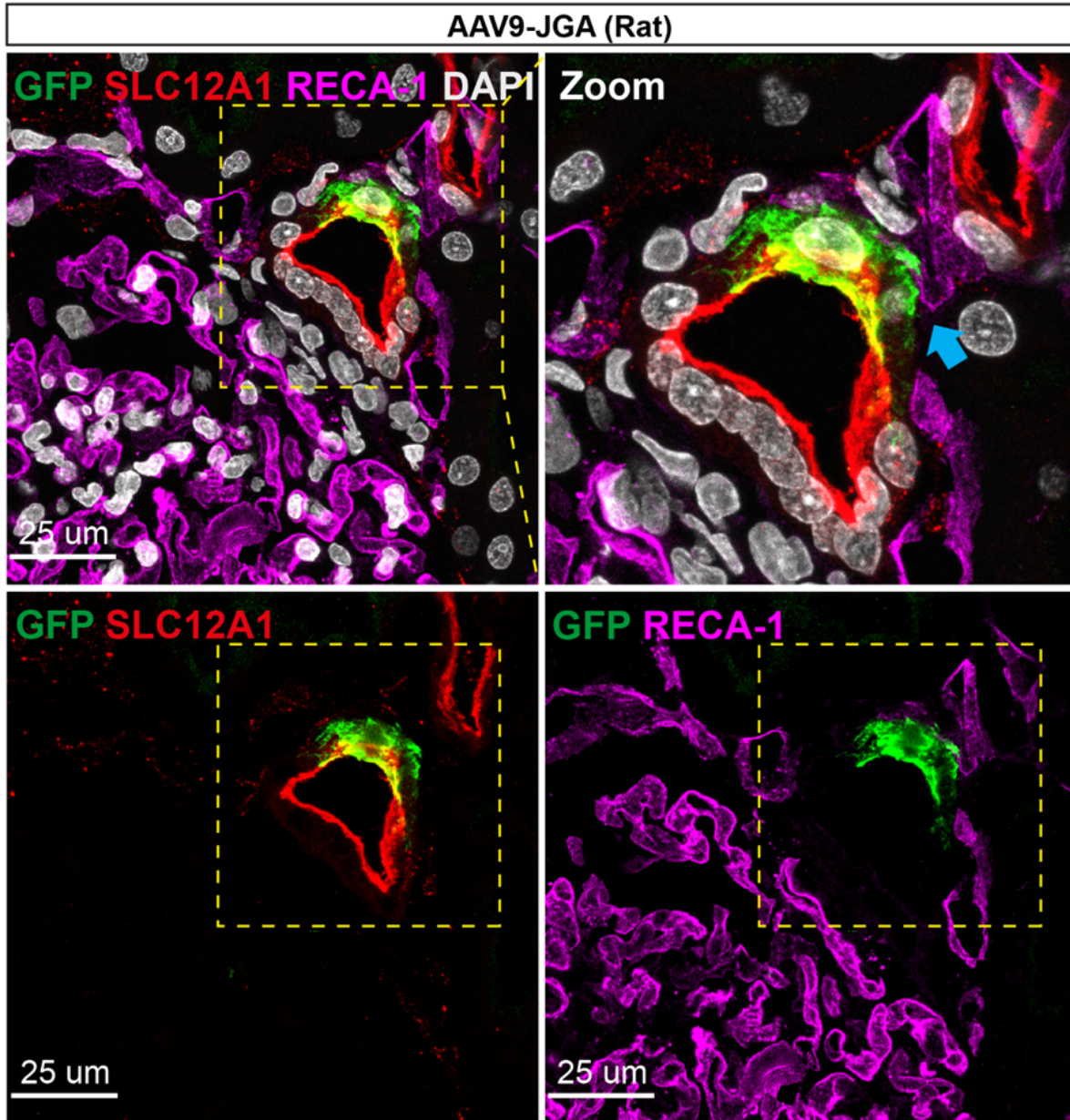


**Figure 3.26 AAV9-JGA transduced the same subtype of TAL cells in rat kidneys.** AAV9-JGA-mediated GFP expression in rat kidneys. TAL was marked by anti-SLC12A1 antibody. Rat endothelium was marked by anti-RECA-1 antibody. Nuclei were counterstained with DAPI. Arrows indicate the direct contact of AAV9-JGA transduced TAL cells with the blood vessel at the joint point of the afferent arteriole and the glomerulus.

## 4 Discussion

### 4.1 Overview

The current generation of viral vector gene therapy represents the culmination of decades of biological and clinical research. To date, the challenges restrict the applicability of viral vectors mainly in three aspects: safety, efficiency, and specificity<sup>148</sup>. Among these viral vectors, AAV has proven to be safe and effective in a broad range of therapeutic applications for a variety of diseases due to its unique biological and biophysical properties<sup>125</sup>. AAV can be engineered for very specific functionality in gene therapy applications. One of the engineered applications is the random display peptide libraries, which have proven to be a powerful tool for generating cell-specific vectors in a number of organs and tissues such as the central nervous system, lung and heart<sup>117-122,124,186</sup>. In contrast, the kidney currently lacks effective viral vectors and remains virtually unavailable for gene<sup>152</sup>. Here, we focused our efforts on optimizing previously established in vivo screening protocol of the random AAV display peptide libraries<sup>171</sup> in kidneys to generate efficient kidney cell-specific viral vectors. We developed a selection protocol specifically for kidneys and screened random AAV2 and AAV9 display peptide libraries in vivo. By integrating the experimental and bioinformatics workflows, we identified two AAV variants termed AAV2-GEC and AAV9-JGA, which specifically and efficiently transduced the glomerular endothelium and a subset of the distal tubule epithelium in the kidney, respectively. AAV2-GEC exhibited robust GEC tropism in C57BL/6J, Balb/c mice and SD rats, as well as in disease models causing GEC damage. The potential of AAV2-GEC for kidney-targeting therapy was evaluated by delivering to the GEC an antibody-cleaving enzyme, which successfully eliminated the kidney-bound IgG, thereby prevented the progression of glomerulonephritis. AAV9-JGA transduced the CLDN16/SLC12A1-positive cells of the TAL at the JGA, and maintained robust tropism in C57BL/6J mice and SD rats. We demonstrated that AAV9-JGA reached the TAL through the tubule-afferent arteriole contact after systemic administration, indicating that AAVs can directly reach the tubular segments from the bloodstream without crossing the glomerular filtration barrier.

## **4.2 The selection and NGS analysis processes of the random AAV display peptide library**

The screening of the random AAV display peptide library involves multiple steps and is a veritable “survival of the fittest” approach<sup>187</sup>. The acquisition of promising AAV vector variants is determined by the selection process itself, with the parameters such as the dose of AAV particles administered in each round of screening, the circulation time of the virus in vivo, and the selection pressure applied in the target tissues, etc. Therefore, the screening process should be appropriately optimized for the target tissue. Compared with other organs, the kidney has a complex anatomical structure with more than 26 different cell types<sup>152</sup>, which makes it difficult to obtain kidney-specific vectors from the screening. In contrast, many previous AAV capsid selections have applied whole-organ viral DNA rescue methods to identify capsid variants<sup>117,118,121</sup>. In the present study, we adapted the screening protocol<sup>171</sup> and increased the selection pressure by separating kidneys into the glomerular and tubular compartments for further screening. This increased selection pressure have significantly contributed to the identification of AAV9-JGA and the AAV2-GEC variants in independent trials. If the whole kidney or only one specific cell type was used for selection rounds, this AAV vector would be ignored or excluded, especially for AAV9-JGA, which targets a very small population of cells in the kidney. In addition, the AAV circulation days in vivo were extended in the third and fourth rounds of selection to better eliminate unspecific particles. These optimized selection strategies resulted in a dramatically reduction in library diversity during the selection process. However, a large number of variants were still present in the final enrichment round, making it difficult to identify the most promising candidates. Previous studies of in vivo selection of AAV libraries<sup>118,121</sup> and the NGS data presented here suggest that the final abundance of relevant clones may not be commensurate with their transduction efficiency and specificity for the tissue of interest. In this study, we can quickly assess a large number of variants by using the NGS scoring system<sup>121</sup> which allowed us to identify valuable vectors by evaluating enriched clones for targeted transduction efficiency and specificity. Of note, after four rounds of selection, these two variants only accounted for less than 3% of all NGS reads in the kidney, but the AAV2-GEC and AAV9-JGA had the highest C

scores. Subsequent verification of AAV2-GEC and AAV9-JGA tropism in vivo was also consistent with the scoring, especially the GS scores of off-target organs directly determines which candidates stand out. Our results confirmed the generalizability of this scoring system in the identification of target-specific vectors in vivo.

#### **4.3 The potential of AAV2-GEC as a gene manipulation tool.**

AAV2-GEC maintained robust tropism in GECs of C57BL/6J, Balb/c and BTBR mouse strains, as well as in SD rats. It also maintained robust tropism under different pathological conditions. It is well known that endothelial cells exhibit significant differences in gene expression between species even in the identical vasculature<sup>188</sup>. These potential inter-species differences may result in AAV variants selected in a particular mouse strain not expanding to other strains or species, or translating to humans<sup>188</sup>. Additionally, EC gene expression differs under physiological and pathological conditions. In the kidney, GEC is sensitive to pro-inflammatory factors, pro-thrombotic mediators, and the disruption of glycocalyx<sup>173</sup>. DKD is a typical chronic kidney disease that causes damage to GEC. Hyperglycemia, oxidative stress and binding of advanced glycation end products (AGEs) promote glycocalyx disruption and result in the loss of GEC fenestrae<sup>173</sup>. The intercellular crosstalk between podocytes and GEC contributes to the pathogenesis of various glomerular diseases<sup>189</sup>. Especially, abnormal secretion of VEGF by stressed podocytes leads to GEC de-differentiation and dysfunction<sup>189,190</sup>. Thus, DKD and podocyte-injury models, causing significant changes in GEC phenotypes and also their tropisms, are suitable to evaluate the targeting specificity of AAV2-GEC in pathological settings. Our results indicate that AAV2-GEC has conserved GEC tropism under both physiological and pathological conditions at least among rodents. It is important to test the targeting specificity of AAV2-GEC in larger animals and non-human primates to evaluate its translational potential in the future.

GEC are a primary target for therapeutic interventions in kidney genetic diseases, as well as in the context of anti-inflammation, inhibition of coagulation, and protection of glycocalyx in glomerular diseases<sup>190-192</sup>. Many gene defects have been identified in GEC.

Most of these genes participate in the complement pathway underlying the pathogenesis of atypical hemolytic uremic syndrome (aHUS) and C3-dominant glomerulopathy<sup>193,194</sup>. Mutations in factor H (CFH), factor I (CFI), C3, factor B (F8), membrane cofactor protein (MCP), and thrombomodulin (THBD) contribute to 50% of all aHUS cases<sup>195</sup>. Two non-complement genes, diacylglycerol kinase epsilon (DGKE) and inverted formin 2 gene (INF2), can cause childhood onset of aHUS, which are also related to steroid-resistant nephrotic syndrome<sup>196,197</sup>. GEC play an essential role in maintaining the GFB, actively interact with podocytes and mesangial cells, as well as directly contact the circulating factors from the bloodstream<sup>173,198</sup>. Therefore, GEC are a therapeutic target to improve their own cellular functions, such as the modification of gene defects, and the preservation of glycocalyx, which is a key for the treatment of DKD and focal segmental glomerulosclerosis<sup>198</sup>. Importantly, GEC can also be used as a bio-factory to produce and distribute therapeutic molecules such as enzymes, to intervene the functionability of neighboring cells or to prevent the pathogenesis in glomeruli. This concept could be especially useful for the treatment of kidney autoimmune diseases, such as lupus nephritis, IgA nephropathy and anti-GBM disease<sup>190</sup>. Since inflammation and coagulation are common complications in the kidney leading to the decline in the glomerular filtration rate and ultimately kidney failure, efficient removal of pathogenic antibodies depositing on the GFB is critical for the preservation of kidney function<sup>190</sup>.

To proof the feasibility of this concept, we used AAV2-GEC to deliver IdeS in the GEC for the treatment of glomerulonephritis. IdeS is a streptococcal IgG-degrading enzyme, which showed remarkable ability in cleaving circulating antibodies in experimental anti-GBM glomerulonephritis<sup>199</sup>, and has been tested in a phase II trial in severe anti-GBM disease<sup>200</sup>. Anti-GBM glomerulonephritis is a subtype of autoimmune glomerulonephritis caused by the presence of antibodies against the type IV collagen alpha 3 chain in the GBM<sup>190</sup>. Removal of kidney-bound and circulating antibodies at a rapid pace is essential for the treatment of anti-GBM glomerulonephritis to prevent the progression to end-stage kidney failure<sup>201</sup>. AAV2-GEC delivery of IdeS in the GEC efficiently produced IdeS in the kidney, and sufficiently cleaved anti-GBM IgG, thereby successfully prevented the progression of anti-GBM glomerulonephritis. Compared to the one-dose infusion of IdeS in patients, which cleaves and removes IgG within 6 hours<sup>200</sup>, AAV2-GEC-mediated IdeS expression

took around 3 days in mice, and the serum concentration of IdeS peaked at 7 days after intravenous injection. It is important to note that unlike in humans, experimental anti-GBM glomerulonephritis induces transient phenotypes and presents a recovery course after one week in mice<sup>199</sup>. Thus, the AAV2-GEC-IdeS had to be injected before the induction of anti-GBM glomerulonephritis to evaluate the treatment effects, which is a limitation of this study.

Notably, one-dose infusion of IdeS cannot prevent the occurrence of rebound antibodies, and the majority of patients will need additional sessions of plasma exchange or immunoadsorption after one week<sup>200,201</sup>. A second dose of IdeS is currently not suggested due to the concerns for anti-IdeS antibodies and immune complex-mediated hypersensitivity<sup>86,200,201</sup>. Interestingly, in AAV2-GEC-IdeS injected mice, the serum IdeS was maintained at a comparable level measured at 7 days for over 240 days, suggesting that IdeS secreted by GEC was not neutralized by antibodies and the transduced GEC were not eliminated by the immune system. Moreover, the prolonged and sustained expression of IdeS mediated by GEC may provide a solution to remove rebound antibodies. Taken together, this proof-of-concept experiment suggests the therapeutic potential of AAV2-GEC, which targets GEC not only for kidney genetic diseases but also for multiple other kidney diseases. For the translational use in the future, vector engineering works will be useful to enable the improvement of the expression efficiency and the precise regulation of the cargo gene expression in pathological settings.

In conclusion, this study establishes an AAV *in vivo* screening approach for renal glomeruli. It identifies a novel GEC-targeting AAV vector with robust tropism maintained cross species in both physiological and pathological settings. The identification of AAV-GEC demonstrates the feasibility of future GFB-targeting strategies for novel kidney therapies.

#### **4.4 The potential of AAV9-JGA as a gene manipulation tool.**

We identified a new vector, AAV9-JGA, which efficiently and specifically targets CLDN16/SLC12A1-positive cells of the TAL at the JGA after systemic administration.

AAV9-JGA mediates prolonged GFP expression in the CLDN16/SLC12A1-positive cells with lower off-target organ transduction. Importantly, the AAV9-JGA-targeted TAL cells at the JGA are CLDN16-positive but not CLDN10-positive, suggesting that these two types of TAL cells exhibit different characteristics. Previous studies revealed the mosaic expression pattern and delineated the anatomical distribution of CLDN16 and CLDN10 in human and rodent kidneys<sup>180,181,202</sup>. CLDN16 is primarily expressed in the kidney, especially in TAL of the nephron, where it is responsible for the paracellular transport of the majority of divalent cations such as Mg<sup>2+</sup> and Ca<sup>2+</sup><sup>203,204</sup>. CLDN10 has two splice variants, -10a and -10b, which are predominantly found in the proximal tubule and TAL, respectively<sup>204,205</sup>. Consensus studies suggest that CLDN10b independently regulates Na<sup>+</sup> by increasing paracellular permeability, whereas the function of CLDN10a remains unclear<sup>180,202,205</sup>. CLDN16 heritable mutations are associated with familial hypomagnesemia with hypercalciuria and nephrocalcinosis (FHHNC), which leads to end-stage renal disease in humans<sup>204</sup>. CLDN16-deficient mice are defective in paracellular cation selectivity and suffer from severe renal magnesium and calcium wasting<sup>206</sup>, which explains the devastating phenotype of FHHNC patients. Claudin-10b mutations in TAL lead to HELIX syndrome, which is characterized by hypohidrosis, electrolyte imbalance, lacrimal gland dysfunction, ichthyosis, and xerostomia<sup>204</sup>.

The single-cell study<sup>181</sup> showed that TAL subtypes express distinct marker genes, some of which encode plasma membrane proteins. It is unclear which plasma membrane proteins function as receptors and contribute to the binding of AAV9-JGA to CLDN16-positive TAL cells, but the tropism is likely to play a role in transduction selectivity. In the future, we will perform single-cell RNA sequencing to further characterize the difference between the CLDN10- and CLDN16-positive TAL cells.

TAL rejoins its parent glomerulus, forming a JGA region that serves as a specific functional coupling framework between tubule and vascular elements<sup>140</sup>. Communication between tubules and glomeruli is critical for maintaining renal homeostasis, particularly tubuloglomerular feedback (TGF), which regulates glomerular filtration rate and renal hemodynamics<sup>184</sup>. Increasing evidence reports renal protection after kidney disease-targeted interventions, such as renin–angiotensin–aldosterone system (RAAS)

modulators and sodium-glucose cotransporter 2 (SGLT2) inhibitors, indicating the importance of intraglomerular pressure reduction via TGF, which is essential for the preservation of kidney function <sup>207</sup>. However, therapeutic approaches particularly targeting TGF are absent, since the JGA represents a very small population in the kidney and the mechanisms of TGF have not been fully elucidated. AAV9-JGA could be a useful tool for basic research, and its therapeutic potential needs to be further investigated in the future.

#### **4.5 A possible route of AAV9-JGA transduction of TALs after intravenous injection**

Previous studies and our own research have shown that several AAV serotypes can transduce a subset of SLC12A1-positive TAL cells at the JGA. This suggests that the TAL cell subpopulation at the JGA is generally susceptible to AAV transduction following intravenous injection. Our findings demonstrate that the circulating AAV9-JGA probably enters the kidney by passing through the fenestrated endothelium of the AA at the JGA, thereby reaches the TAL cells through tubule-afferent arteriole contact.

Notably, we found that AAV serotype transduction in TAL cells appears to be route dependent, as no evidence of TAL transduction by AAV serotypes has been found in non-intravenous renal injection models <sup>153,160</sup>. After intravenous injection, AAVs in the bloodstream circulate into the kidney via the renal artery, reach the nephron and enter the glomerulus through the afferent arteriole. Since the glomerular filtration barrier (GFB) selectively filters blood solutes with molecular weights less than 50 kDa and diameters less than 7 nm <sup>133</sup>. AAV, which has a capsid diameter of approximately 25 nm, has been suggested to be unlikely to pass through the GFB but to instead get stuck in the glomeruli and recirculated into the bloodstream from the efferent arteriole of the glomerulus <sup>152</sup>.

Physical contacts between TAL and AA of the same nephron in the region of the MD plaque (a part of the distal tubule) are frequently observed in the renal cortex. Recent studies suggest that these contacts may be involved in TGF <sup>182-184</sup>. Besides, the AA itself exhibits a heterogeneous morphology in the renal cortex <sup>208,209</sup>. In mammals, including humans, the proximal AA is composed of a non-permeable endothelium, whereas the

endothelium of the juxtaglomerular (distal) AA has uneven pores ranging from 60 to 240 nm in diameter<sup>185,209,210</sup>. These pores are structurally similar to glomerular endothelium but lack glycoprotein diaphragms<sup>185,210</sup>. Therefore, we hypothesized that the juxtaglomerular AA fenestrae may facilitate the entry of AAV from the bloodstream into the renal tubule. Consistently, we found that AAV9-JGA-mediated GFP expression was always neighboring AA in the kidney and that AAV9-JGA particles appeared between the AA endothelium and the TAL basement membrane shortly after intravenous injection. Since the AAV9-JGA specifically transduced CLDN16/SLC12A1-positive but not CLDN10-positive TAL subtype at the JGA, although they exhibit mosaic expression patterns in this area, suggesting the unique cell entry receptor in the CLDN16/SLC12A1-positive cells. In conclusion, our findings reveal a natural AAV transduction route in the kidney. AAV9-JGA specific transduction of CLDN16/SLC12A1-positive TAL cells is determined by a combination of anatomical features of JGA and its tropism.

#### **4.6 Outlook**

In this project, we described for the first time two novel kidney-specific AAV variants, which specifically target CLDN16/SLC12A1-positive cells of the TAL at the JGA and the glomerular endothelial cells, respectively. Our findings support the cross-species transduction of these AAV variants in rodents. As preclinical validation, future studies in larger animals are necessary to test whether AAV9-JGA and AAV2-GEC have potential in the clinic.

GECs pose a potential efficacious cellular target to halt disease development and progression in kidney diseases<sup>211</sup>. Aberrant gene expression patterns largely contribute to GECs dysfunction, which needs cell-specific delivery to therapeutically intervene. Our findings presented in this study appear to be extremely promising. The BTBR ob/ob mouse is a robust model for diabetic nephropathy in type 2 diabetes<sup>212</sup>. In vivo studies have demonstrated that VEGFR2 is a functional receptor for GREMLIN in the kidney, and activation of a GREMLIN/VEGFR2 pathway is involved in diabetic kidney disease in

BTBR ob/ob diabetic mice<sup>213,214</sup>. It is planned to knockdown of VEGFR2 by using AAV2-GEC-shRNA to inhibit downstream signaling, thereby mitigate renal damage progression.

CLDN16- and CLDN10-positive TAL cells exhibit a mosaic expression pattern and delineate the anatomical distribution of human and rodent kidneys<sup>180</sup>. It is unclear which plasma membrane proteins function as receptors and contribute to the binding of AAV9-JGA to CLDN16-positive TAL cells. Since plasma membrane protein markers of CLDN16-positive TAL cells were identified by our single-cell data (data not shown), in vitro experiments can be carried out to identify possible receptors for AAV9-JGA. Furthermore, to investigate the functional role of these TAL cells, we can generate a mouse model of CLDN16/SLC12A1 positive cell ablation by AAV9-JGA mediated delivering a diphtheria toxin receptor (DTR).

## 5 Summary

Kidney diseases represent a major and steadily increasing global health burden. Since the kidney is composed of a large number of different cell types, assembled in various tissues with highly diverging functions and disease susceptibilities, cell-specific targeting strategies are urgently needed. Here, we describe a novel approach to discover kidney-specific AAV vectors and screened both random AAV2 and AAV9 display peptide library in mice using an iterative in vivo selection protocol. Thereby we identified two AAV variants, termed “AAV2-GEC” and “AAV9-JGA”, which enable specific targeting of the glomerular endothelial cells and the CLDN16/SLC12A1-positive cells of the TAL at the JGA after systemic administration, respectively. The selective tropism of both variants was validated across species (mice and rats) and both variants exhibit stable long-term transgene expression without histological toxicity. In addition, AAV2-GEC maintained selective tropism in different mouse strains under disease conditions. We evaluated the potential of AAV2-GEC for GFB-targeting therapy and delivered to the GEC the genetic information of a bacterial cysteine proteinase that degrades IgG. This therapeutic strategy provided sustained clearance of kidney-bound antibodies and successfully prevented the progression of anti-glomerular basement membrane glomerulonephritis in mice. Furthermore, we demonstrated a general susceptibility of AAV9-JGA-targeted cells to AAV transduction and revealed a natural AAV transduction route in the kidney after systemic administration. Together, this study establishes an AAV in vivo screening approach for kidney-specific targets. We identify two novel kidney-specific targeting AAV vectors, one for glomerular endothelial cells and another for kidney epithelial cells, demonstrating the feasibility of future cell-specific kidney therapies.

## 6 Zusammenfassung

Nierenkrankheiten stellen weltweit eine große und stetig zunehmende Gesundheitsbelastung dar. Da die Niere aus einer großen Anzahl verschiedener Zelltypen besteht und aus verschiedenen Geweben mit sehr unterschiedlichen Funktionen und Krankheitsanfälligkeiten zusammengesetzt ist, werden dringend zellspezifische Targeting-Strategien benötigt. In dieser Arbeit wird ein neuer Ansatz zur Isolation nierenspezifischer AAV-Vektoren beschrieben. Dazu selektionierten wir eine randomisierte AAV2- sowie eine AAV9-Display-Peptidbibliothek in Mäusen mit Hilfe eines iterativen In-vivo-Auswahlprotokolls. Dabei haben wir zwei AAV-Varianten identifiziert, „AAV2-GEC“ und „AAV9-JGA“, die nach systemischer Verabreichung spezifisch die glomerulären Endothelzellen bzw. die CLDN16/SLC12A1-positiven Zellen des TAL an der JGA angreifen können. Der selektive Tropismus beider Varianten wurde in verschiedene Spezies (Maus und Ratte) validiert und beide Varianten weisen eine stabile Langzeit-Transgenexpression auf, ohne das histologische Anzeichen von Toxizität festgestellt werden konnten. Darüber hinaus bewahrte AAV2-GEC seinen selektiven Tropismus in verschiedenen Mausstämmen unter Krankheitsbedingungen. Zur Untersuchung des therapeutischen Potenzials von AAV2-GEC für eine zielgerichtete Behandlung von GFB brachten wir die genetische Information einer bakteriellen Cysteinproteinase, die IgG abbaut, spezifisch in die GEC ein. Diese therapeutische Strategie ermöglichte eine nachhaltige Eliminierung von nierengebundenen Antikörpern und verhinderte erfolgreich das Fortschreiten der Glomerulonephritis gegen die glomeruläre Basalmembran bei Mäusen. Darüber hinaus konnten wir eine generelle Anfälligkeit von AAV9-JGA-transduzierten Zellen für AAV-Transduktion nachweisen und einen natürlichen AAV-Transduktionsweg in der Niere nach systemischer Verabreichung aufzeigen. Zusammenfassend lässt sich sagen, dass diese Studie einen AAV-in-vivo-Screening-Ansatz für nierenspezifische Zielstrukturen darstellt. Wir haben zwei neuartige nierenspezifische AAV-Targeting-Vektoren identifiziert, einen für glomeruläre Endothelzellen und einen weiteren für Nierenepithelzellen, was die Durchführbarkeit zukünftiger zellspezifischer Nierentherapien zeigt.

## 7 List of abbreviations

AA	Afferent artery
AAV	Adeno-associated virus
AAVR	Universal AAV receptor
AdV5	Adenovirus type 5
$\alpha$ SMA	Alpha-smooth muscle actin
bp	base-pair
BS	Bowman's capsule
BSA	Bovine serum albumin
BM	Basement membrane
C1q	Complement component 1q
C3	Complement component 3
C score	Combine score
Cap	Capsid
CD	Collecting duct
CD31	The cluster of differentiation 31: Platelet endothelial cell adhesion molecule (PECAM-1)
cDNA	Complementary DNA
CLDN10	Claudin-10
CLDN16	Claudin-16
CLIC/GEEC	Clathrin-independent carriers/ Glycosylphosphatidylinositol-anchored protein enriched compartments
CMV	Cytomegalovirus
Col V	Collagenase V
DKD	Diabetic kidney disease
DMEM	Dulbecco's modified eagle medium
DTR	Diphtheria toxin receptor
E score	Enrichment score
EA	Efferent artery
EDTA	Ethylenediaminetetraacetic acid

eGFP	Enhanced GFP
ELISA	Enzyme-linked immunosorbent assay
FHHNC	Familial hypomagnesemia with hypercalciuria and nephrocalcinosis
FGFR1	Fibroblast growth factor receptor 1
GBM	Glomerular basement membrane
GC	Granular cell
gDNA	Genomic DNA
GEC	Glomerular endothelial cell
GFB	Glomerular filtration barrier
GFP	Green fluorescent protein
GFR	Glomerular filtration rate
GS score	General specificity score
HE	Hematoxylin and eosin
HEK 293T	Human embryonic kidney 293 cells with the simian virus 40 large T antigen
HGFR	Hepatocyte growth factor receptor
HSPG	Heparan sulfate proteoglycans
HSV-1	Herpes simplex virus type 1
IdeS	IgG-degrading enzyme of streptococcus pyogenes
IHC	Immunohistochemistry
ITR	Inverted terminal repeat
JGA	Juxtaglomerular apparatus
kDa	Kilodalton
LamR	Laminin receptor
MC	Mesangial cell
MD	Macula densa
MOI	Multiplicity of infection
NGS	Next-generation sequencing
NKCC2	Sodium-potassium-chloride cotransporter
NOS1	Nitric Oxide Synthase 1

NTN	Nephrotoxic nephritis
ORF	Open reading frame
PBS	Phosphate buffered saline
PBS-MK	Phosphate buffered saline with magnesium and potassium
PCR	Polymerase chain reaction
PDGFR	Platelet-derived growth factor receptor
PEC	Parietal epithelial cell
PEG	Polyethylene glycol
PEI	Polyethylenimine
PFA	Paraformaldehyde
PKD	Polycystic kidney disease
PT	Proximal tubules
qPCR	quantitative Polymerase Chain Reaction
RAAS	Renin-angiotensin-aldosterone system
rAAV	Recombinant AAV
RAC1	Rac family small GTPase 1
RCR	Rolling circle replication
Rep	Replication
RHR	Replication-rolling hairpin replication
RU	Retrograde ureteral
SC	Subcapsular injection
scAAV	Self-complementary AAV
SD	Slit diaphragm
SGLT2	Sodium-glucose cotransporter 2
SLC12A1	Solute Carrier Family 12 Member 1
ssAAV	Single-stranded AAV
SYNPO	Synaptopodin
TAL	Thick ascending limb
TGF	Tubuloglomerular feedback
TRS	Terminal resolution site
UACR	Urine albumin-creatinine ratio

UKE	Universitätsklinikum Hamburg-Eppendorf
VEGFR1/2	Vascular endothelial growth factor receptor 1/2
v/v	volume per volume
vg/dg	Vector copy numbers per diploid genome
w/v	Weight per volume
WT	Wild-type

## 8 Reference

- 1 Nonnenmacher, M. & Weber, T. Intracellular transport of recombinant adeno-associated virus vectors. *Gene Ther* **19**, 649-658, doi:10.1038/gt.2012.6 (2012).
- 2 Atchison, R. W., Casto, B. C. & Hammon, W. M. Adenovirus-Associated Defective Virus Particles. *Science* **149**, 754-756, doi:10.1126/science.149.3685.754 (1965).
- 3 Berns, K. I. & Giraud, C. Biology of adeno-associated virus. *Curr Top Microbiol Immunol* **218**, 1-23, doi:10.1007/978-3-642-80207-2\_1 (1996).
- 4 Hamilton, H., Gomos, J., Berns, K. I. & Falck-Pedersen, E. Adeno-associated virus site-specific integration and AAVS1 disruption. *Journal of virology* **78**, 7874-7882, doi:10.1128/JVI.78.15.7874-7882.2004 (2004).
- 5 Srivastava, A., Lusby, E. W. & Berns, K. I. Nucleotide sequence and organization of the adeno-associated virus 2 genome. *Journal of virology* **45**, 555-564, doi:10.1128/JVI.45.2.555-564.1983 (1983).
- 6 Koczot, F. J., Carter, B. J., Garon, C. F. & Rose, J. A. Self-complementarity of terminal sequences within plus or minus strands of adenovirus-associated virus DNA. *Proc Natl Acad Sci U S A* **70**, 215-219, doi:10.1073/pnas.70.1.215 (1973).
- 7 Kyostio, S. R., Wonderling, R. S. & Owens, R. A. Negative regulation of the adeno-associated virus (AAV) P5 promoter involves both the P5 rep binding site and the consensus ATP-binding motif of the AAV Rep68 protein. *Journal of virology* **69**, 6787-6796, doi:10.1128/JVI.69.11.6787-6796.1995 (1995).
- 8 Samulski, R. J. & Muzyczka, N. AAV-Mediated Gene Therapy for Research and Therapeutic Purposes. *Annu Rev Virol* **1**, 427-451, doi:10.1146/annurev-virology-031413-085355 (2014).
- 9 Sonntag, F. *et al.* The assembly-activating protein promotes capsid assembly of different adeno-associated virus serotypes. *Journal of virology* **85**, 12686-12697, doi:10.1128/JVI.05359-11 (2011).
- 10 Sonntag, F., Schmidt, K. & Kleinschmidt, J. A. A viral assembly factor promotes AAV2 capsid formation in the nucleolus. *Proc Natl Acad Sci U S A* **107**, 10220-10225, doi:10.1073/pnas.1001673107 (2010).
- 11 Ogden, P. J., Kelsic, E. D., Sinai, S. & Church, G. M. Comprehensive AAV capsid fitness landscape reveals a viral gene and enables machine-guided design. *Science* **366**, 1139-1143, doi:10.1126/science.aaw2900 (2019).
- 12 Elmore, Z. C. *et al.* The membrane associated accessory protein is an adeno-associated viral egress factor. *Nat Commun* **12**, 6239, doi:10.1038/s41467-021-26485-4 (2021).

- 13 McCarty, D. M. Self-complementary AAV vectors; advances and applications. *Mol Ther* **16**, 1648-1656, doi:10.1038/mt.2008.171 (2008).
- 14 Tattersall, P. & Ward, D. C. Rolling hairpin model for replication of parvovirus and linear chromosomal DNA. *Nature* **263**, 106-109, doi:10.1038/263106a0 (1976).
- 15 Astell, C. R., Chow, M. B. & Ward, D. C. Sequence analysis of the termini of virion and replicative forms of minute virus of mice DNA suggests a modified rolling hairpin model for autonomous parvovirus DNA replication. *Journal of virology* **54**, 171-177, doi:10.1128/JVI.54.1.171-177.1985 (1985).
- 16 Hauswirth, W. W. & Berns, K. I. Origin and termination of adeno-associated virus DNA replication. *Virology* **78**, 488-499, doi:10.1016/0042-6822(77)90125-8 (1977).
- 17 Chandler, M. *et al.* Breaking and joining single-stranded DNA: the HUH endonuclease superfamily. *Nat Rev Microbiol* **11**, 525-538, doi:10.1038/nrmicro3067 (2013).
- 18 Meier, A. F. *et al.* Herpes simplex virus co-infection facilitates rolling circle replication of the adeno-associated virus genome. *PLoS Pathog* **17**, e1009638, doi:10.1371/journal.ppat.1009638 (2021).
- 19 Huang, L. Y., Halder, S. & Agbandje-McKenna, M. Parvovirus glycan interactions. *Curr Opin Virol* **7**, 108-118, doi:10.1016/j.coviro.2014.05.007 (2014).
- 20 Kashiwakura, Y. *et al.* Hepatocyte growth factor receptor is a coreceptor for adeno-associated virus type 2 infection. *Journal of virology* **79**, 609-614, doi:10.1128/JVI.79.1.609-614.2005 (2005).
- 21 Kern, A. *et al.* Identification of a heparin-binding motif on adeno-associated virus type 2 capsids. *Journal of virology* **77**, 11072-11081, doi:10.1128/jvi.77.20.11072-11081.2003 (2003).
- 22 Summerford, C. & Samulski, R. J. Membrane-associated heparan sulfate proteoglycan is a receptor for adeno-associated virus type 2 virions. *Journal of virology* **72**, 1438-1445, doi:10.1128/JVI.72.2.1438-1445.1998 (1998).
- 23 Opie, S. R., Warrington, K. H., Jr., Agbandje-McKenna, M., Zolotukhin, S. & Muzyczka, N. Identification of amino acid residues in the capsid proteins of adeno-associated virus type 2 that contribute to heparan sulfate proteoglycan binding. *Journal of virology* **77**, 6995-7006, doi:10.1128/jvi.77.12.6995-7006.2003 (2003).
- 24 Bell, C. L., Gurda, B. L., Van Vliet, K., Agbandje-McKenna, M. & Wilson, J. M. Identification of the galactose binding domain of the adeno-associated virus serotype 9 capsid. *Journal of virology* **86**, 7326-7333, doi:10.1128/JVI.00448-12 (2012).

- 25 Lerch, T. F. & Chapman, M. S. Identification of the heparin binding site on adeno-associated virus serotype 3B (AAV-3B). *Virology* **423**, 6-13, doi:10.1016/j.virol.2011.10.007 (2012).
- 26 Zhang, R. *et al.* Adeno-associated virus 2 bound to its cellular receptor AAVR. *Nat Microbiol* **4**, 675-682, doi:10.1038/s41564-018-0356-7 (2019).
- 27 Tseng, Y. S. & Agbandje-McKenna, M. Mapping the AAV Capsid Host Antibody Response toward the Development of Second Generation Gene Delivery Vectors. *Front Immunol* **5**, 9, doi:10.3389/fimmu.2014.00009 (2014).
- 28 Huang, L. Y. *et al.* Characterization of the Adeno-Associated Virus 1 and 6 Sialic Acid Binding Site. *Journal of virology* **90**, 5219-5230, doi:10.1128/JVI.00161-16 (2016).
- 29 Afione, S. *et al.* Identification and mutagenesis of the adeno-associated virus 5 sialic acid binding region. *Journal of virology* **89**, 1660-1672, doi:10.1128/JVI.02503-14 (2015).
- 30 Bartlett, J. S., Wilcher, R. & Samulski, R. J. Infectious entry pathway of adeno-associated virus and adeno-associated virus vectors. *Journal of virology* **74**, 2777-2785, doi:10.1128/jvi.74.6.2777-2785.2000 (2000).
- 31 Johnson, F. B. & Dudleemajil, E. Clathrin-Associated Endocytosis as a Route of Entry into Cells for Parvoviruses. *Molecular Regulation of Endocytosis*, 183-216, doi:10.5772/48510 (2012).
- 32 Sanlioglu, S. *et al.* Endocytosis and nuclear trafficking of adeno-associated virus type 2 are controlled by rac1 and phosphatidylinositol-3 kinase activation. *Journal of virology* **74**, 9184-9196, doi:10.1128/jvi.74.19.9184-9196.2000 (2000).
- 33 Weinberg, M. S. *et al.* Recombinant adeno-associated virus utilizes cell-specific infectious entry mechanisms. *Journal of virology* **88**, 12472-12484, doi:10.1128/JVI.01971-14 (2014).
- 34 Nonnenmacher, M. & Weber, T. Adeno-associated virus 2 infection requires endocytosis through the CLIC/GEEC pathway. *Cell Host Microbe* **10**, 563-576, doi:10.1016/j.chom.2011.10.014 (2011).
- 35 Wu, Z., Miller, E., Agbandje-McKenna, M. & Samulski, R. J. Alpha2,3 and alpha2,6 N-linked sialic acids facilitate efficient binding and transduction by adeno-associated virus types 1 and 6. *Journal of virology* **80**, 9093-9103, doi:10.1128/JVI.00895-06 (2006).
- 36 Qing, K. *et al.* Human fibroblast growth factor receptor 1 is a co-receptor for infection by adeno-associated virus 2. *Nat Med* **5**, 71-77, doi:10.1038/4758 (1999).

- 37 Akache, B. *et al.* The 37/67-kilodalton laminin receptor is a receptor for adeno-associated virus serotypes 8, 2, 3, and 9. *Journal of virology* **80**, 9831-9836, doi:10.1128/JVI.00878-06 (2006).
- 38 Asokan, A., Hamra, J. B., Govindasamy, L., Agbandje-McKenna, M. & Samulski, R. J. Adeno-associated virus type 2 contains an integrin alpha5beta1 binding domain essential for viral cell entry. *Journal of virology* **80**, 8961-8969, doi:10.1128/JVI.00843-06 (2006).
- 39 Handa, A., Muramatsu, S. I., Qiu, J., Mizukami, H. & Brown, K. E. Adeno-associated virus (AAV)-3-based vectors transduce haematopoietic cells not susceptible to transduction with AAV-2-based vectors. *J Gen Virol* **81**, 2077-2084, doi:10.1099/0022-1317-81-8-2077 (2000).
- 40 Ling, C. *et al.* Human hepatocyte growth factor receptor is a cellular coreceptor for adeno-associated virus serotype 3. *Hum Gene Ther* **21**, 1741-1747, doi:10.1089/hum.2010.075 (2010).
- 41 Kaludov, N., Brown, K. E., Walters, R. W., Zabner, J. & Chiorini, J. A. Adeno-associated virus serotype 4 (AAV4) and AAV5 both require sialic acid binding for hemagglutination and efficient transduction but differ in sialic acid linkage specificity. *Journal of virology* **75**, 6884-6893, doi:10.1128/JVI.75.15.6884-6893.2001 (2001).
- 42 Di Pasquale, G. *et al.* Identification of PDGFR as a receptor for AAV-5 transduction. *Nat Med* **9**, 1306-1312, doi:10.1038/nm929 (2003).
- 43 Ng, R. *et al.* Structural characterization of the dual glycan binding adeno-associated virus serotype 6. *Journal of virology* **84**, 12945-12957, doi:10.1128/JVI.01235-10 (2010).
- 44 Weller, M. L. *et al.* Epidermal growth factor receptor is a co-receptor for adeno-associated virus serotype 6. *Nat Med* **16**, 662-664, doi:10.1038/nm.2145 (2010).
- 45 Shen, S., Bryant, K. D., Brown, S. M., Randell, S. H. & Asokan, A. Terminal N-linked galactose is the primary receptor for adeno-associated virus 9. *J Biol Chem* **286**, 13532-13540, doi:10.1074/jbc.M110.210922 (2011).
- 46 Hahm, H. S. *et al.* Automated Glycan Assembly of Oligo-N-Acetyllactosamine and Keratan Sulfate Probes to Study Virus-Glycan Interactions. *Chem-Us* **2**, 114-124, doi:10.1016/j.chempr.2016.12.004 (2017).
- 47 Mietzsch, M. *et al.* Structural Study of Aavrh.10 Receptor and Antibody Interactions. *Journal of virology* **95**, e0124921, doi:10.1128/JVI.01249-21 (2021).
- 48 Bantel-Schaal, U., Hub, B. & Kartenbeck, J. Endocytosis of adeno-associated virus type 5 leads to accumulation of virus particles in the Golgi compartment. *Journal of virology* **76**, 2340-2349, doi:10.1128/jvi.76.5.2340-2349.2002 (2002).

- 49 Nonnenmacher, M. E., Cintrat, J. C., Gillet, D. & Weber, T. Syntaxin 5-dependent retrograde transport to the trans-Golgi network is required for adeno-associated virus transduction. *Journal of virology* **89**, 1673-1687, doi:10.1128/JVI.02520-14 (2015).
- 50 Wu, Z., Asokan, A. & Samulski, R. J. Adeno-associated virus serotypes: vector toolkit for human gene therapy. *Mol Ther* **14**, 316-327, doi:10.1016/j.ymthe.2006.05.009 (2006).
- 51 Bleker, S., Sonntag, F. & Kleinschmidt, J. A. Mutational analysis of narrow pores at the fivefold symmetry axes of adeno-associated virus type 2 capsids reveals a dual role in genome packaging and activation of phospholipase A2 activity. *Journal of virology* **79**, 2528-2540, doi:10.1128/JVI.79.4.2528-2540.2005 (2005).
- 52 Kronenberg, S., Bottcher, B., von der Lieth, C. W., Bleker, S. & Kleinschmidt, J. A. A conformational change in the adeno-associated virus type 2 capsid leads to the exposure of hidden VP1 N termini. *Journal of virology* **79**, 5296-5303, doi:10.1128/JVI.79.9.5296-5303.2005 (2005).
- 53 Buning, H. AAV Entry: Filling in the Blanks. *Mol Ther* **28**, 346-347, doi:10.1016/j.ymthe.2020.01.015 (2020).
- 54 Mizukami, H., Young, N. S. & Brown, K. E. Adeno-associated virus type 2 binds to a 150-kilodalton cell membrane glycoprotein. *Virology* **217**, 124-130, doi:10.1006/viro.1996.0099 (1996).
- 55 Pillay, S. *et al.* Adeno-associated Virus (AAV) Serotypes Have Distinctive Interactions with Domains of the Cellular AAV Receptor. *Journal of virology* **91**, doi:10.1128/JVI.00391-17 (2017).
- 56 Zhang, R. *et al.* Divergent engagements between adeno-associated viruses with their cellular receptor AAVR. *Nat Commun* **10**, 3760, doi:10.1038/s41467-019-11668-x (2019).
- 57 Dudek, A. M. *et al.* An Alternate Route for Adeno-associated Virus (AAV) Entry Independent of AAV Receptor. *Journal of virology* **92**, doi:10.1128/JVI.02213-17 (2018).
- 58 Dudek, A. M. *et al.* GPR108 Is a Highly Conserved AAV Entry Factor. *Mol Ther* **28**, 367-381, doi:10.1016/j.ymthe.2019.11.005 (2020).
- 59 Pillay, S. *et al.* An essential receptor for adeno-associated virus infection. *Nature* **530**, 108-112, doi:10.1038/nature16465 (2016).
- 60 Hamilton, B. A., Li, X., Pezzulo, A. A., Abou Alaiwa, M. H. & Zabner, J. Polarized AAVR expression determines infectivity by AAV gene therapy vectors. *Gene Ther* **26**, 240-249, doi:10.1038/s41434-019-0078-3 (2019).

- 61 Cotmore, S. F., D'Abramo A, M., Jr., Ticknor, C. M. & Tattersall, P. Controlled conformational transitions in the MVM virion expose the VP1 N-terminus and viral genome without particle disassembly. *Virology* **254**, 169-181, doi:10.1006/viro.1998.9520 (1999).
- 62 Ros, C., Baltzer, C., Mani, B. & Kempf, C. Parvovirus uncoating in vitro reveals a mechanism of DNA release without capsid disassembly and striking differences in encapsidated DNA stability. *Virology* **345**, 137-147, doi:10.1016/j.virol.2005.09.030 (2006).
- 63 Colella, P., Ronzitti, G. & Mingozi, F. Emerging Issues in AAV-Mediated In Vivo Gene Therapy. *Mol Ther Methods Clin Dev* **8**, 87-104, doi:10.1016/j.omtm.2017.11.007 (2018).
- 64 Hoggan, M. D., Blacklow, N. R. & Rowe, W. P. Studies of small DNA viruses found in various adenovirus preparations: physical, biological, and immunological characteristics. *Proc Natl Acad Sci U S A* **55**, 1467-1474, doi:10.1073/pnas.55.6.1467 (1966).
- 65 Samulski, R. J., Berns, K. I., Tan, M. & Muzyczka, N. Cloning of adeno-associated virus into pBR322: rescue of intact virus from the recombinant plasmid in human cells. *Proc Natl Acad Sci U S A* **79**, 2077-2081, doi:10.1073/pnas.79.6.2077 (1982).
- 66 Laughlin, C. A., Tratschin, J. D., Coon, H. & Carter, B. J. Cloning of infectious adeno-associated virus genomes in bacterial plasmids. *Gene* **23**, 65-73, doi:10.1016/0378-1119(83)90217-2 (1983).
- 67 Flotte, T. R. *et al.* Stable in vivo expression of the cystic fibrosis transmembrane conductance regulator with an adeno-associated virus vector. *Proc Natl Acad Sci U S A* **90**, 10613-10617, doi:10.1073/pnas.90.22.10613 (1993).
- 68 Kaplitt, M. G. *et al.* Long-term gene expression and phenotypic correction using adeno-associated virus vectors in the mammalian brain. *Nat Genet* **8**, 148-154, doi:10.1038/ng1094-148 (1994).
- 69 Flotte, T. *et al.* A phase I study of an adeno-associated virus-CFTR gene vector in adult CF patients with mild lung disease. *Hum Gene Ther* **7**, 1145-1159, doi:10.1089/hum.1996.7.9-1145 (1996).
- 70 Gao, G. *et al.* Adeno-associated viruses undergo substantial evolution in primates during natural infections. *Proc Natl Acad Sci U S A* **100**, 6081-6086, doi:10.1073/pnas.0937739100 (2003).
- 71 Erles, K., Sebokova, P. & Schlehofer, J. R. Update on the prevalence of serum antibodies (IgG and IgM) to adeno-associated virus (AAV). *J Med Virol* **59**, 406-411, doi:10.1002/(sici)1096-9071(199911)59:3<406::aid-jmv22>3.0.co;2-n (1999).

- 72 Smith, R. H. Adeno-associated virus integration: virus versus vector. *Gene Ther* **15**, 817-822, doi:10.1038/gt.2008.55 (2008).
- 73 Xiao, X., Li, J. & Samulski, R. J. Production of high-titer recombinant adeno-associated virus vectors in the absence of helper adenovirus. *Journal of virology* **72**, 2224-2232, doi:10.1128/JVI.72.3.2224-2232.1998 (1998).
- 74 Ferrari, F. K., Samulski, T., Shenk, T. & Samulski, R. J. Second-strand synthesis is a rate-limiting step for efficient transduction by recombinant adeno-associated virus vectors. *Journal of virology* **70**, 3227-3234, doi:10.1128/JVI.70.5.3227-3234.1996 (1996).
- 75 Fisher, K. J. *et al.* Transduction with recombinant adeno-associated virus for gene therapy is limited by leading-strand synthesis. *Journal of virology* **70**, 520-532, doi:10.1128/JVI.70.1.520-532.1996 (1996).
- 76 McCarty, D. M., Monahan, P. E. & Samulski, R. J. Self-complementary recombinant adeno-associated virus (scAAV) vectors promote efficient transduction independently of DNA synthesis. *Gene Ther* **8**, 1248-1254, doi:10.1038/sj.gt.3301514 (2001).
- 77 Louis Jeune, V., Joergensen, J. A., Hajjar, R. J. & Weber, T. Pre-existing anti-adeno-associated virus antibodies as a challenge in AAV gene therapy. *Hum Gene Ther Methods* **24**, 59-67, doi:10.1089/hgtb.2012.243 (2013).
- 78 Vandamme, C., Adjali, O. & Mingozi, F. Unraveling the Complex Story of Immune Responses to AAV Vectors Trial After Trial. *Hum Gene Ther* **28**, 1061-1074, doi:10.1089/hum.2017.150 (2017).
- 79 Arjomandnejad, M., Dasgupta, I., Flotte, T. R. & Keeler, A. M. Immunogenicity of Recombinant Adeno-Associated Virus (AAV) Vectors for Gene Transfer. *BioDrugs*, 1-19, doi:10.1007/s40259-023-00585-7 (2023).
- 80 Ronzitti, G., Gross, D. A. & Mingozi, F. Human Immune Responses to Adeno-Associated Virus (AAV) Vectors. *Front Immunol* **11**, 670, doi:10.3389/fimmu.2020.00670 (2020).
- 81 Verdera, H. C., Kuranda, K. & Mingozi, F. AAV Vector Immunogenicity in Humans: A Long Journey to Successful Gene Transfer. *Mol Ther* **28**, 723-746, doi:10.1016/j.ymthe.2019.12.010 (2020).
- 82 Corti, M. *et al.* B-Cell Depletion is Protective Against Anti-AAV Capsid Immune Response: A Human Subject Case Study. *Mol Ther Methods Clin Dev* **1**, 14033-, doi:10.1038/mtm.2014.33 (2014).
- 83 Meliani, A. *et al.* Antigen-selective modulation of AAV immunogenicity with tolerogenic rapamycin nanoparticles enables successful vector re-administration. *Nat Commun* **9**, 4098, doi:10.1038/s41467-018-06621-3 (2018).

- 84 Monteilhet, V. *et al.* A 10 patient case report on the impact of plasmapheresis upon neutralizing factors against adeno-associated virus (AAV) types 1, 2, 6, and 8. *Mol Ther* **19**, 2084-2091, doi:10.1038/mt.2011.108 (2011).
- 85 Tse, L. V. *et al.* Structure-guided evolution of antigenically distinct adeno-associated virus variants for immune evasion. *Proc Natl Acad Sci U S A* **114**, E4812-E4821, doi:10.1073/pnas.1704766114 (2017).
- 86 Jordan, S. C. *et al.* IgG Endopeptidase in Highly Sensitized Patients Undergoing Transplantation. *N Engl J Med* **377**, 442-453, doi:10.1056/NEJMoa1612567 (2017).
- 87 Mihai, S. *et al.* In vivo enzymatic modulation of IgG antibodies prevents immune complex-dependent skin injury. *Exp Dermatol* **26**, 691-696, doi:10.1111/exd.13163 (2017).
- 88 Leborgne, C. *et al.* IgG-cleaving endopeptidase enables in vivo gene therapy in the presence of anti-AAV neutralizing antibodies. *Nat Med* **26**, 1096-1101, doi:10.1038/s41591-020-0911-7 (2020).
- 89 Ros-Ganan, I. *et al.* Optimising the IgG-degrading enzyme treatment regimen for enhanced adeno-associated virus transduction in the presence of neutralising antibodies. *Clin Transl Immunology* **11**, e1375, doi:10.1002/cti2.1375 (2022).
- 90 Bobo, T. A. *et al.* IgG-cleavage protein allows therapeutic AAV gene delivery in passively immunized MPS IIIA mice. *Gene Ther*, doi:10.1038/s41434-022-00368-9 (2022).
- 91 Bryant, L. M. *et al.* Lessons learned from the clinical development and market authorization of Glybera. *Hum Gene Ther Clin Dev* **24**, 55-64, doi:10.1089/humc.2013.087 (2013).
- 92 Ameri, H. Prospect of retinal gene therapy following commercialization of voretigene neparvovec-rzyl for retinal dystrophy mediated by RPE65 mutation. *J Curr Ophthalmol* **30**, 1-2, doi:10.1016/j.joco.2018.01.006 (2018).
- 93 Maguire, A. M. *et al.* Efficacy, Safety, and Durability of Voretigene Neparvovec-rzyl in RPE65 Mutation-Associated Inherited Retinal Dystrophy: Results of Phase 1 and 3 Trials. *Ophthalmology* **126**, 1273-1285, doi:10.1016/j.ophtha.2019.06.017 (2019).
- 94 Administration, U. F. a. D. FDA approves novel gene therapy to treat patients with a rare form of inherited vision loss. (2018).
- 95 Mendell, J. R. *et al.* Single-Dose Gene-Replacement Therapy for Spinal Muscular Atrophy. *N Engl J Med* **377**, 1713-1722, doi:10.1056/NEJMoa1706198 (2017).

- 96 Al-Zaidy, S. *et al.* Health outcomes in spinal muscular atrophy type 1 following AVXS-101 gene replacement therapy. *Pediatr Pulmonol* **54**, 179-185, doi:10.1002/ppul.24203 (2019).
- 97 Urquhart, L. FDA new drug approvals in Q2 2019. *Nat Rev Drug Discov* **18**, 575, doi:10.1038/d41573-019-00121-9 (2019).
- 98 Colon-Thillet, R., Jerome, K. R. & Stone, D. Optimization of AAV vectors to target persistent viral reservoirs. *Virology* **18**, 85, doi:10.1186/s12985-021-01555-7 (2021).
- 99 Munch, R. C. *et al.* Off-target-free gene delivery by affinity-purified receptor-targeted viral vectors. *Nat Commun* **6**, 6246, doi:10.1038/ncomms7246 (2015).
- 100 Reul, J., Muik, A. & Buchholz, C. J. Ligand Coupling to the AAV Capsid for Cell-Specific Gene Transfer. *Methods Mol Biol* **1950**, 35-50, doi:10.1007/978-1-4939-9139-6\_3 (2019).
- 101 Eichhoff, A. M. *et al.* Nanobody-Enhanced Targeting of AAV Gene Therapy Vectors. *Mol Ther Methods Clin Dev* **15**, 211-220, doi:10.1016/j.omtm.2019.09.003 (2019).
- 102 Ponnazhagan, S., Mahendra, G., Kumar, S., Thompson, J. A. & Castillas, M., Jr. Conjugate-based targeting of recombinant adeno-associated virus type 2 vectors by using avidin-linked ligands. *Journal of virology* **76**, 12900-12907, doi:10.1128/jvi.76.24.12900-12907.2002 (2002).
- 103 Hudry, E. *et al.* Efficient Gene Transfer to the Central Nervous System by Single-Stranded Anc80L65. *Mol Ther Methods Clin Dev* **10**, 197-209, doi:10.1016/j.omtm.2018.07.006 (2018).
- 104 Maheshri, N., Koerber, J. T., Kaspar, B. K. & Schaffer, D. V. Directed evolution of adeno-associated virus yields enhanced gene delivery vectors. *Nat Biotechnol* **24**, 198-204, doi:10.1038/nbt1182 (2006).
- 105 Asuri, P. *et al.* Directed evolution of adeno-associated virus for enhanced gene delivery and gene targeting in human pluripotent stem cells. *Mol Ther* **20**, 329-338, doi:10.1038/mt.2011.255 (2012).
- 106 Pulicherla, N. *et al.* Engineering liver-detargeted AAV9 vectors for cardiac and musculoskeletal gene transfer. *Mol Ther* **19**, 1070-1078, doi:10.1038/mt.2011.22 (2011).
- 107 Li, W. *et al.* Engineering and selection of shuffled AAV genomes: a new strategy for producing targeted biological nanoparticles. *Mol Ther* **16**, 1252-1260, doi:10.1038/mt.2008.100 (2008).

- 108 Grimm, D. *et al.* In vitro and in vivo gene therapy vector evolution via multispecies interbreeding and retargeting of adeno-associated viruses. *Journal of virology* **82**, 5887-5911, doi:10.1128/JVI.00254-08 (2008).
- 109 Lisowski, L. *et al.* Selection and evaluation of clinically relevant AAV variants in a xenograft liver model. *Nature* **506**, 382-386, doi:10.1038/nature12875 (2014).
- 110 Ran, G. *et al.* Site-Directed Mutagenesis Improves the Transduction Efficiency of Capsid Library-Derived Recombinant AAV Vectors. *Mol Ther Methods Clin Dev* **17**, 545-555, doi:10.1016/j.omtm.2020.03.007 (2020).
- 111 Wooley, D. P. *et al.* A directed evolution approach to select for novel Adeno-associated virus capsids on an HIV-1 producer T cell line. *J Virol Methods* **250**, 47-54, doi:10.1016/j.jviromet.2017.09.008 (2017).
- 112 Muller, O. J. *et al.* Random peptide libraries displayed on adeno-associated virus to select for targeted gene therapy vectors. *Nat Biotechnol* **21**, 1040-1046, doi:10.1038/nbt856 (2003).
- 113 Varadi, K. *et al.* Novel random peptide libraries displayed on AAV serotype 9 for selection of endothelial cell-directed gene transfer vectors. *Gene Ther* **19**, 800-809, doi:10.1038/gt.2011.143 (2012).
- 114 Borner, K. *et al.* Pre-arrayed Pan-AAV Peptide Display Libraries for Rapid Single-Round Screening. *Mol Ther* **28**, 1016-1032, doi:10.1016/j.ymthe.2020.02.009 (2020).
- 115 Dalkara, D. *et al.* In vivo-directed evolution of a new adeno-associated virus for therapeutic outer retinal gene delivery from the vitreous. *Sci Transl Med* **5**, 189ra176, doi:10.1126/scitranslmed.3005708 (2013).
- 116 Isgrig, K. *et al.* AAV2.7m8 is a powerful viral vector for inner ear gene therapy. *Nat Commun* **10**, 427, doi:10.1038/s41467-018-08243-1 (2019).
- 117 Deverman, B. E. *et al.* Cre-dependent selection yields AAV variants for widespread gene transfer to the adult brain. *Nat Biotechnol* **34**, 204-209, doi:10.1038/nbt.3440 (2016).
- 118 Korbelin, J. *et al.* A brain microvasculature endothelial cell-specific viral vector with the potential to treat neurovascular and neurological diseases. *EMBO Mol Med* **8**, 609-625, doi:10.15252/emmm.201506078 (2016).
- 119 Chen, X. *et al.* Engineered AAVs for non-invasive gene delivery to rodent and non-human primate nervous systems. *Neuron* **110**, 2242-2257 e2246, doi:10.1016/j.neuron.2022.05.003 (2022).

- 120 Goertsen, D. *et al.* AAV capsid variants with brain-wide transgene expression and decreased liver targeting after intravenous delivery in mouse and marmoset. *Nat Neurosci* **25**, 106-115, doi:10.1038/s41593-021-00969-4 (2022).
- 121 Korbelen, J. *et al.* Pulmonary Targeting of Adeno-associated Viral Vectors by Next-generation Sequencing-guided Screening of Random Capsid Displayed Peptide Libraries. *Mol Ther* **24**, 1050-1061, doi:10.1038/mt.2016.62 (2016).
- 122 Goertsen, D., Goeden, N., Flytzanis, N. C. & Gradinaru, V. Targeting the lung epithelium after intravenous delivery by directed evolution of underexplored sites on the AAV capsid. *Mol Ther Methods Clin Dev* **26**, 331-342, doi:10.1016/j.omtm.2022.07.010 (2022).
- 123 Pavlou, M. *et al.* Novel AAV capsids for intravitreal gene therapy of photoreceptor disorders. *EMBO Mol Med* **13**, e13392, doi:10.15252/emmm.202013392 (2021).
- 124 Rode, L. *et al.* AAV capsid engineering identified two novel variants with improved in vivo tropism for cardiomyocytes. *Mol Ther* **30**, 3601-3618, doi:10.1016/j.ymthe.2022.07.003 (2022).
- 125 Wang, D., Tai, P. W. L. & Gao, G. Adeno-associated virus vector as a platform for gene therapy delivery. *Nat Rev Drug Discov* **18**, 358-378, doi:10.1038/s41573-019-0012-9 (2019).
- 126 Adachi, K., Enoki, T., Kawano, Y., Veraz, M. & Nakai, H. Drawing a high-resolution functional map of adeno-associated virus capsid by massively parallel sequencing. *Nat Commun* **5**, 3075, doi:10.1038/ncomms4075 (2014).
- 127 Shen, S. *et al.* Glycan binding avidity determines the systemic fate of adeno-associated virus type 9. *Journal of virology* **86**, 10408-10417, doi:10.1128/JVI.01155-12 (2012).
- 128 Korbelen, J. *et al.* Optimization of design and production strategies for novel adeno-associated viral display peptide libraries. *Gene Ther* **24**, 470-481, doi:10.1038/gt.2017.51 (2017).
- 129 Ravindra Kumar, S. *et al.* Multiplexed Cre-dependent selection yields systemic AAVs for targeting distinct brain cell types. *Nat Methods* **17**, 541-550, doi:10.1038/s41592-020-0799-7 (2020).
- 130 Ebook. Biology. *United Kingdom: McGraw-Hill Education*, 1020-1022 (2014).
- 131 Puelles, V. G. *et al.* Glomerular number and size variability and risk for kidney disease. *Curr Opin Nephrol Hypertens* **20**, 7-15, doi:10.1097/MNH.0b013e3283410a7d (2011).

- 132 Pollak, M. R., Quaggin, S. E., Hoenig, M. P. & Dworkin, L. D. The glomerulus: the sphere of influence. *Clin J Am Soc Nephrol* **9**, 1461-1469, doi:10.2215/CJN.09400913 (2014).
- 133 Du, B. J., Yu, M. X. & Zheng, J. Transport and interactions of nanoparticles in the kidneys. *Nat Rev Mater* **3**, 358-374, doi:10.1038/s41578-018-0038-3 (2018).
- 134 Haraldsson, B., Nystrom, J. & Deen, W. M. Properties of the glomerular barrier and mechanisms of proteinuria. *Physiol Rev* **88**, 451-487, doi:10.1152/physrev.00055.2006 (2008).
- 135 Levick, J. R. & Smaje, L. H. An analysis of the permeability of a fenestra. *Microvasc Res* **33**, 233-256, doi:10.1016/0026-2862(87)90020-3 (1987).
- 136 Byron, A. *et al.* Glomerular cell cross-talk influences composition and assembly of extracellular matrix. *J Am Soc Nephrol* **25**, 953-966, doi:10.1681/ASN.2013070795 (2014).
- 137 Timpl, R. Structure and biological activity of basement membrane proteins. *Eur J Biochem* **180**, 487-502, doi:10.1111/j.1432-1033.1989.tb14673.x (1989).
- 138 Grahammer, F. New structural insights into podocyte biology. *Cell Tissue Res* **369**, 5-10, doi:10.1007/s00441-017-2590-3 (2017).
- 139 Lemley, K. V. *et al.* The glomerular mesangium: capillary support function and its failure under experimental conditions. *Clin Investig* **70**, 843-856, doi:10.1007/BF00180755 (1992).
- 140 Barajas, L. Anatomy of the juxtaglomerular apparatus. *Am J Physiol* **237**, F333-343, doi:10.1152/ajprenal.1979.237.5.F333 (1979).
- 141 JaBJ, S. Function of the Juxtaglomerular Apparatus: control of glomerular hemodynamics and renin secretion. *The Kidney: Physiology & Pathophysiology* 1053-1068 (1992).
- 142 Peti-Peterdi, J. & Harris, R. C. Macula densa sensing and signaling mechanisms of renin release. *J Am Soc Nephrol* **21**, 1093-1096, doi:10.1681/ASN.2009070759 (2010).
- 143 Schnabel, E. & Kriz, W. Morphometric studies of the extraglomerular mesangial cell field in volume expanded and volume depleted rats. *Anat Embryol (Berl)* **170**, 217-222, doi:10.1007/BF00319007 (1984).
- 144 Francois, H. & Coffman, T. M. Prostanoids and blood pressure: which way is up? *J Clin Invest* **114**, 757-759, doi:10.1172/JCI22929 (2004).

- 145 Ma, C. C., Wang, Z. L., Xu, T., He, Z. Y. & Wei, Y. Q. The approved gene therapy drugs worldwide: from 1998 to 2019. *Biotechnol Adv* **40**, 107502, doi:10.1016/j.biotechadv.2019.107502 (2020).
- 146 Arabi, F., Mansouri, V. & Ahmadbeigi, N. Gene therapy clinical trials, where do we go? An overview. *Biomed Pharmacother* **153**, 113324, doi:10.1016/j.biopha.2022.113324 (2022).
- 147 Mali, S. Delivery systems for gene therapy. *Indian J Hum Genet* **19**, 3-8, doi:10.4103/0971-6866.112870 (2013).
- 148 Bulcha, J. T., Wang, Y., Ma, H., Tai, P. W. L. & Gao, G. Viral vector platforms within the gene therapy landscape. *Signal Transduct Target Ther* **6**, 53, doi:10.1038/s41392-021-00487-6 (2021).
- 149 Zu, H. & Gao, D. Non-viral Vectors in Gene Therapy: Recent Development, Challenges, and Prospects. *AAPS J* **23**, 78, doi:10.1208/s12248-021-00608-7 (2021).
- 150 Chavez, M., Chen, X., Finn, P. B. & Qi, L. S. Advances in CRISPR therapeutics. *Nat Rev Nephrol* **19**, 9-22, doi:10.1038/s41581-022-00636-2 (2023).
- 151 Schrezenmeier, E. *et al.* The underestimated burden of monogenic kidney disease in adults waitlisted for kidney transplantation. *Genet Med* **23**, 1219-1224, doi:10.1038/s41436-021-01127-8 (2021).
- 152 Rubin, J. D. & Barry, M. A. Improving Molecular Therapy in the Kidney. *Mol Diagn Ther* **24**, 375-396, doi:10.1007/s40291-020-00467-6 (2020).
- 153 Davis, L. & Park, F. Gene therapy research for kidney diseases. *Physiol Genomics* **51**, 449-461, doi:10.1152/physiolgenomics.00052.2019 (2019).
- 154 Corridon, P. R. *et al.* A method to facilitate and monitor expression of exogenous genes in the rat kidney using plasmid and viral vectors. *Am J Physiol Renal Physiol* **304**, F1217-1229, doi:10.1152/ajprenal.00070.2013 (2013).
- 155 Tariq, I. *et al.* Lipodendriplexes mediated enhanced gene delivery: a cellular to pre-clinical investigation. *Sci Rep* **10**, 21446, doi:10.1038/s41598-020-78123-6 (2020).
- 156 Han, S. J. *et al.* Renal proximal tubular NEMO plays a critical role in ischemic acute kidney injury. *JCI Insight* **5**, doi:10.1172/jci.insight.139246 (2020).
- 157 Tang, T. T. *et al.* Kim-1 Targeted Extracellular Vesicles: A New Therapeutic Platform for RNAi to Treat AKI. *J Am Soc Nephrol* **32**, 2467-2483, doi:10.1681/ASN.2020111561 (2021).

- 158 Rodriguez-Castejon, J. *et al.* alpha-Galactosidase A Augmentation by Non-Viral Gene Therapy: Evaluation in Fabry Disease Mice. *Pharmaceutics* **13**, doi:10.3390/pharmaceutics13060771 (2021).
- 159 Ortiz, P. A., Hong, N. J., Plato, C. F., Varela, M. & Garvin, J. L. An in vivo method for adenovirus-mediated transduction of thick ascending limbs. *Kidney Int* **63**, 1141-1149, doi:10.1046/j.1523-1755.2003.00827.x (2003).
- 160 Rubin, J. D., Nguyen, T. V., Allen, K. L., Ayasoufi, K. & Barry, M. A. Comparison of Gene Delivery to the Kidney by Adenovirus, Adeno-Associated Virus, and Lentiviral Vectors After Intravenous and Direct Kidney Injections. *Hum Gene Ther* **30**, 1559-1571, doi:10.1089/hum.2019.127 (2019).
- 161 Hillestad, M. L., Guenzel, A. J., Nath, K. A. & Barry, M. A. A vector-host system to fingerprint virus tropism. *Hum Gene Ther* **23**, 1116-1126, doi:10.1089/hum.2011.116 (2012).
- 162 Chen, S. *et al.* Gene delivery in renal tubular epithelial cells using recombinant adeno-associated viral vectors. *J Am Soc Nephrol* **14**, 947-958, doi:10.1097/01.asn.0000057858.45649.f7 (2003).
- 163 Ozgur-Gunes, Y. *et al.* Correction of a knock-in mouse model of acrodysostosis with gene therapy using a rAAV9-CAG-human PRKAR1A vector. *Gene Ther* **29**, 441-448, doi:10.1038/s41434-021-00286-2 (2022).
- 164 Lang, J. F., Toulmin, S. A., Brida, K. L., Eisenlohr, L. C. & Davidson, B. L. Standard screening methods underreport AAV-mediated transduction and gene editing. *Nat Commun* **10**, 3415, doi:10.1038/s41467-019-11321-7 (2019).
- 165 Rocca, C. J., Ur, S. N., Harrison, F. & Cherqui, S. rAAV9 combined with renal vein injection is optimal for kidney-targeted gene delivery: conclusion of a comparative study. *Gene Ther* **21**, 618-628, doi:10.1038/gt.2014.35 (2014).
- 166 Cahoon, J. M. *et al.* Intravitreal AAV2.COMP-Ang1 Prevents Neurovascular Degeneration in a Murine Model of Diabetic Retinopathy. *Diabetes* **64**, 4247-4259, doi:10.2337/db14-1030 (2015).
- 167 Ikeda, Y., Sun, Z., Ru, X., Vandenberghe, L. H. & Humphreys, B. D. Efficient Gene Transfer to Kidney Mesenchymal Cells Using a Synthetic Adeno-Associated Viral Vector. *J Am Soc Nephrol* **29**, 2287-2297, doi:10.1681/ASN.2018040426 (2018).
- 168 Zincarelli, C., Soltys, S., Rengo, G. & Rabinowitz, J. E. Analysis of AAV serotypes 1-9 mediated gene expression and tropism in mice after systemic injection. *Mol Ther* **16**, 1073-1080, doi:10.1038/mt.2008.76 (2008).
- 169 Asico, L. D. *et al.* Nephron segment-specific gene expression using AAV vectors. *Biochem Biophys Res Commun* **497**, 19-24, doi:10.1016/j.bbrc.2018.01.169 (2018).

- 170 Michelfelder, S. *et al.* Vectors selected from adeno-associated viral display peptide libraries for leukemia cell-targeted cytotoxic gene therapy. *Exp Hematol* **35**, 1766-1776, doi:10.1016/j.exphem.2007.07.018 (2007).
- 171 Korbelin, J. & Trepel, M. How to Successfully Screen Random Adeno-Associated Virus Display Peptide Libraries In Vivo. *Hum Gene Ther Methods* **28**, 109-123, doi:10.1089/hgtb.2016.177 (2017).
- 172 Kocylowski, M. K. *et al.* A slit-diaphragm-associated protein network for dynamic control of renal filtration. *Nat Commun* **13**, 6446, doi:10.1038/s41467-022-33748-1 (2022).
- 173 Jourde-Chiche, N. *et al.* Endothelium structure and function in kidney health and disease. *Nat Rev Nephrol* **15**, 87-108, doi:10.1038/s41581-018-0098-z (2019).
- 174 Liu, S. *et al.* Single-cell transcriptomics reveals a mechanosensitive injury signaling pathway in early diabetic nephropathy. *Genome Med* **15**, 2, doi:10.1186/s13073-022-01145-4 (2023).
- 175 Finch, N. C. *et al.* Reduced Glomerular Filtration in Diabetes Is Attributable to Loss of Density and Increased Resistance of Glomerular Endothelial Cell Fenestrations. *J Am Soc Nephrol* **33**, 1120-1136, doi:10.1681/ASN.2021030294 (2022).
- 176 Watakabe, A. *et al.* Comparative analyses of adeno-associated viral vector serotypes 1, 2, 5, 8 and 9 in marmoset, mouse and macaque cerebral cortex. *Neurosci Res* **93**, 144-157, doi:10.1016/j.neures.2014.09.002 (2015).
- 177 El-Shamayleh, Y., Ni, A. M. & Horwitz, G. D. Strategies for targeting primate neural circuits with viral vectors. *J Neurophysiol* **116**, 122-134, doi:10.1152/jn.00087.2016 (2016).
- 178 Hordeaux, J. *et al.* The Neurotropic Properties of AAV-PHP.B Are Limited to C57BL/6J Mice. *Mol Ther* **26**, 664-668, doi:10.1016/j.ymthe.2018.01.018 (2018).
- 179 Huang, Q. *et al.* Delivering genes across the blood-brain barrier: LY6A, a novel cellular receptor for AAV-PHP.B capsids. *PLoS One* **14**, e0225206, doi:10.1371/journal.pone.0225206 (2019).
- 180 Milatz, S. *et al.* Mosaic expression of claudins in thick ascending limbs of Henle results in spatial separation of paracellular Na<sup>+</sup> and Mg<sup>2+</sup> transport. *Proc Natl Acad Sci U S A* **114**, E219-E227, doi:10.1073/pnas.1611684114 (2017).
- 181 Chen, L., Chou, C. L. & Knepper, M. A. Targeted Single-Cell RNA-seq Identifies Minority Cell Types of Kidney Distal Nephron. *J Am Soc Nephrol* **32**, 886-896, doi:10.1681/ASN.2020101407 (2021).

- 182 Komlosi, P., Bell, P. D. & Zhang, Z. R. Tubuloglomerular feedback mechanisms in nephron segments beyond the macula densa. *Curr Opin Nephrol Hypertens* **18**, 57-62, doi:10.1097/MNH.0b013e32831daf54 (2009).
- 183 Ren, H. *et al.* Direct physical contact between intercalated cells in the distal convoluted tubule and the afferent arteriole in mouse kidneys. *PLoS One* **8**, e70898, doi:10.1371/journal.pone.0070898 (2013).
- 184 Romero, C. A. & Carretero, O. A. Tubule-vascular feedback in renal autoregulation. *Am J Physiol Renal Physiol* **316**, F1218-F1226, doi:10.1152/ajprenal.00381.2018 (2019).
- 185 Rosivall, L., Razga, Z. & Ormos, J. Morphological characterization of human juxtaglomerular apparatus. *Kidney Int Suppl* **32**, S9-12 (1991).
- 186 Lin, R. *et al.* Directed evolution of adeno-associated virus for efficient gene delivery to microglia. *Nat Methods* **19**, 976-985, doi:10.1038/s41592-022-01547-7 (2022).
- 187 Hanlon, K. S. *et al.* Selection of an Efficient AAV Vector for Robust CNS Transgene Expression. *Mol Ther Methods Clin Dev* **15**, 320-332, doi:10.1016/j.omtm.2019.10.007 (2019).
- 188 Hennigs, J. K., Matuszcak, C., Trepel, M. & Korbelen, J. Vascular Endothelial Cells: Heterogeneity and Targeting Approaches. *Cells* **10**, doi:10.3390/cells10102712 (2021).
- 189 Mahtal, N., Lenoir, O. & Tharaux, P. L. Glomerular Endothelial Cell Crosstalk With Podocytes in Diabetic Kidney Disease. *Front Med (Lausanne)* **8**, 659013, doi:10.3389/fmed.2021.659013 (2021).
- 190 Anders, H. J., Kitching, A. R., Leung, N. & Romagnani, P. Glomerulonephritis: immunopathogenesis and immunotherapy. *Nat Rev Immunol*, 1-19, doi:10.1038/s41577-022-00816-y (2023).
- 191 Daehn, I. S. & Duffield, J. S. The glomerular filtration barrier: a structural target for novel kidney therapies. *Nat Rev Drug Discov* **20**, 770-788, doi:10.1038/s41573-021-00242-0 (2021).
- 192 Zinn, E. *et al.* In Silico Reconstruction of the Viral Evolutionary Lineage Yields a Potent Gene Therapy Vector. *Cell Rep* **12**, 1056-1068, doi:10.1016/j.celrep.2015.07.019 (2015).
- 193 Li, A. S., Ingham, J. F. & Lennon, R. Genetic Disorders of the Glomerular Filtration Barrier. *Clin J Am Soc Nephrol* **15**, 1818-1828, doi:10.2215/CJN.11440919 (2020).
- 194 Lemaire, M., Noone, D., Lapeyraque, A. L., Licht, C. & Fremeaux-Bacchi, V. Inherited Kidney Complement Diseases. *Clin J Am Soc Nephrol* **16**, 942-956, doi:10.2215/CJN.11830720 (2021).

- 195 Bresin, E. *et al.* Combined complement gene mutations in atypical hemolytic uremic syndrome influence clinical phenotype. *J Am Soc Nephrol* **24**, 475-486, doi:10.1681/ASN.2012090884 (2013).
- 196 Challis, R. C. *et al.* Thrombotic Microangiopathy in Inverted Formin 2-Mediated Renal Disease. *J Am Soc Nephrol* **28**, 1084-1091, doi:10.1681/ASN.2015101189 (2017).
- 197 Lemaire, M. *et al.* Recessive mutations in DGKE cause atypical hemolytic-uremic syndrome. *Nat Genet* **45**, 531-536, doi:10.1038/ng.2590 (2013).
- 198 Dumas, S. J. *et al.* Phenotypic diversity and metabolic specialization of renal endothelial cells. *Nat Rev Nephrol* **17**, 441-464, doi:10.1038/s41581-021-00411-9 (2021).
- 199 Shin, J. I., Geetha, D., Szpirt, W. M., Windpessl, M. & Kronbichler, A. Anti-glomerular basement membrane disease (Goodpasture disease): From pathogenesis to plasma exchange to IdeS. *Ther Apher Dial* **26**, 24-31, doi:10.1111/1744-9987.13718 (2022).
- 200 Uhlin, F. *et al.* Endopeptidase Cleavage of Anti-Glomerular Basement Membrane Antibodies in vivo in Severe Kidney Disease: An Open-Label Phase 2a Study. *J Am Soc Nephrol* **33**, 829-838, doi:10.1681/ASN.2021111460 (2022).
- 201 Yang, R. *et al.* Successful treatment of experimental glomerulonephritis with IdeS and EndoS, IgG-degrading streptococcal enzymes. *Nephrol Dial Transplant* **25**, 2479-2486, doi:10.1093/ndt/gfq115 (2010).
- 202 Prot-Bertoye, C. *et al.* Differential localization patterns of claudin 10, 16, and 19 in human, mouse, and rat renal tubular epithelia. *Am J Physiol Renal Physiol* **321**, F207-F224, doi:10.1152/ajprenal.00579.2020 (2021).
- 203 Muller, D., Kausalya, P. J., Meij, I. C. & Hunziker, W. Familial hypomagnesemia with hypercalciuria and nephrocalcinosis: blocking endocytosis restores surface expression of a novel Claudin-16 mutant that lacks the entire C-terminal cytosolic tail. *Hum Mol Genet* **15**, 1049-1058, doi:10.1093/hmg/ddl020 (2006).
- 204 Jo, C. H., Kim, S. & Kim, G. H. Claudins in kidney health and disease. *Kidney Res Clin Pract* **41**, 275-287, doi:10.23876/j.krcp.21.279 (2022).
- 205 Prot-Bertoye, C. & Houillier, P. Claudins in Renal Physiology and Pathology. *Genes (Basel)* **11**, doi:10.3390/genes11030290 (2020).
- 206 Hou, J. *et al.* Claudin-16 and claudin-19 interaction is required for their assembly into tight junctions and for renal reabsorption of magnesium. *Proc Natl Acad Sci U S A* **106**, 15350-15355, doi:10.1073/pnas.0907724106 (2009).

- 207 Kalantar-Zadeh, K., Jafar, T. H., Nitsch, D., Neuen, B. L. & Perkovic, V. Chronic kidney disease. *Lancet* **398**, 786-802, doi:10.1016/S0140-6736(21)00519-5 (2021).
- 208 Apelt, K., Bijkerk, R., Lebrin, F. & Rabelink, T. J. Imaging the Renal Microcirculation in Cell Therapy. *Cells* **10**, doi:10.3390/cells10051087 (2021).
- 209 Rosivall, L. & Peti-Peterdi, J. Heterogeneity of the afferent arteriole--correlations between morphology and function. *Nephrol Dial Transplant* **21**, 2703-2707, doi:10.1093/ndt/gfl308 (2006).
- 210 Rosivall, L. *et al.* Renin-angiotensin system affects endothelial morphology and permeability of renal afferent arteriole. *Acta Physiol Hung* **94**, 7-17, doi:10.1556/APhysiol.94.2007.1-2.3 (2007).
- 211 Sol, M. *et al.* Glomerular Endothelial Cells as Instigators of Glomerular Sclerotic Diseases. *Front Pharmacol* **11**, 573557, doi:10.3389/fphar.2020.573557 (2020).
- 212 Hudkins, K. L. *et al.* BTBR Ob/Ob mutant mice model progressive diabetic nephropathy. *J Am Soc Nephrol* **21**, 1533-1542, doi:10.1681/ASN.2009121290 (2010).
- 213 Mezzano, S. *et al.* Gremlin and renal diseases: ready to jump the fence to clinical utility? *Nephrol Dial Transplant* **33**, 735-741, doi:10.1093/ndt/gfx194 (2018).
- 214 Lavoz, C. *et al.* VEGFR2 Blockade Improves Renal Damage in an Experimental Model of Type 2 Diabetic Nephropathy. *J Clin Med* **9**, doi:10.3390/jcm9020302 (2020).

## 9 Acknowledgment

Completing this doctoral thesis has been a significant milestone in my academic journey, and I owe a debt of gratitude to the individuals and institutions who have supported and inspired me along the way.

First and foremost, I would like to thank my supervisor Prof. Dr. med. Tobias B. Huber to give me the chance to do my doctoral study at Huber Laboratory. I am grateful to Dr. Shun Lu, Dr. Shuya Liu and Dr. Jakob Körbelin for their unwavering guidance, patience, and expertise throughout this research journey. Their invaluable insights, constructive feedback, and continuous encouragement have been instrumental in shaping this thesis.

I appreciate the members of my thesis committee, Prof. Dr. med. Catherine Meyer-Schwesinger and Prof. Dr. med. Friedrich Koch-Nolte. Their insightful feedback, constructive criticism, and rigorous examination of my work have elevated the quality and rigor of this thesis.

I would like to thank Dr. Julia Hagenstein for the professional technical support, PD Dr. Oliver Kretz for the EM micrographs, Dr. Nuray Akyüz for the NGS, and Dr. Malik Alawi for the bioinformatics evaluation.

I would like to acknowledge Melanie Schaper, Anja Obser, Silvia Chilla, Ilka Edenhofer, Nina Ziegert and Valerie Oberüber, as well as Microscopy Imaging Facility and Vector Core at University Medical Center Hamburg-Eppendorf, Germany, for the excellent technical support. I would like to acknowledge the financial support provided by the China Scholarship Council.

I would like to thank all Huber Laboratory members to create a productive and efficient working environment.

Lastly, I would like to express my deepest gratitude to my wife and our parents. Their unwavering love, encouragement, and understanding have been the bedrock of my journey. Their sacrifices, belief in my abilities, and constant encouragement have been a constant source of inspiration.

## 10 Curriculum vitae

### **Basic Information**

Name: Guochao Wu

Date of birth: 09.20.1992

E-mail: g.wu@uke.de

### **Education**

2018- PhD student in III. Department of Medicine, University Medical Center Hamburg-Eppendorf.

2014-2017 Master Degree in Animal Nutrition and Feed Science, College of Animal Science, Jilin University.

2010-2014 Bachelor Degree in Animal Science, College of Animal Science, Jilin University.

### **Publications**

**Wu G**, Liu S, Hagenstein J, Hengel F, Schaper M, Akyüz N, Alawi M, Liao Z, Failla AV, Dierlamm J, Körbelin J, Lu S, Huber TB. A novel kidney glomerular endothelium-targeting AAV delivers bacterial proteinase to treat glomerulonephritis. 2023.06. Manuscript preparation.

Lu S, **Wu G**, Liu S, Hagenstein J, Akyüz N, Alawi M, Braren I, Zhao Y, Bonn S, Dierlamm J, Kretz O, Körbelin J, Huber TB. In vivo-directed evolution discovers a kidney epithelial-specific AAV and reveals a natural transduction route after system administration. 2023.06. Manuscript preparation.

Solagna F, Tezze C, Lindenmeyer MT, Lu S, **Wu G**, Liu S, Zhao Y, Mitchell R, Meyer C, Omairi S, Kilic T. Pro-cachectic factors link experimental and human chronic kidney disease to skeletal muscle wasting programs. The Journal of Clinical Investigation. 2021 Jun 1;131(11).

Aypek H, Krisp C, Lu S, Liu S, Kylies D, Kretz O, **Wu G**, Moritz M, Amann K, Benz K, Tong P. Loss of the collagen IV modifier prolyl 3-hydroxylase 2 causes thin basement membrane nephropathy. Journal of Clinical Investigation. 2022 May 2;132(9):e147253.

Liu S, Zhao Y, Lu S, Zhang T, Lindenmeyer MT, Nair V, Gies SE, **Wu G**, Nelson RG, Czogalla J, Aypek H. Single-cell transcriptomics reveals a mechanosensitive injury signaling pathway in early diabetic nephropathy. *Genome Medicine*. 2023 Dec;15(1):1-9.

### **Patents**

Huber TB, Lu S, Körbelin J, **Wu G**, Liu S. 2023. 01. An AAV2-vector variant for targeted transfer of genes. Patent application submitted to European patent office. Application number: EP23154267.1.

Huber TB, Lu S, Körbelin J, **Wu G**, Liu S. 2023. 01. An AAV9 capsid variant for targeted gene transfer. Patent application submitted to European patent office. Application number: EP23154266.3.

## 11 Eidesstattliche Versicherung

Ich versichere ausdrücklich, dass ich die Arbeit selbständig und ohne fremde Hilfe verfasst, andere als die von mir angegebenen Quellen und Hilfsmittel nicht benutzt und die aus den benutzten Werken wörtlich oder inhaltlich entnommenen Stellen einzeln nach Ausgabe (Auflage und Jahr des Erscheinens), Band und Seite des benutzten Werkes kenntlich gemacht habe.

Ferner versichere ich, dass ich die Dissertation bisher nicht einem Fachvertreter an einer anderen Hochschule zur Überprüfung vorgelegt oder mich anderweitig um Zulassung zur Promotion beworben habe.

Ich erkläre mich einverstanden, dass meine Dissertation vom Dekanat der Medizinischen Fakultät mit einer gängigen Software zur Erkennung von Plagiaten überprüft werden kann.

Unterschrift: .....